The Pennsylvania State University

The Graduate School

College of Engineering

PARAMETRIC TRADE STUDY OF MULTIPLE LIBRATION POINT ORBITS IN THE CIRCULAR RESTRICTED FOUR-BODY PROBLEM

A Thesis in

Aerospace Engineering

by

Peter C. Scarcella

Submitted in Partial Fulfillment
of the Requirements
for the Degree of

Master of Science

May 2016

The thesis of Peter Scarcella was reviewed and approved* by the following:

David B. Spencer
Professor of Aerospace Engineering
Thesis Advisor

Sven G. Bilén
Professor of Engineering Design, Electrical Engineering, and Aerospace Engineering

George A. Lesieutre
Professor of Aerospace Engineering
Head of the Department of Aerospace Engineering

*Signatures are on file in the Graduate School

ABSTRACT

Studying an asteroid up close has been up until more recently nothing more than wishful thinking. With NASA's Asteroid Redirect Mission in the planning stages, the prospect of bringing an asteroid back to the vicinity of the Earth is tantalizing. Once an asteroid has been retrieved and brought back to the Earth–Moon system and placed into orbit for study, human crews will visit it and study it up close. This thesis explores the orbital dynamics of an asteroid in orbit around the Earth–Moon libration point, EML1. The dynamics of the motions for a spacecraft in close proximity to an asteroid are found using the circular restricted four-body problem (CR4BP). Treating the problem as the superposition of two circular restricted three-body problems (CR3BP), the asteroid becomes an additional gravitational perturbation to a spacecraft close to the asteroid. Two sets of coupled equations of motion, one for the asteroid and one for the spacecraft are derived and solved simultaneously. A trade study to examine the near-term behavior of a spacecraft's orbit relative to the asteroid is conducted via a series of simulations utilizing a variety of variables such as the asteroid's location and mass relative to the spacecraft, the size of orbit, and the varying of initial conditions. The characteristics being studied are the stability of the spacecraft's orbit over a short duration as well as the range between the spacecraft and its target asteroid over the mission duration. In addition, the minimum safe stand-off distance between both objects is determined to ensure no collisions or orbital instability. The ultimate goal is to obtain various datasets to deduce the most stable conditions for placing an asteroid and to determine where to fly a spacecraft in formation with the asteroid in orbit about the EML1 libration point. The results show the viability of a couple orbits as well as the prevalence of impacts. How the data can be utilized for future missions was also studied.

TABLE OF CONTENTS

LIST OF FIGURES

LIST OF TABLES

ACKNOWLEDGMENTS

I would like to grant my deepest appreciation to my advisor, Dr. David Spencer for his indispensable guidance during the development process of this thesis.

In addition, I would also like to give my gratitude toward Dr. George Lesieutre and Dr. Sven Bilén for their support of the students of the Department of Aerospace Engineering.

I would also like to extend my gratefulness to Dr. Florian Renk of the European Space Operations Centre (ESOC) within the European Space Agency (ESA) for supplying me with the initial conditions for my orbits. Without that data, this work would have been impossible.

I would like to express my immense gratitude towards my parents Peter and Patricia Scarcella, and my sister Janessa Cottage for their continued support and love in my pursuit of this masters degree and in everyday life.

Lastly, I want to express my thankfulness to my close friends for the friendship and laughter they provide me on a daily basis.

LIST OF SYMBOLS

$L1$ ..... Collinear libration point between Earth and Moon

$L2$ ..... Collinear libration point beyond Moon

μ .....Gravitational Parameter (km^3/sec^2)

m_1 ..... Mass of Earth (kg)

m_2 ..... Mass of Moon (kg)

m_3 ..... Mass of Asteroid (metric tons)

m_4 .....Mass of Spacecraft (kg)

ω..... Angular Velocity about the Barycenter (rad/sec)

G.....Gravitational Constant ($km^3kg^{-1}sec^{-2}$)

$\vec{a}_1$.....Position Vector from Barycenter to Body One (m)

$\vec{a}_2$..... Position Vector from Barycenter to Body Two (m)

$\vec{r}_{31}$ ..... Position Vector from Body Three to Body One (m)

$\vec{r}_{32}$.....Position Vector from Body Three to Body Two (m)

$\vec{r}_{41}$..... Position Vector from Body Four to Body One (m)

$\vec{r}_{42}$.....Position Vector from Body Four to Body Two (m)

$\vec{r}_{43}$.....Position Vector from Body Four to Body Three (m)

r_{25} ..... Radius of 25–ton Asteroid (m)

r_{75} ..... Radius of 75–ton Asteroid (m)

r_{130} ..... Radius of 130–ton Asteroid (m)

r_{200} ..... Radius of 200–ton Asteroid (m)

Chapter 1

Introduction

The desire to study an asteroid has long been a aspiration of scientists in many different disciplines. Questions ranging from determining the early formation of the solar system to the potential for future mining of vital mineral elements have all been posed as rationale for retrieving a complete asteroid. NASA has been planning for several years now to capture an asteroid for study under their Asteroid Redirect Mission.[*] While the design of the capture device and overall mission design is still in the planning phases, one of the basic ideas is to place the asteroid in a lunar distant retrograde orbit once the asteroid has been brought back. This thesis seeks to look at alternative prospects around the Earth – Moon libration point L1, hereafter referred to as EML1. The location of the aforementioned libration point may be viewed in Figure 1.1.

To examine the dynamics of both an asteroid and a spacecraft in the Earth–Moon system, one needs to take into account the gravitational effects from all sources. However, this can be difficult and it can easily be stated that the gravitational perturbations resulting from the asteroid and spacecraft are negligible. As such, it is useful to utilize the classical restricted three-body problem similar to Bando [1] et al. and Gurfil et al. [2]. It is a widely studied problem in astrodynamics in which three bodies move about a common center-of-mass (henceforth referred to as the barycenter) where the third smaller mass moves relative to the other larger masses. This smaller body has negligible gravitational effects on the motion of the other more massive objects.

[*] http://www.nasa.gov/sites/default/files/atoms/files/nasa-tm-2016-219011-arm-fast-final-report_0.pdf March 20, 2016

The system that this thesis examines, however, is considering four masses in which two of the masses are much more massive than the remaining two.

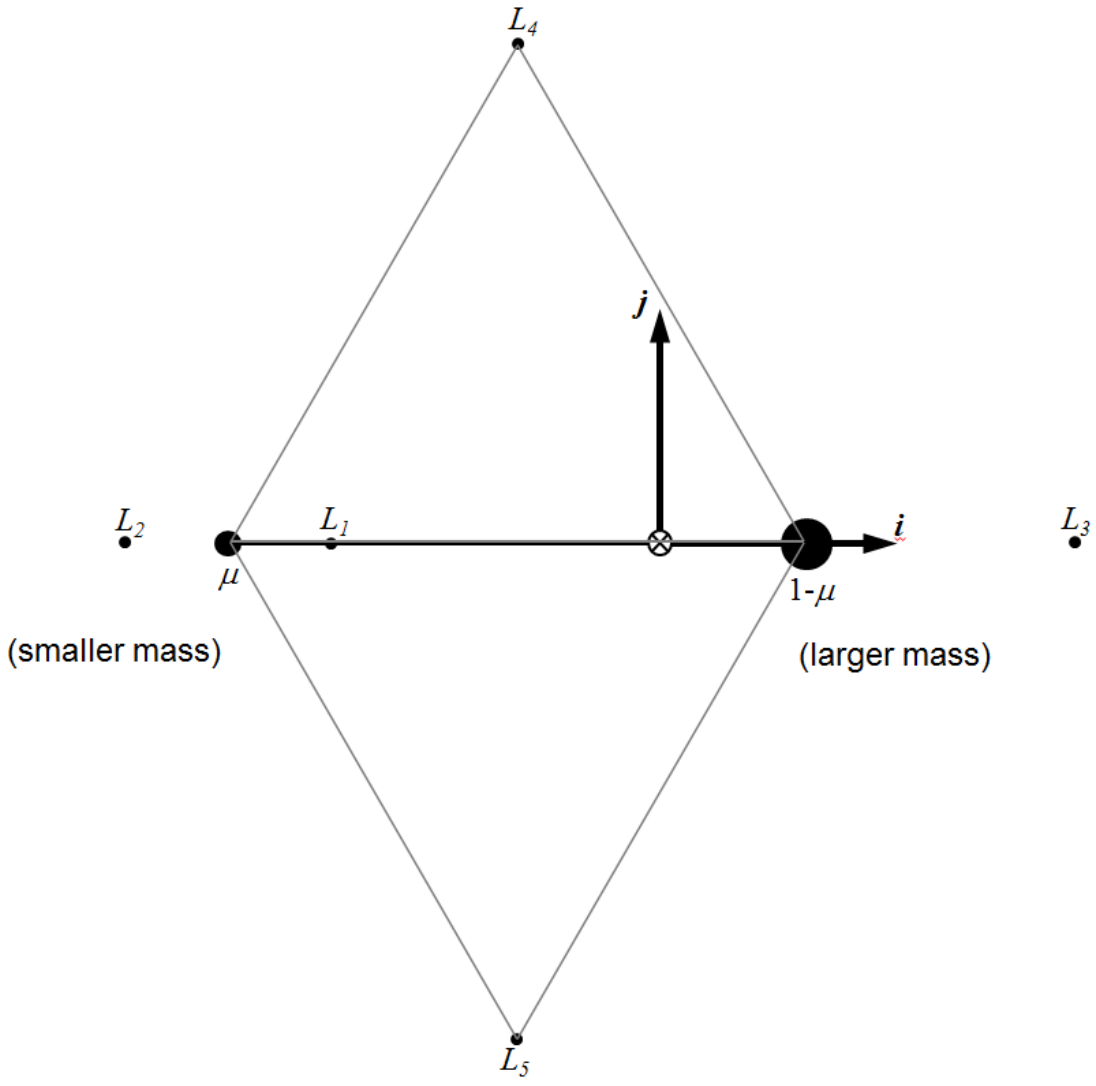

Figure 1.1. Graphical representation of the location of the libration points

Thus, the restricted four-body problem model will be used. This can be achieved by starting with the restricted three-body problem and adding an additional gravitational perturbation. In this scenario, where the spacecraft is moving relative to the asteroid, the effects of the asteroid's

gravity on the spacecraft is the additional gravitational source within the restricted three-body problem wherein the Earth and Moon are the major sources of gravity. The masses are considered to be point masses though other models are viable as outlined in Wang et al. [3], wherein the spacecraft is treated as a rigid body. The model being used here is the circular restricted four body-problem (CR4BP) as circular orbits will be assumed for the Earth–Moon system. This is a good mathematical approximation to study the general behavior of the smaller mass (the spacecraft) relative to the larger bodies.

In effect, two coupled circular restricted three-body problems (CR3BP) are solved simultaneously. The first problem considers the asteroid in the Earth–Moon system and the second problem considers the spacecraft in the same system except with the addition of an extra term containing the gravitational effects of the asteroid onto the spacecraft's orbit. Both of these systems of equations are coupled and solved simultaneously. A more rigorous explanation and derivation of these equations is discussed in Chapter 2.

Once the governing equations of motion are obtained, the idea is to then conduct a trade study in which a variety of orbits and other scenarios are simulated to determine the safest optimal standoff distance between the spacecraft and asteroid. Stability of the orbits is also a key factor, though long-term stability of the spacecraft's orbit is not an issue as the mission would take place over a short duration. Stability is defined as how much the spacecraft drifts closer or further from the asteroid. For larger bodies like 433 Eros, stable orbits are viable roughly 31 km from the surface [4]. The only perturbation being considered in this thesis is the effect of gravity. Other sources of perturbations such as gravity-gradient torques produced by the Sun and Earth [5] solar radiation pressure, solar tides, as well as other variables as seen in Scheeres [6] are factors in this problem but are not considered here. When in close proximity to the asteroid, the effect from the gravity is the largest perturbation as mentioned by Scheeres [7].

Other variables being examined in this thesis include the initial proximity of the spacecraft to the asteroid as well as the mass of the asteroid itself. The Moon's orbit around the Earth is not circular so the position of the libration point will oscillate back and forth as the Moon completes its revolution around the Earth. A more rigorous overview of the stability of libration points can be viewed in texts such as Szebeheley [8] and Curtis [9]. Generating this type of data is important as it can be used to develop better control laws for spacecraft operation close to asteroids. Guelman [10], Mok et al. [11], and Broschart et al. [12] all describe various methods of control schemes near small bodies such as asteroids. The need to develop control laws for spacecraft is vital and thus the need to understand the underlying dynamics is a first step. Other applications of this data involve designing a trajectory to land on an asteroid as per Tardivel et al. [13] or to operate around an asteroid using solar sails as detailed by Morrow [14].

The various scenarios of the trade study are discussed in more detail in Chapter 3, whereas the results are presented and analyzed in Chapter 4. Lastly, the conclusions and proposed future work are discussed in Chapter 5.

Chapter 2

Astrodynamics of the N-Body Problem

The astrodynamics of the circular restricted four-body problem can be broken up into several sections. To begin the derivation of the equations of motion, it is first necessary to define the reference frames used as seen in Section 2.1. As there are four bodies, the model will be broken up into two coupled circular restricted three-body-problems. The dynamics of the CR3BP are discussed in Section 2.2. Treating the asteroid has an additional gravitational source, Section 2.3 will explore the second CR3BP with that extra term coupled with the equations of motion for the Earth, Moon, and spacecraft. The N-Body problem can be studied in more detail in Szebeheley [8].

2.1 Inertial and Rotational Reference Frames

Within the inertial reference frame ($\hat{I}$, $\hat{J}$, $\hat{K}$), one can define a rotating reference frame as $\hat{i}$, $\hat{j}$, $\hat{k}$ as seen in Figure 2.1. As can be seen from the figure, inertial and rotating reference frames are coplanar in the ($\hat{I}$, $\hat{J}$) and ($\hat{i}$, $\hat{j}$) planes. The rotating frame being initially aligned rotates relative to the inertial frame at a rate ω over a time interval $t - t_0$ where t_0 is the time where both frames are initially aligned. The resulting angle $\omega(t - t_0)$ is swept out over the interval. Masses m_1 and m_2 are positioned relative to the smaller mass by their respective vectors $\bar{r}_1$ and $\bar{r}_2$. The equations of motion for the restricted three-body-problem will be found in the rotating frame.

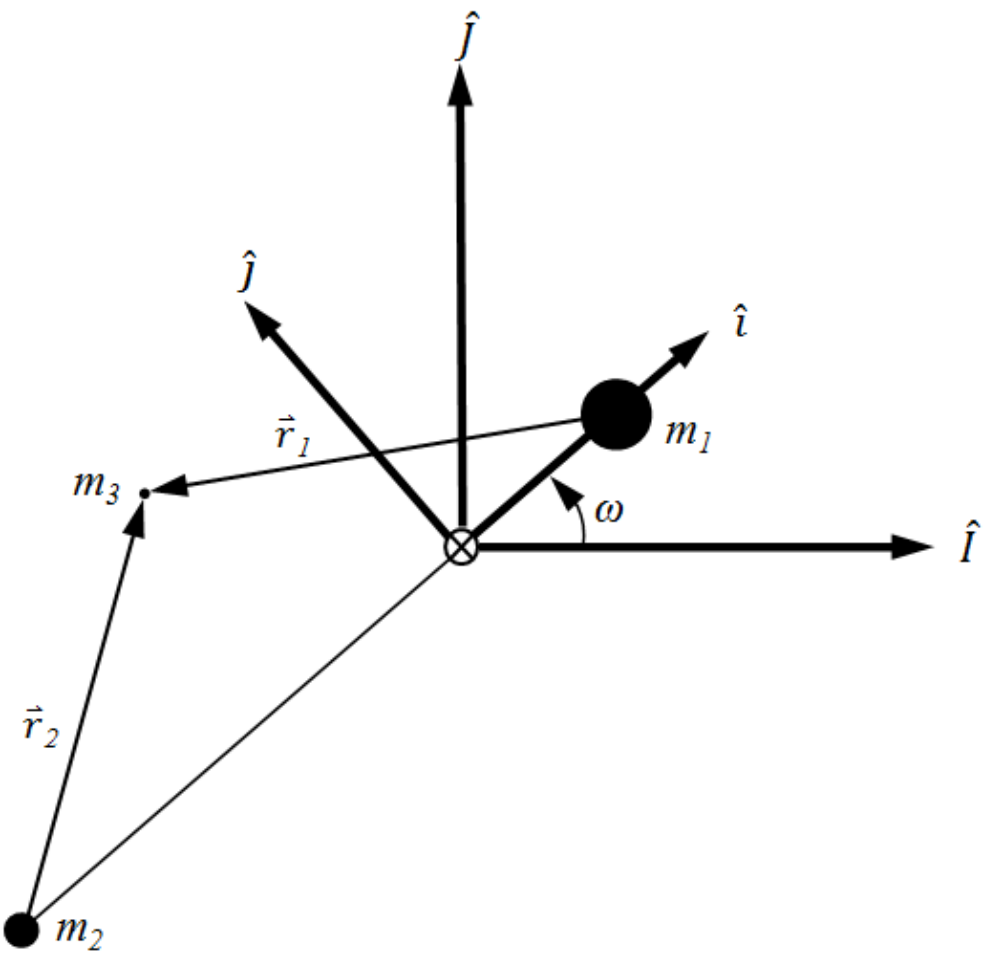

Figure 2.1. Geometry of the Inertial and Rotational Reference Frames

2.2 The Circular Restricted Three-Body Problem (CR3BP)

It is common in orbital mechanics problems such as this to non-dimensionalize the physical parameters to determine a clear relationship between the properties being examined; within the scope of this problem, this would be between the masses. In astrodynamical terms, these are called canonical units. The following derivations are done in a similar manner to

Prussing et al. [15] and Curtis [9]. By letting the sum of the major masses (m_1 and m_2) equal one, the smaller mass ($m_1 >> m_2$) becomes defined proportionally to the larger mass, i.e.,

$$\mu = \frac{m_2}{m_1 + m_2}. \tag{2.1}$$

The smaller mass becomes

$$m_2 = \mu. \tag{2.2}$$

The masses being normalized results in the larger mass being

$$m_1 = 1 - \mu. \tag{2.3}$$

Within the scope of the CR3BP, it is necessary to begin with Newton's second law which relates the force to the mass of an object and its rate of change in velocity. In the restricted three-body problem, the equations-of-motion are

$$m_3 \ddot{\vec{r}} = G\left(\frac{m_3 m_1}{r_{31}^3}\vec{r}_{31}\right) + G\left(\frac{m_3 m_2}{r_{32}^3}\vec{r}_{32}\right). \tag{2.4}$$

The meaning of the variables can be seen from Figure 2.2.

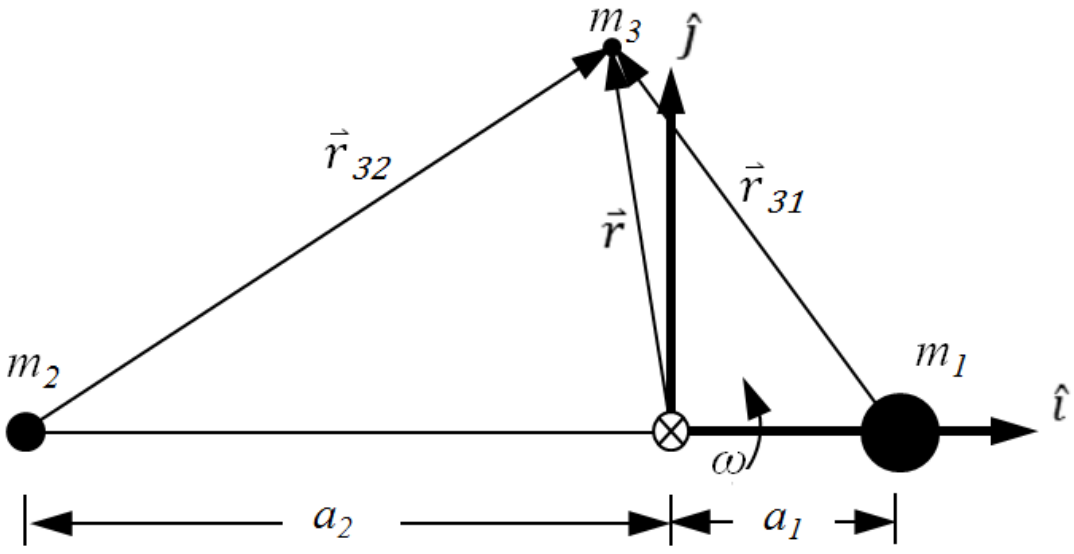

Figure 2.2. Geometry of the CR3BP

It is now necessary to introduce the position vector of the third mass in the rotational frame and its corresponding velocity and acceleration vectors as

$$\vec{r} = x\hat{i} + y\hat{j} + z\hat{k}\,. \tag{2.5}$$

The velocity in the rotating frame is

$$\frac{d\vec{r}}{dt} = \frac{dx}{dt}\hat{i} + \frac{dy}{dt}\hat{j} + \frac{dz}{dt}\hat{k} \tag{2.6}$$

and the acceleration is

$$\frac{d^2\vec{r}}{dt^2} = \frac{d^2x}{dt^2}\hat{i} + \frac{d^2y}{dt^2}\hat{j} + \frac{d^2z}{dt^2}\hat{k}\,. \tag{2.7}$$

From examining Figure 2.2, the relative positions between the smallest mass and both the larger ones are determined. These vectors are found to be

$$\vec{r}_{31} = (x - a_1)\hat{i} + y\hat{j} + z\hat{k}\,, \tag{2.8}$$

$$\vec{r}_{32} = (x - a_2)\hat{i} + y\hat{j} + z\hat{k}\,, \tag{2.9}$$

where a_1 and a_2 are the locations of m_1 and m_2, respectively.

The motion of the Earth and Moon around their barycenter has an acceleration in the rotational reference (Figure 2.1) frame of

$$\ddot{\vec{r}}^{(R)} = \left(\frac{d^2x}{dt^2} - 2\frac{dy}{dt} - x\right)\hat{i} + \left(\frac{d^2y}{dt^2} + 2\frac{dx}{dt} - y\right)\hat{j} + \frac{d^2z}{dt^2}\hat{k} \tag{2.10}$$

This acceleration is equivalent to the gravitational acceleration

$$\ddot{\vec{r}} = -\frac{(1-\mu)}{r_{31}^3}\vec{r}_{31} - \frac{\mu}{r_{32}^3}\vec{r}_{32}. \tag{2.11}$$

Equating Equations (2.10) and (2.11) and substituting the relative position vectors from Equations (2.8) and (2.9), the rotational acceleration ($\ddot{\vec{r}}^{(R)}$) becomes

$$\ddot{\vec{r}}^{(R)} = -\frac{(1-\mu)}{r_{31}^3}\vec{r}_{31}\left[(x-\mu)\hat{i} + y\hat{j} + z\hat{k}\right] - \frac{\mu}{r_{32}^3}\vec{r}_{32}\left[(x+1-\mu)\hat{i} + y\hat{j} + z\hat{k}\right] \tag{2.12}$$

Finally, equating Equation (2.12) with (2.10) while also separating the $\hat{i}$, $\hat{j}$, $\hat{k}$ components yields three non-linear differential equations.

$$\frac{d^2x}{dt^2} - 2\frac{dy}{dt} - x = -\frac{(1-\mu)(x-\mu)}{r_{31}^3} - \frac{\mu(x+1-\mu)}{r_{32}^3}, \tag{2.13}$$

$$\frac{d^2y}{dt^2} + 2\frac{dx}{dt} - y = -\frac{(1-\mu)y}{r_{31}^3} - \frac{\mu y}{r_{32}^3}, \text{ and} \tag{2.14}$$

$$\frac{d^2z}{dt^2} = -\frac{(1-\mu)z}{r_{31}^3} - \frac{\mu z}{r_{32}^3}. \tag{2.15}$$

Equations (2.12) through (2.14) describe the motion of the asteroid relative to both the Earth and Moon in three dimensions. These equations do not take into account the spacecraft (the fourth body) in our system. Expanding upon the restricted three-body problem and considering the asteroid as an additional gravitational source is the fundamental model used in this research.

2.3 The Circular Restricted Four-Body Problem (CR4BP)

Consider the system described in the previous section. In this section, a fourth body will be added: the spacecraft. As mentioned in Chapter 1, the problem will be treated as two coupled circular restricted three-body problems. To accomplish this task, the moon is treated as an additional term in the equations of motion providing the additional gravitational acceleration.

The analysis begins in the same manner as the previous section. Equations (2.1) – (2.7) are derived in the same way. An additional normalized mass parameter is needed for the third body as the previous Equations (2.1) – (2.3) relate μ to m_1 and m_2. The expression for the third body (the asteroid) is

$$\mu_3 = \frac{Gm_3}{\mu_1 + \mu_2} \tag{2.16}$$

where G is the gravitational constant and μ_1 and μ_2 are the gravitational parameters for the Earth and Moon, respectively.

The derivation deviates from this point as Figure 2.3 is considered. Similar to the previous section, the relative position vectors are taken between the smallest mass (this time the spacecraft) and the larger two masses m_1 and m_2.

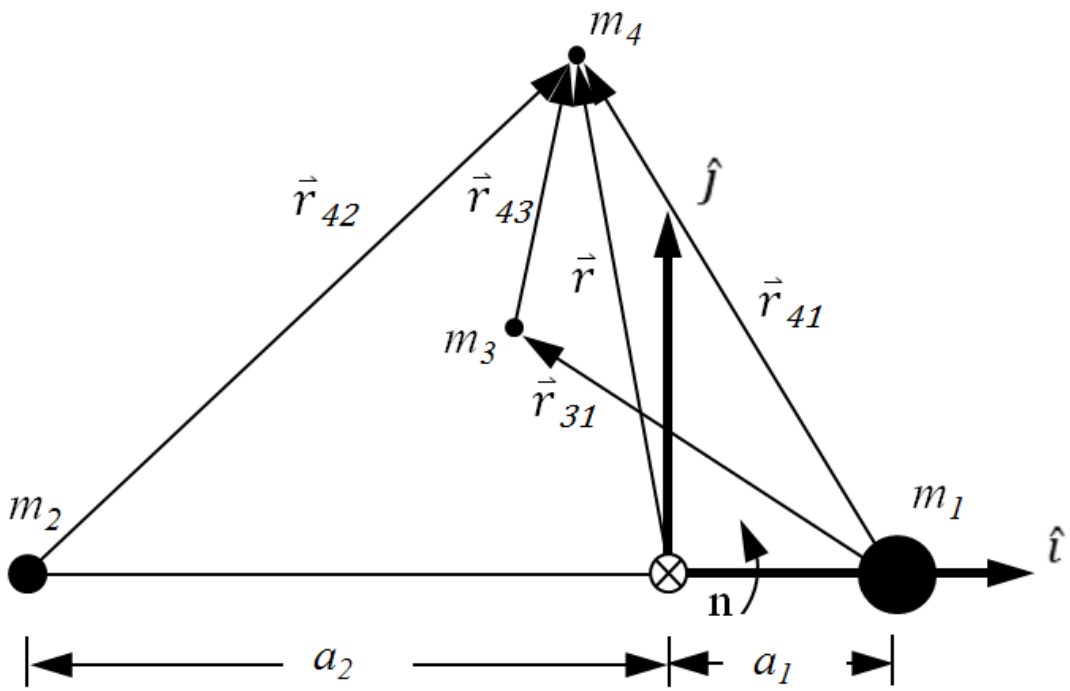

Figure 2.3. Geometry of the CR4BP

However, an additional vector is derived ($\vec{r}_{43}$) in a similar manner to Huang [16], which is the position vector between the spacecraft (m_4) and the moon (m_3).

$$\vec{r}_{41} = (x_s - a_1)\hat{i} + y_s\hat{j} + z_s\hat{k}, \tag{2.17}$$

$$\vec{r}_{42} = (x_s - a_2)\hat{i} + y_s\hat{j} + z_s\hat{k}, \text{ and} \tag{2.18}$$

$$\vec{r}_{43} = (x_s - x_a)\hat{i} + (y_s - y_a)\hat{j} + (z_s - z_a)\hat{k}, \tag{2.19}$$

where x_s, y_s, and z_s are the coordinates of the satellite and x_a, y_a, and z_a are the coordinates of the asteroid. The acceleration of the Earth and Moon around the barycenter is the same as the one in Equation (2.10). The acceleration due to the gravity differs from Equation (2.11) as it now has an extra term

$$\ddot{\vec{r}} = -\frac{(1-\mu)}{r_{41}^3}\vec{r}_{41} - \frac{\mu}{r_{42}^3}\vec{r}_{42} - \frac{\mu_3}{r_{43}^3}\vec{r}_{43} \tag{2.20}$$

Equating Equations (2.10) and (2.20) and substituting the relative position vectors (2.17-2.19) yields the rotational acceleration

$$\ddot{\vec{r}}^{(I)} = -\frac{(1-\mu)}{r_{41}^3}\vec{r}_{41}\left[(x_s-\mu)\hat{i} + y_s\hat{j} + z_s\hat{k}\right] - \frac{\mu}{r_{42}^3}\vec{r}_{42}\left[(x_s+1-\mu)\hat{i} + y_s\hat{j} + z_s\hat{k}\right]$$

$$-\frac{\mu_3}{r_{43}^3}\left[(x_s-x_a)\hat{i} + (y_s-y_a)\hat{j} + (z_s-z_a)\hat{k}\right] \tag{2.21}$$

Finally, relating Equations (2.10) and (2.21) with each other and separating the $\hat{i}$, $\hat{j}$, $\hat{k}$ components yields three non-linear differential equations for the spacecraft

$$\frac{d^2x_s}{dt^2} - 2\frac{dy_s}{dt} - x_s = -\frac{(1-\mu)(x_s-\mu)}{r_{41}^3} - \frac{\mu(x_s+1-\mu)}{r_{42}^3} - \frac{\mu_3(x_s-x_a)}{r_{43}^3} \tag{2.22}$$

$$\frac{d^2y_s}{dt^2} + 2\frac{dx_s}{dt} - y_s = -\frac{(1-\mu)y_s}{r_{41}^3} - \frac{\mu y_s}{r_{42}^3} - \frac{\mu_3(y_s-y_a)}{r_{43}^3} \tag{2.23}$$

$$\frac{d^2z_s}{dt^2} = -\frac{(1-\mu)z_s}{r_{41}^3} - \frac{\mu z_s}{r_{42}^3} - \frac{\mu_3(z_s-z_a)}{r_{43}^3} \tag{2.24}$$

Equations (2.22) – (2.24) show the governing equations of motion for the spacecraft in three dimensions. These equations are coupled with the asteroid via the x_a, y_a, and z_a terms. These relations along with Equations (2.13) – (2.15) are the governing equations for the very restricted four-body problem [16]. The parameters for the trade study will be examined in the following chapter.

Chapter 3

Trade Study Parameters

This chapter discusses the various scenarios and metrics of the trade study. These include the libration point orbits, the relative positions of the spacecraft with respect to the asteroid, and both the size and mass of the asteroid itself.

3.1 Libration Point Orbits

The trade study begins by looking at two halo orbits of different sizes; Figures 3.1 and 3.2 show the generated large halo orbit where Figures 3.3 and 3.4 show the small halo orbit. It should be noted that the small halo orbit has a slight discontinuity that is viewable in Figure 3.4; this will be explored in Chapter 4. Both orbits have roughly the same orbital period. Halo orbits of different sizes were chosen over roughly the same orbital period to determine if the size of the given orbit has any effect on the stability or prevalence of impacts. The initial conditions for each starting position in the orbits are supplied in Table 3.1 for the large and small halo orbits. Subsequent starting positions were obtained from the original initial conditions by integrating over a very small time step.

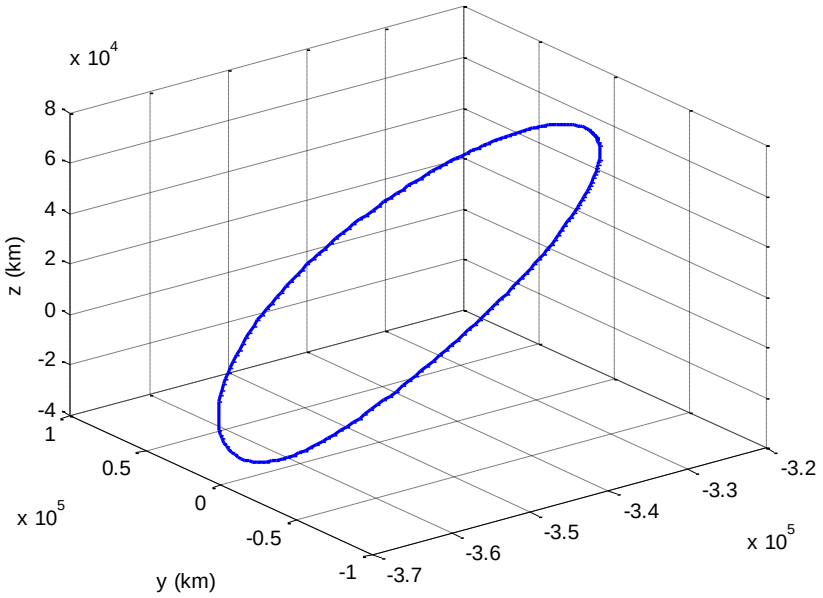

Figure 3.1. Large halo orbit generated from initial conditions

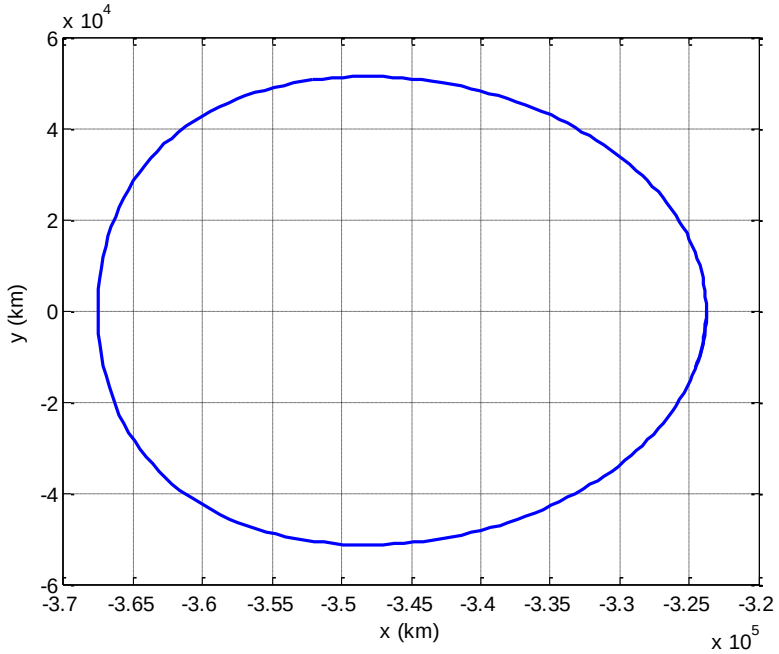

Figure 3.2. Large halo orbit generated from initial conditions in x-y plane

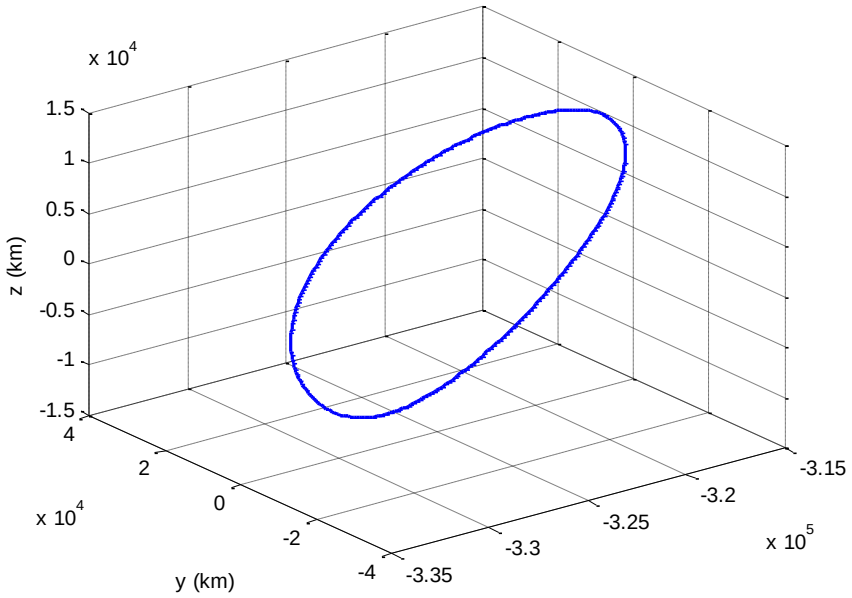

Figure 3.3. Small halo orbit generated from initial conditions

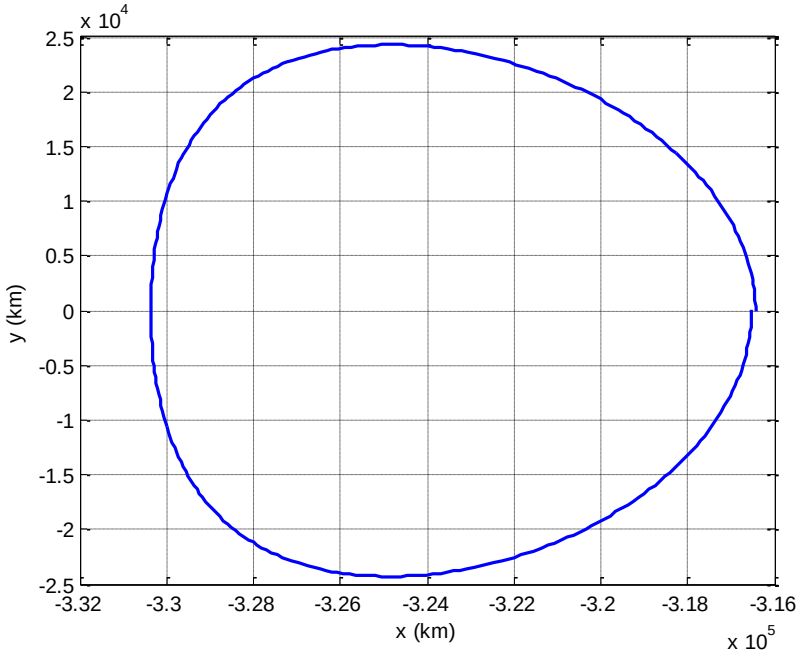

Figure 3.4. Small halo orbit generated from initial conditions in x-y plane

Table 3.1. Initial conditions for halo orbits (μ = 0.01215058162343)

	Large Halo Orbit (DU)	***Small Halo Orbit (DU)***
x	-0.84225833074	-0.823445341829
y	0	0
z	0.163024589129	0.030939510780
$\dot{x}$	0	0
$\dot{y}$	-0.263218103238	-0.140698846709
$\dot{z}$	0	0

As can be seen from Table 3.2, the initial ranges are listed from the spacecraft to the center of the asteroid. The initial range is defined as the initial separation distance between the spacecraft and the center of the asteroid at the beginning of the orbit. These ranges were chosen for each sized halo orbit due to the effects that occur through those initial distances. The specific numbers are arbitrary as there would not be much difference between 506 meters versus 500 meters. The differences in the initial ranges between the large and small halo orbits are explained in Chapter 4.

Table 3.2. Initial ranges between spacecraft and asteroid

Case	*Initial Separation Distance (m)*
1	910[†]
2	811[‡]
3	506
4	303
5	270[§]
6	202
7	172
8	151
9	101
10	71
11	50
12	38

Lastly, whether the spacecraft is trailing or leading the asteroid will be examined. This was done to see if that has any effect on the stability or impacts.

[†] Range conducted for the two revolution case only
[‡] Range conducted for small halo orbit case only
[§] Range conducted for small halo orbit case only

3.2 The Asteroid

The size and masses of the asteroids were chosen based on NASA's mission documents for the Asteroid Redirect Mission.[**] The asteroid masses and diameters seen in Table 3.3 were chosen within the range of mission parameters. It will be assumed that the asteroids are spherical objects with diameters of the upper bound of the values seen in Table 3.3. The diameters were determined based on the densities of granite and pumice.

Table 3.3. Asteroid masses being examined in all cases[††]

Mass (tons)	Diameter (m)
25	3 – 4
75	4 – 7
130	5 – 10
200	5.5 – 13

These diameters will be used in determining whether or not the spacecraft collides with the asteroid. If the minimum distance between the spacecraft and the asteroid drops below the radius of the asteroid, then it is assumed an impact has occurred. Near-misses will also be noted as the spacecraft passing within 25 meters of the surface of the asteroid. While not directly impacting the asteroid, the spacecraft will be too close based on numerical accuracy. Anything beyond the 25–meter range will be considered safe formation flying. The results of these scenarios are examined in Chapter 4.

[**] http://www.nasa.gov/feature/asteroid-redirect-mission-documents March 30, 2016
[††] http://www.nasa.gov/sites/default/files/files/Chodas-ARRM-Obs-Status-Dec-2013.pptx.pdf April 3, 2016

Chapter 4

Results and Discussion

This chapter focuses on the results based off the scenarios elaborated upon in the previous chapter. The first test case involves the large halo orbit previously shown in Figures 3.1 and 3.2. Within this orbit, several cases are examined at different initial conditions where the spacecraft trails the asteroid initially over several different ranges. Then the spacecraft is positioned so that it leads the asteroid over the same initial ranges. Furthermore, the dynamics of the situations are examined over both one and two revolutions of the orbit. The second case imposes a similar set-up except the halo orbit is smaller (Figures 3.3 and 3.4). The same constraints are applied with different starting ranges between the two objects for both the spacecraft trailing and leading the asteroid. It should also be noted that the plots for the relative positions and velocities occur in the $\hat{i} - \hat{j} - \hat{k}$ frame where the coordinate directions on the plots are noted by *X*, *Y*, and *Z*, respectively.

4.1 Large Halo Orbit

The largest initial separation distance between the spacecraft and asteroid are examined first with subsequent distances becoming smaller. The orbit propagation is shown over one revolution (12.166 days) first, then followed by two complete revolutions. In the latter case, stability over the long duration will be considered the examining factor. Some plots that are examined include range between the spacecraft and asteroid, relative velocities and positions in different coordinate directions and planes, and the difference in range between massless asteroids

from the asteroid with mass. The latter plot is useful to establish a baseline with the massless asteroid to show the effect of the gravitational perturbations to the case where the spacecraft has no gravitational influences (other than from the Earth and Moon).

4.1.1 Spacecraft Trailing Asteroid Over One Revolution of Large Halo Orbit

The first initial separation range being examined is at 506 meters. At this initial positioning, the gravitational perturbations have little effect over the one revolution duration. The range is defined as the magnitude of the difference in the position vectors from the spacecraft to the asteroid; this relative position is defined in Figure 2.3. From Figure 4.1, five masses are shown; the zero ton–mass is the baseline case where the spacecraft is effectively orbiting by itself. From this point onward, the baseline case will refer to the zero mass asteroid.

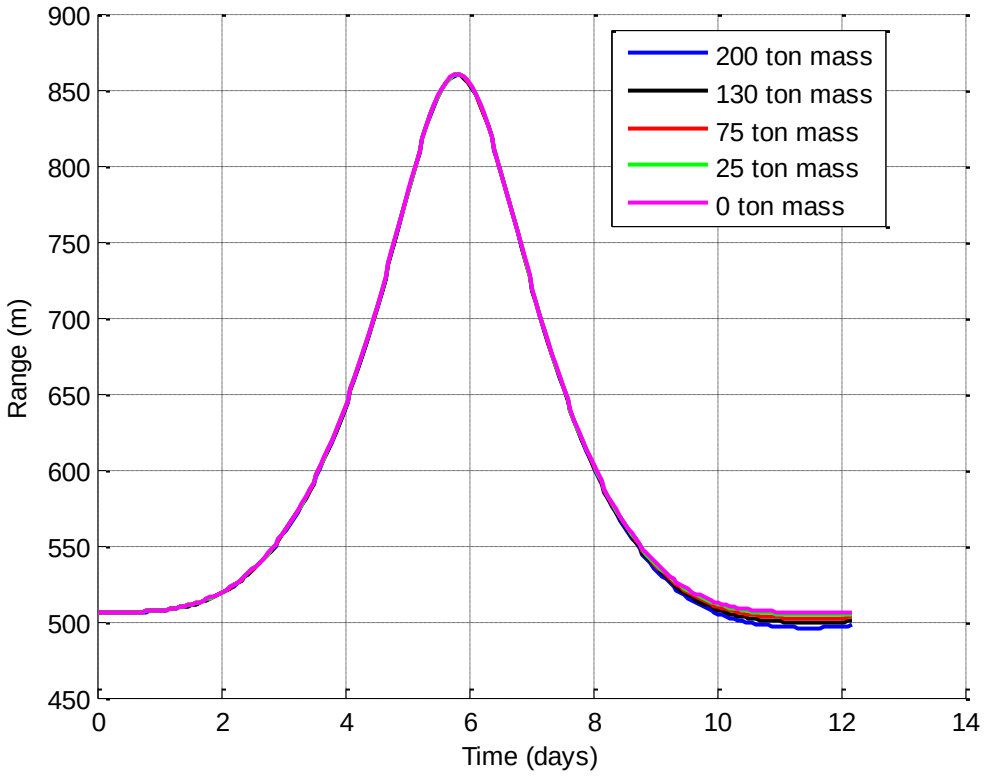

Figure 4.1. Range between spacecraft and asteroid with 506–m initial separation

The other cases include an asteroid with mass so it can be seen how the presence of gravity alters the range between the spacecraft and the asteroid. Figure 4.1 shows that the increase in the mass of the asteroid at this range has very little effect on the spacecraft's trajectory.

The deviation from the baseline flight path can be more easily demonstrated from Figure 4.2. This figure was generated by subtracting the baseline range vector (the range vector from the 0–ton–mass) from the range vector that had a spacecraft formation flying with an asteroid that has mass. The resulting data shows the difference in range from a spacecraft with no accompanying mass with a spacecraft with an additional gravitational source.

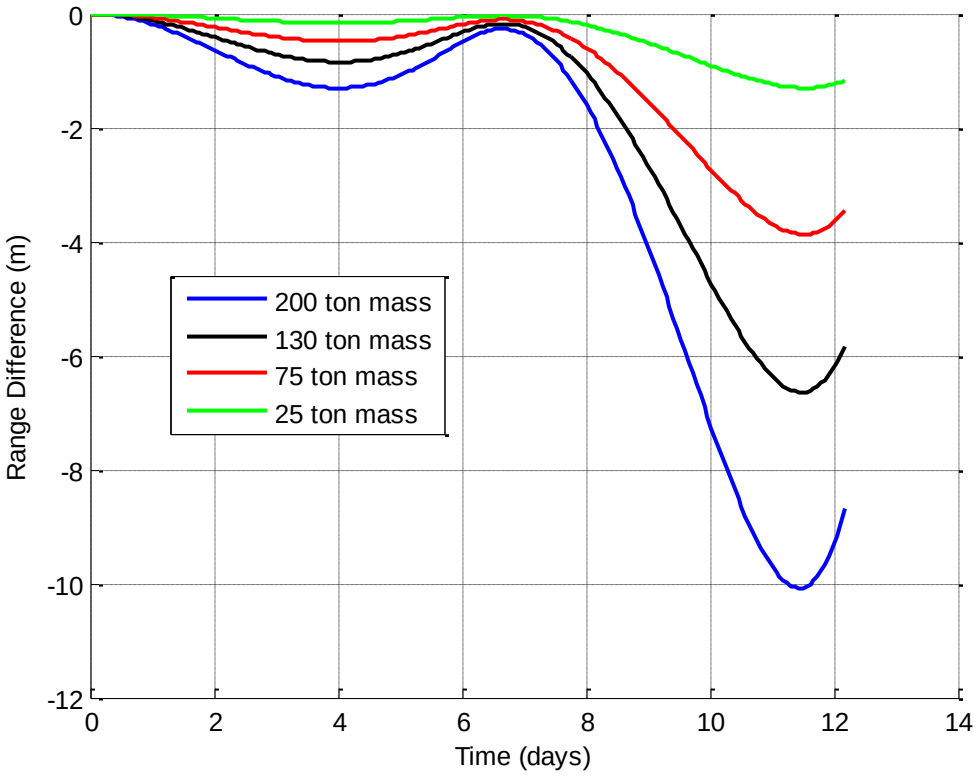

Figure 4.2. Range difference between spacecraft and massless asteroid from asteroids of varying mass with initial 506–m separation

At this initial range, the spacecraft formation flying with an asteroid of mass does not deviate much from baseline case. The spacecraft barely deviates from the flight path even in the 200–ton–mass case, wherein the maximum deviation is slightly over 10– meters. To gain a better understanding of how the spacecraft moves relative to the asteroid, the relative position vector of the spacecraft and asteroid (as defined in Figure 2.3) was plotted in the $\hat{i}-\hat{j}$, $\hat{i}-\hat{k}$, and $\hat{j}-\hat{k}$ planes (Figure 2.1), in addition to the $\hat{i}-\hat{j}-\hat{k}$ space. The resulting plots as seen in Figures 4.3 and 4.4 for the baseline case and the 200–ton–mass case respectively show minimal differences between both figures. As can be seen from the 200–ton–mass, the spacecraft slightly overshoots its orbit upon returning to the starting position.

From the previously discussed figures, it can be concluded that the spacecraft's orbit regardless of the mass it is flying alongside, has negligible effect on the trajectory. Over one revolution, the orbit is stable.

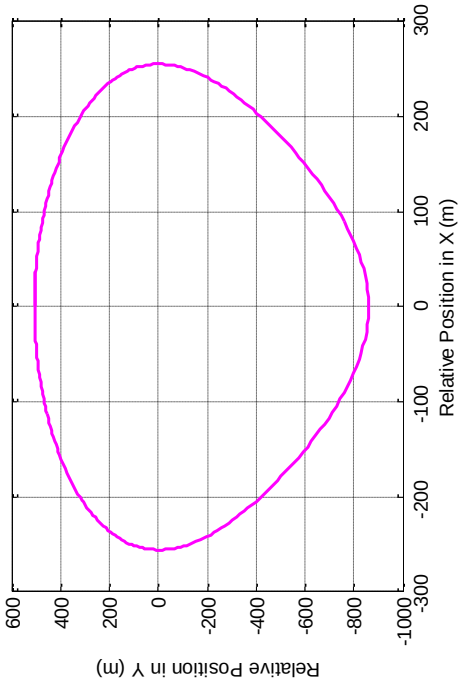

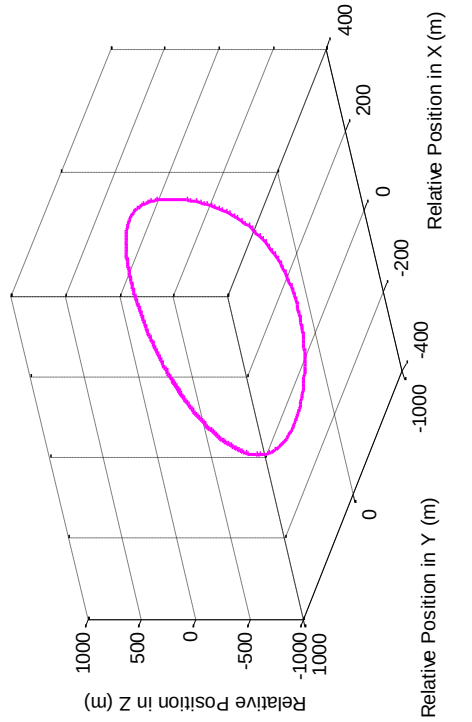

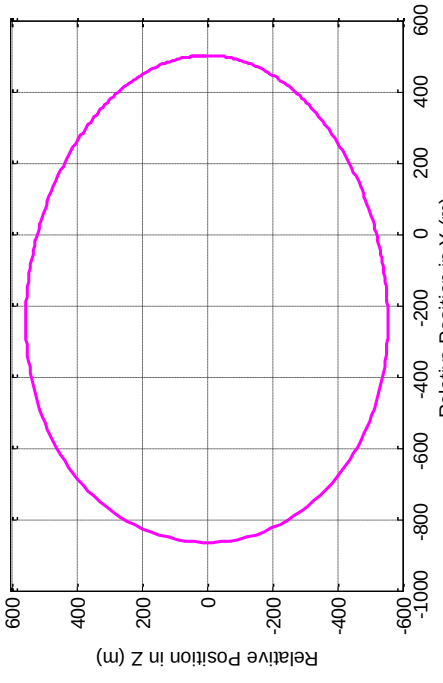

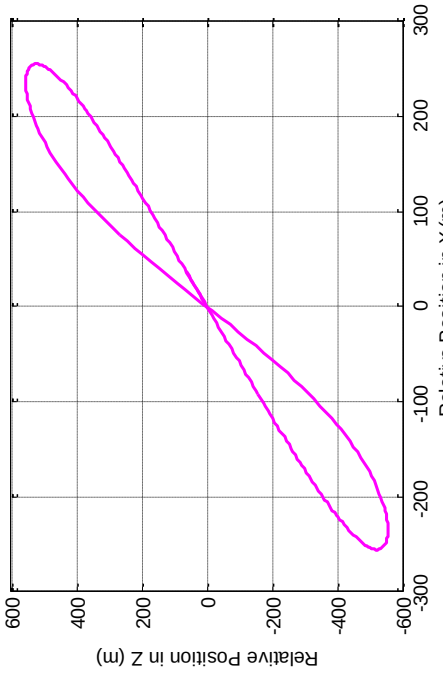

Figure 4.3. The spacecraft's relative position vector around the 0–ton asteroid at an initial distance of 506– m

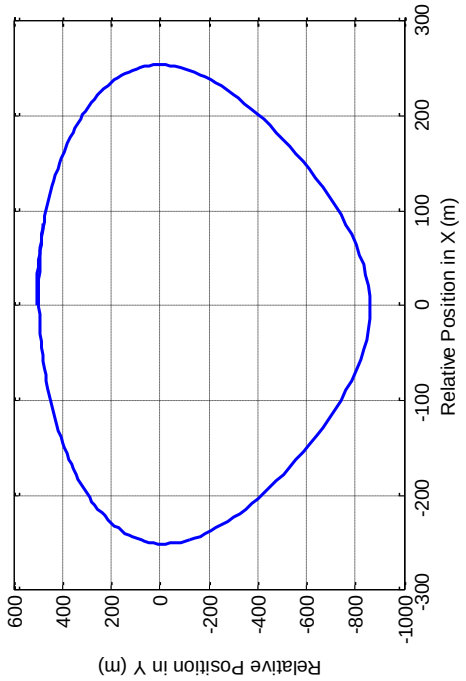

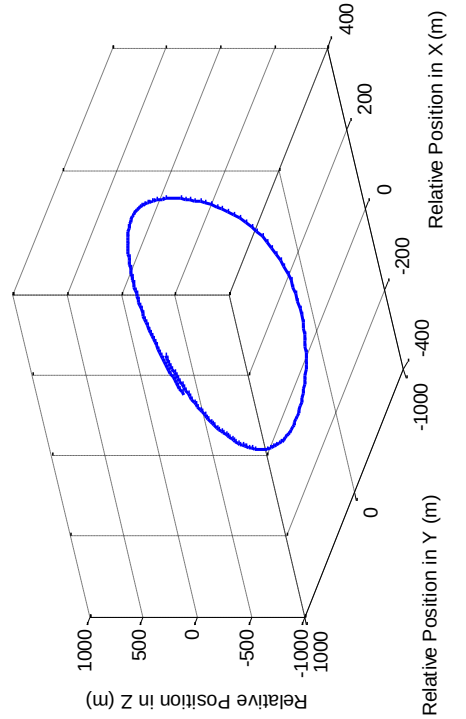

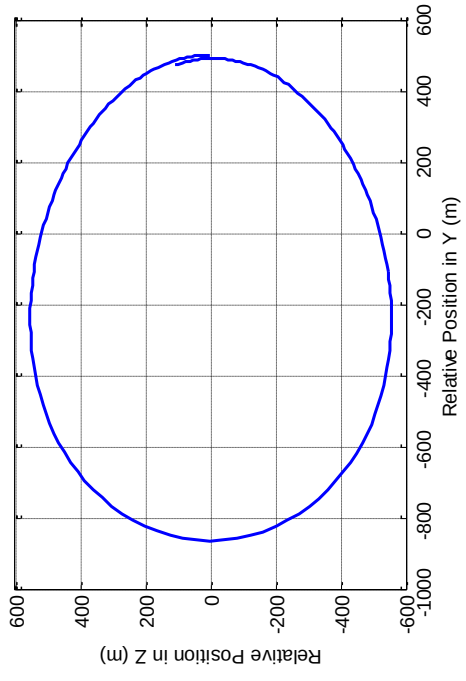

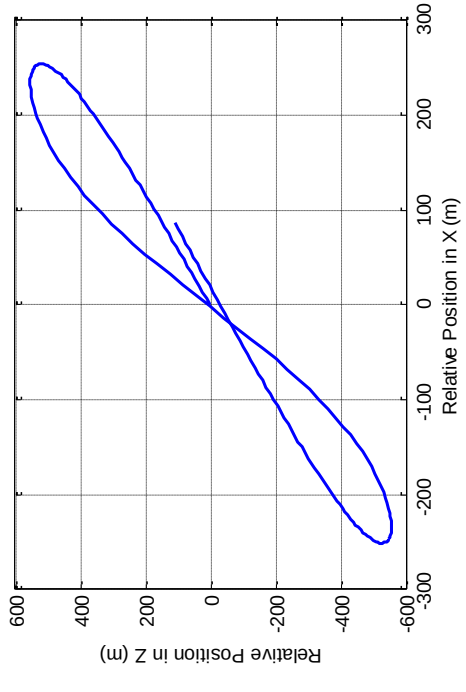

Figure 4.4. The spacecraft's relative position vector around the 200–ton asteroid at an initial distance of 506– m

Next, the 303–meter initial range between the spacecraft and asteroid is analyzed. At about 200 meters closer than the previous case, some additional gravitational effects can be seen. Figure 4.5 again shows the range as previously defined between the spacecraft and the asteroid for each of the masses. As the mass of the asteroid increases, more deviation from the baseline case is starting to occur. To gain insight as to what is starting to occur, examining Figure 4.6 shows the range differences between the baseline ranges and the ranges with an asteroid of mass; when the spacecraft orbits with asteroids of heavier mass, the spacecraft is pulled closer to the asteroid before being sent on a trajectory farther from the asteroid. Comparing Figure 4.6 to its counterpart from the first initial separation distance in Figure 4.2 shows that the deviation has increased.

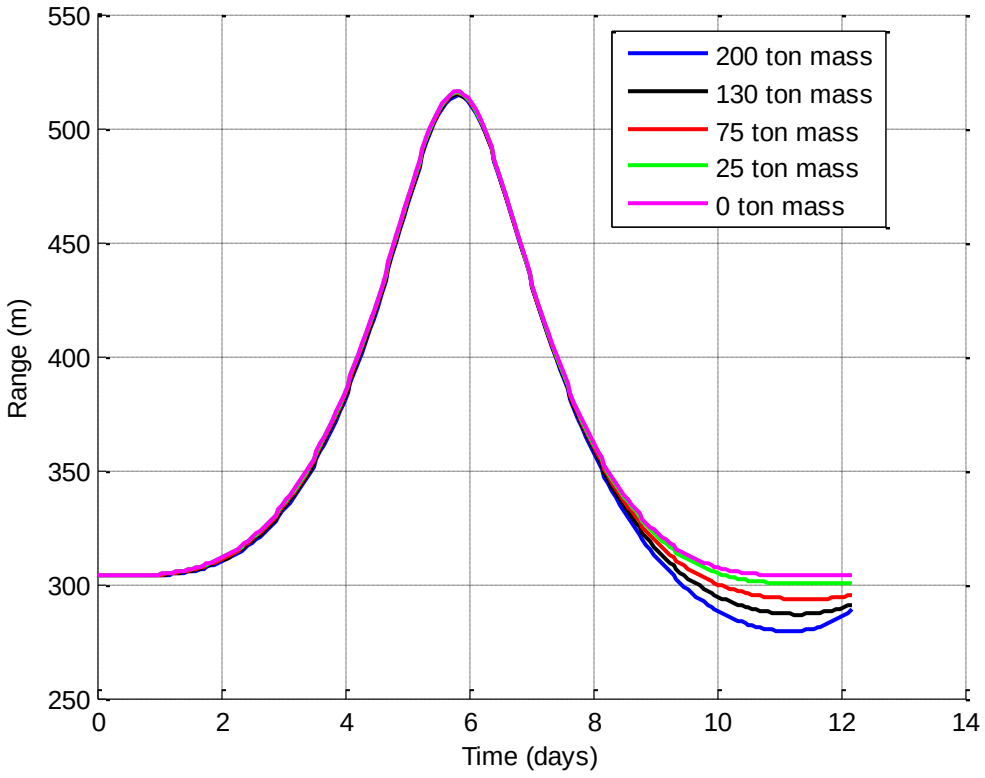

Figure 4.5. Range between spacecraft and asteroid with 303–m initial separation

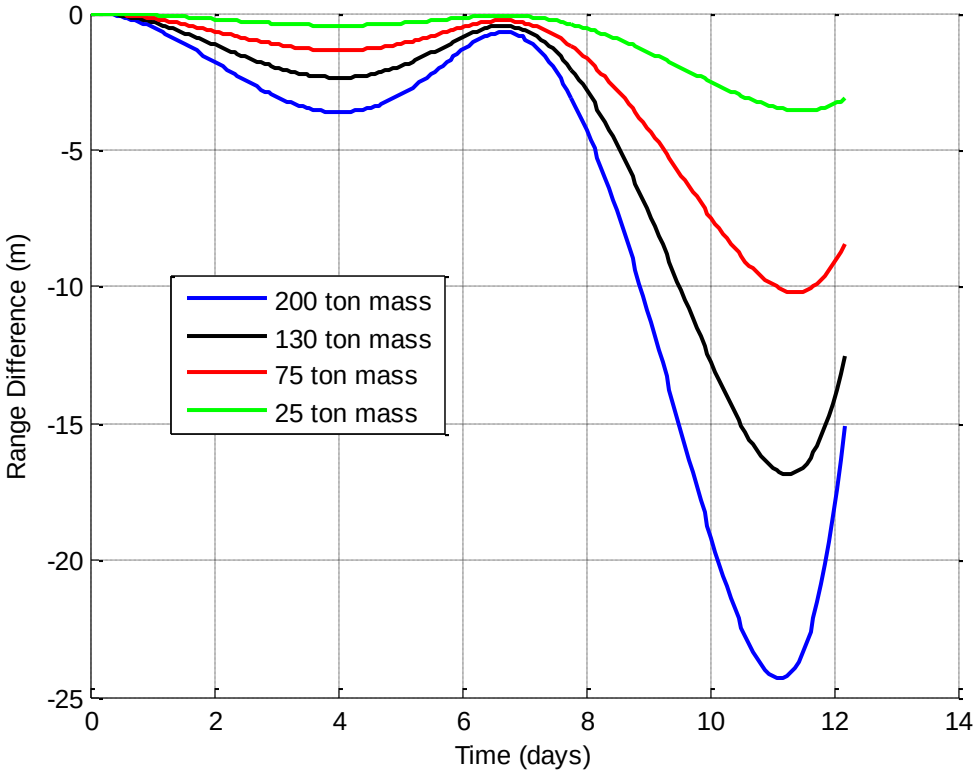

Figure 4.6. Range difference between spacecraft and massless asteroid from asteroids of varying mass with initial 303–m separation

As the deviation from the baseline case is still relatively small, the position of the spacecraft relative to the asteroid will be looked at for the 75–, 130–, and 200–ton–masses only. Figures 4.7–4.10 show the relative position vector between both objects in different planes. From all the planes, it can be seen that the spacecraft as the mass of the asteroid increases begins to drift from the asteroid. To get a sense of the magnitudes of these drifts, the relative position vector of the baseline case is subtracted from the relative position vectors with asteroids of mass. This shows how much the spacecraft drifts when formation flying with asteroids compared to when the spacecraft is orbiting alone as in the baseline case.

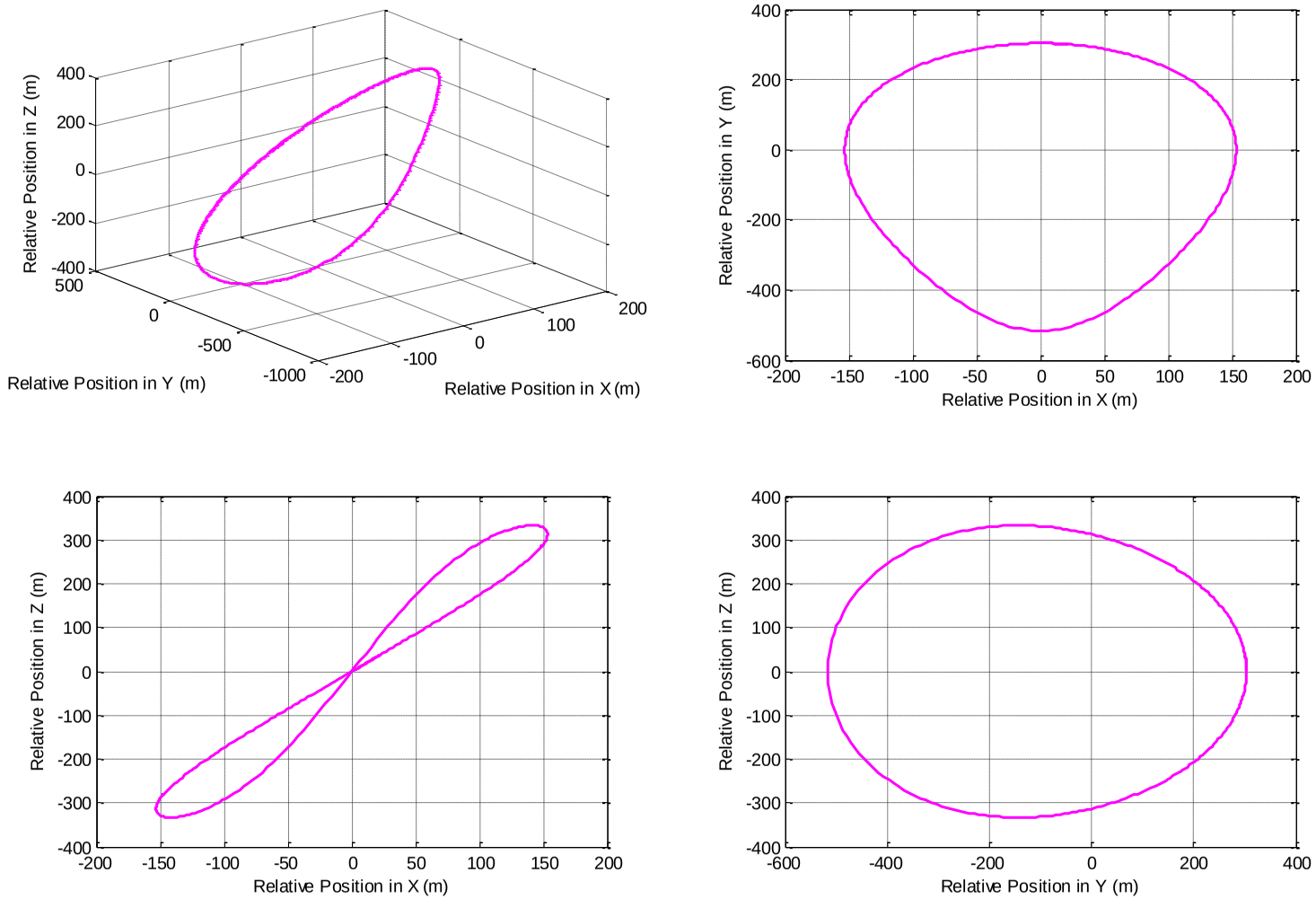

Figure 4.7. The spacecraft's relative position vector around the 0–ton asteroid at an initial distance of 303– m

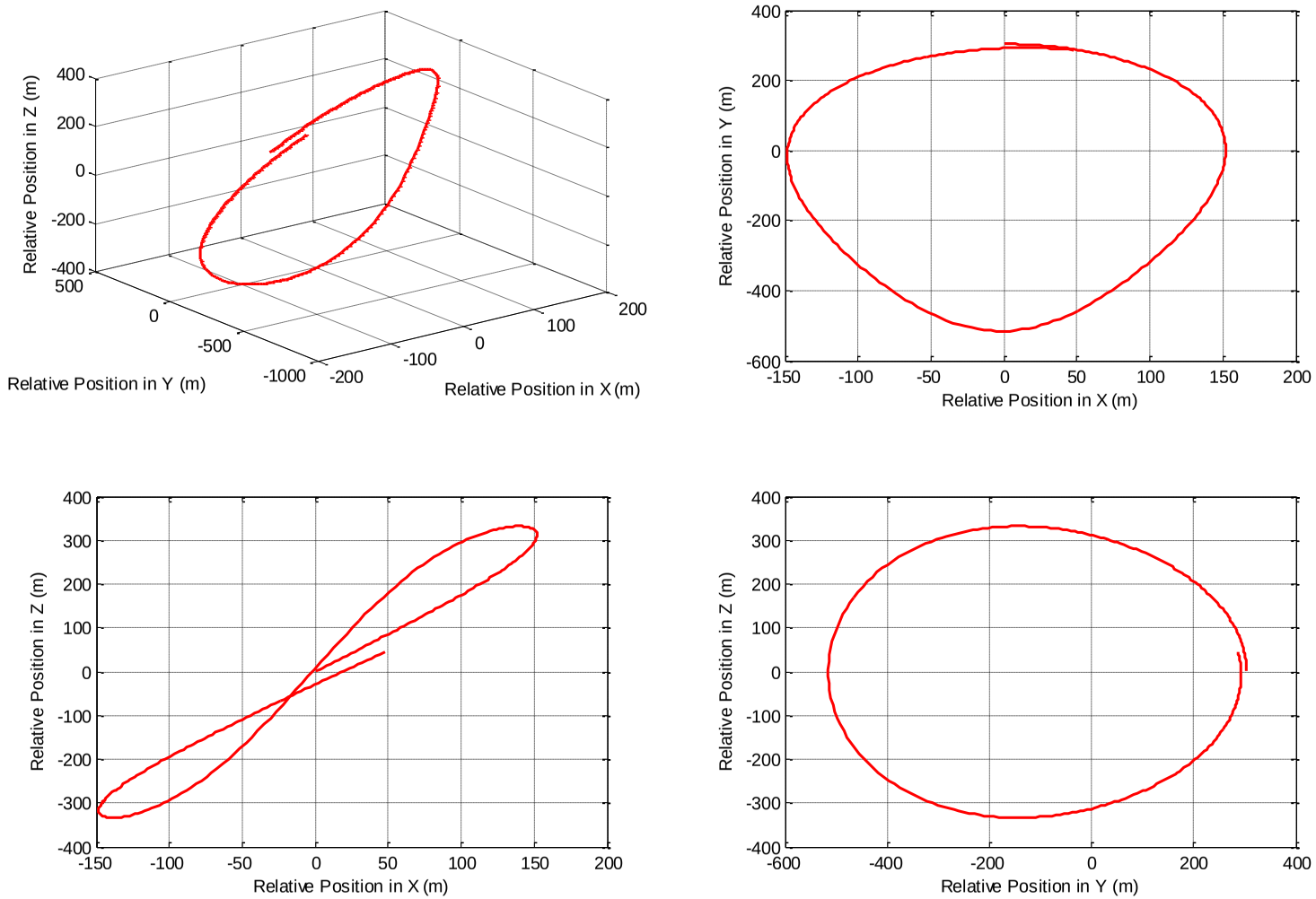

Figure 4.8. The spacecraft's relative position vector around the 75–ton asteroid at an initial distance of 303– m

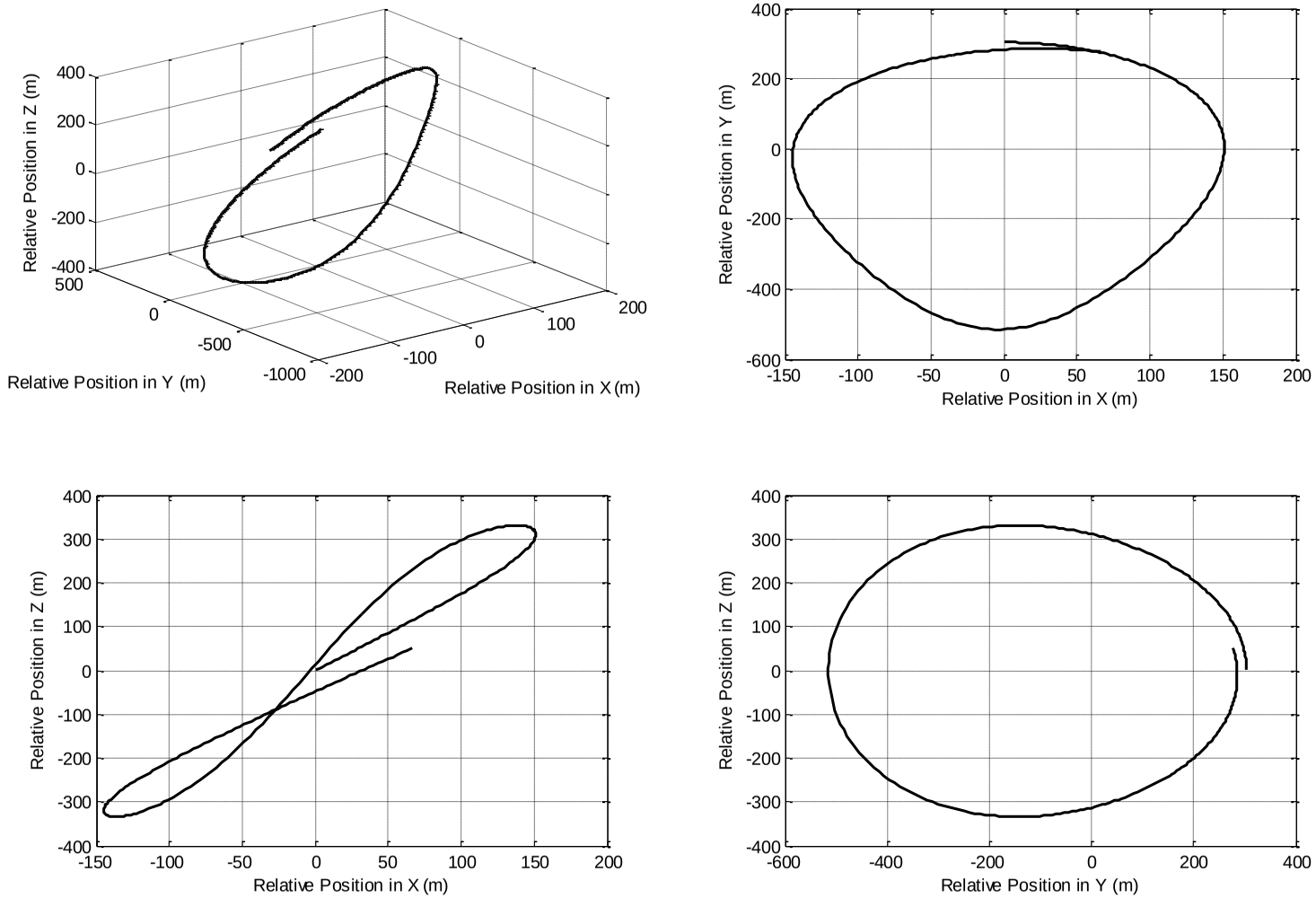

Figure 4.9. The spacecraft's relative position vector around the 130–ton asteroid at an initial distance of 303– m

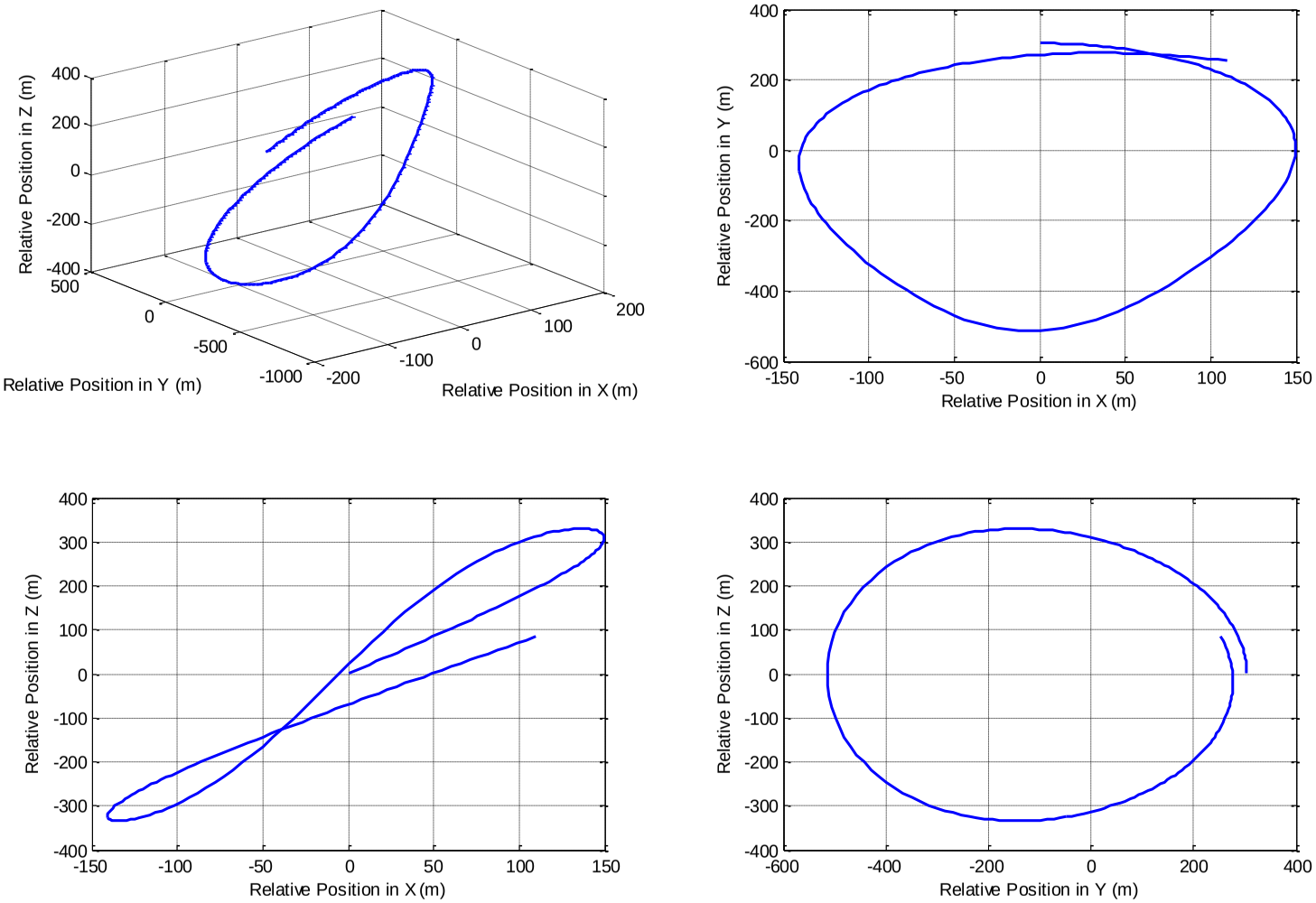

Figure 4.10. The spacecraft's relative position vector around the 200–ton asteroid at an initial distance of 303–m

Figure 4.11 shows these results in each coordinate direction over time; the $\delta X, \delta Y,$ and δZ terms are defined as the difference between the spacecraft and asteroid's position vectors in each coordinate direction. It becomes clear that, in the $\hat{i}$ and $\hat{k}$ directions, the spacecraft moves further away compared to the baseline case. However in the $\hat{j}$ direction, the spacecraft moves closer. Examining the various planes in Figures 4.7– 4.10 shows these trends. In the $\hat{i} - \hat{j}$ plane, the spacecraft is further in the positive $\hat{i}$ direction than it would have been without an asteroid and a bit lower in the $\hat{j}$ direction. The $\hat{i} - \hat{k}$ plane shows the relative positon grow in each direction and the $\hat{j} - \hat{k}$ plane shows the relative position closer in the $\hat{j}$ direction but further apart in the $\hat{k}$ direction. The net effect as seen in the ranges of Figure 4.4 is that the spacecraft initially moves closer to the asteroid but, instead of heading for an impact, the spacecraft is propelled away. It can also be seen especially with the larger masses that the spacecraft is overshooting its initial orbital starting position in the $\hat{i} - \hat{j}$ and $\hat{j} - \hat{k}$ planes. Even at this initial distance, the orbit is still relatively stable over the duration of the period.

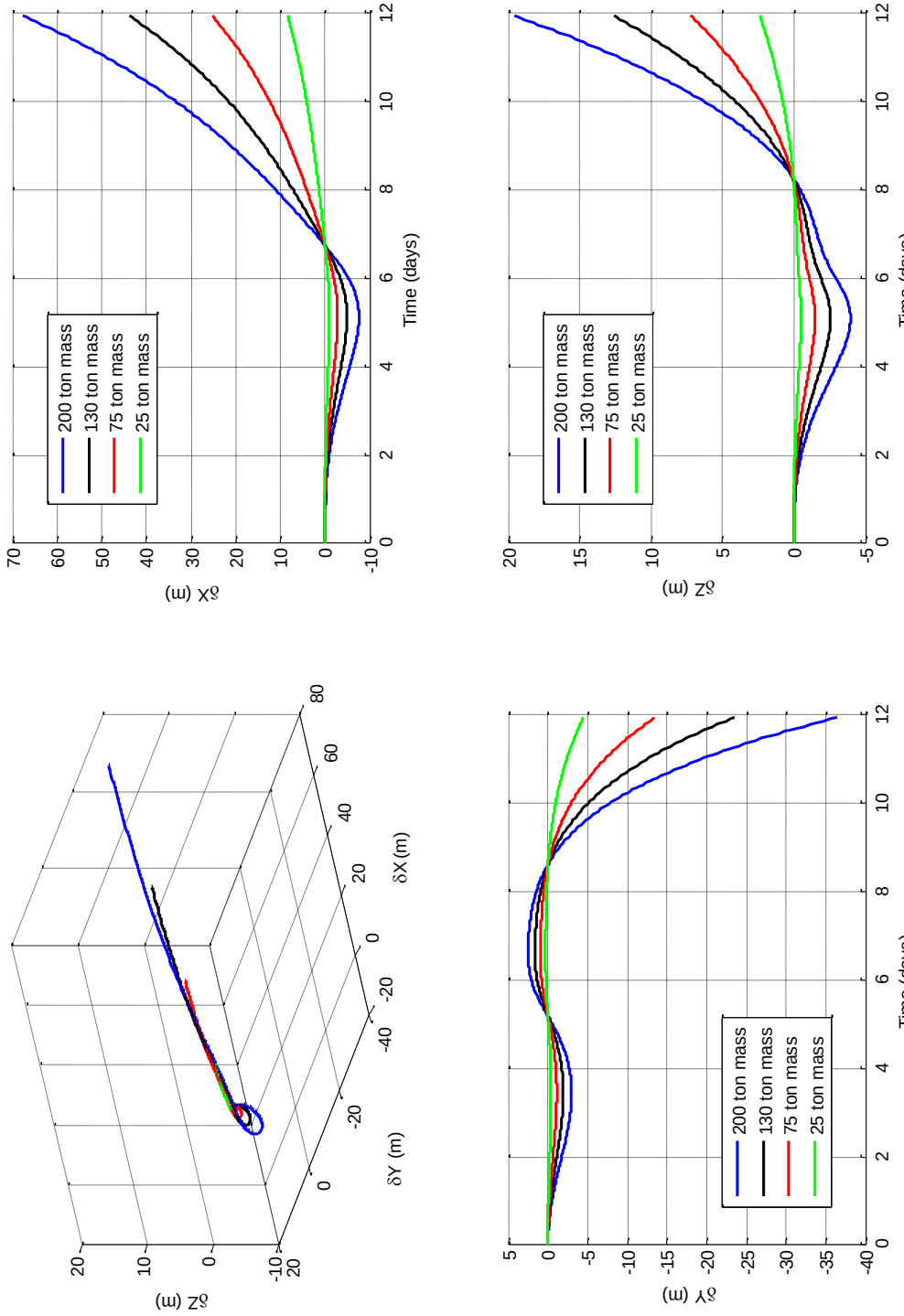

Figure 4.11. Relative position vector deviation from the baseline case at 303–m

At an initial range of 202– meters, the spacecraft still is not impacting the asteroid; the spacecraft again moves closer towards the end of the orbit but, as the orbit completes, the spacecraft has roughly returned to the same range as the base case for all masses except the 200–ton–mass. As shown in Figure 4.12, the spacecraft counterintuitively is moving further from the higher massed objects rather than closer.

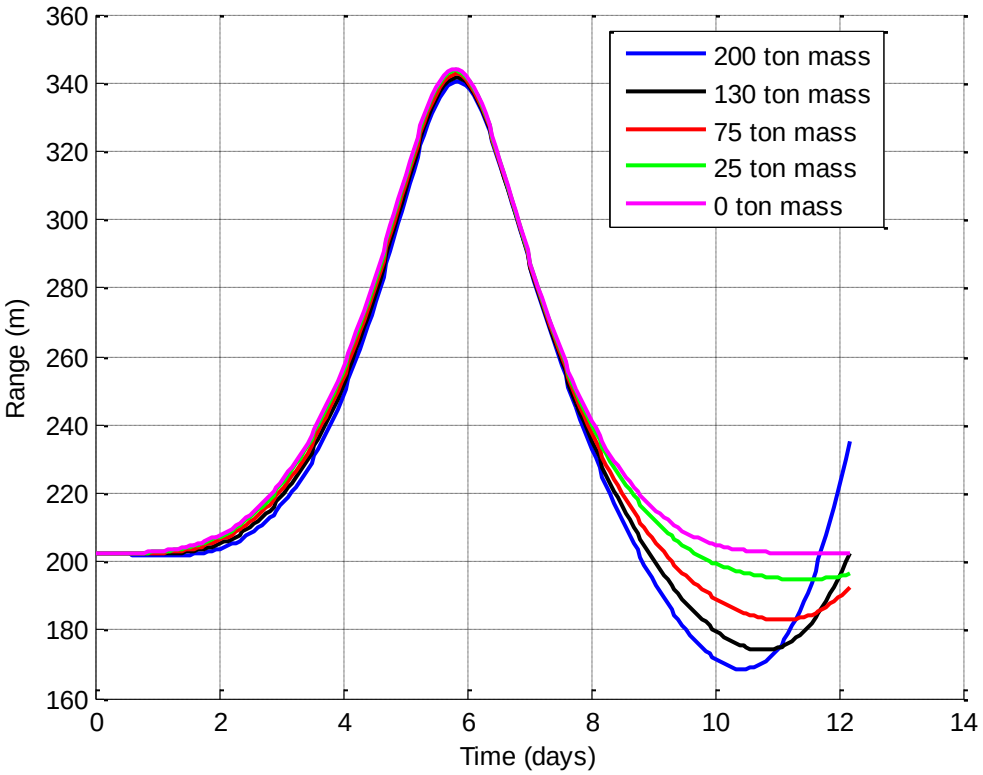

Figure 4.12. Range between spacecraft and asteroid with 202–m initial separation

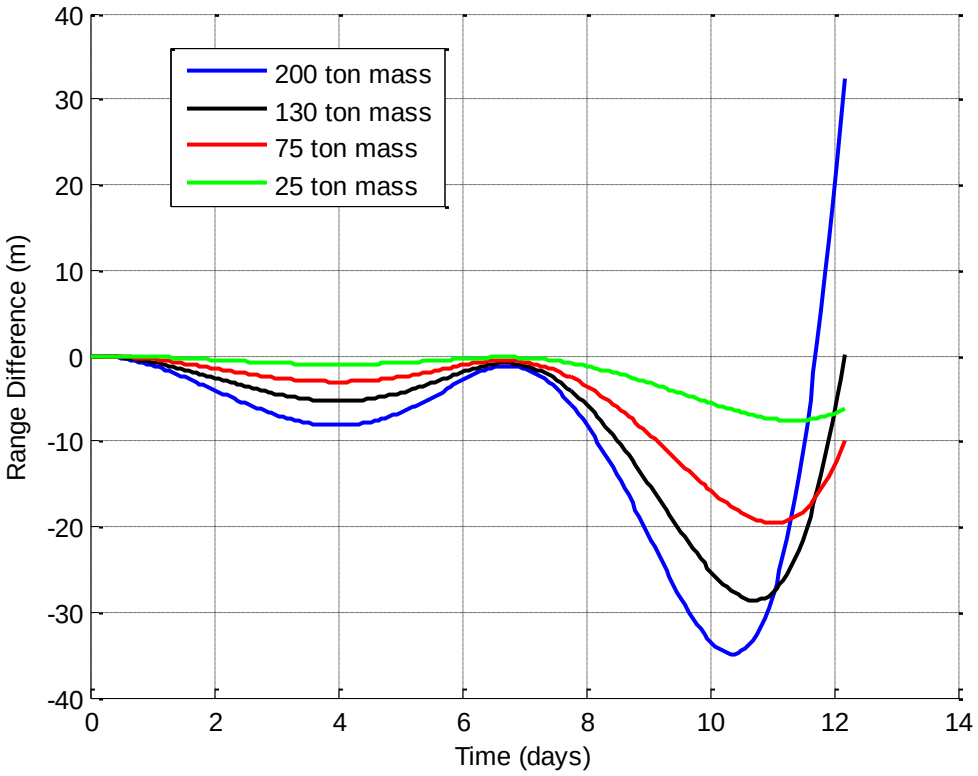

Figure 4.13. Range difference between spacecraft and massless asteroid from asteroids of varying mass with initial 202–m separation

Again looking at the differences in the range compared to the baseline range, Figure 4.13 shows how the spacecraft is ultimately moving away from the asteroid towards the end of the orbit. There are two points at which the spacecraft moves closer to the asteroid; the first is a relatively small deviation that ends with the spacecraft roughly returning to the zero a little over 6 days into the orbit. At this point, the spacecraft moves much closer to the asteroid without hitting it and again heads away. However, the motion back away from the asteroid is much faster than the previous movement earlier in the orbit. The– 200–ton–mass clearly begins to sharply increase in range from the baseline ranges with the other masses looking to do the same if the orbit were to continue.

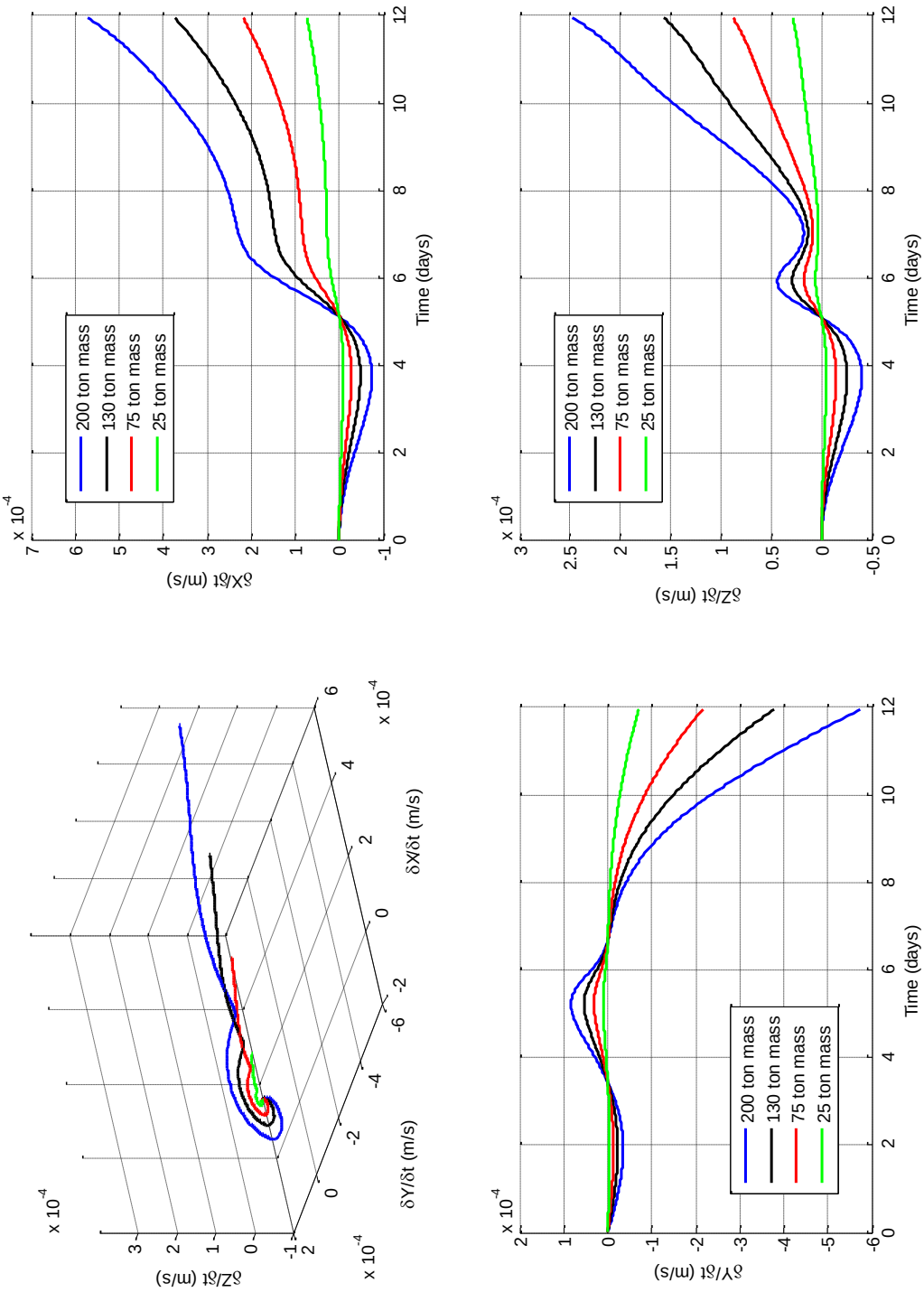

Figure 4.14. Relative velocity vector deviation from the baseline case at 202–m

Looking at the difference in the relative velocity vectors of the asteroid and the spacecraft from the baseline case (difference defined by the $\delta X/\delta t, \delta Y/\delta t,$ and $\delta Z/\delta t$ terms in each coordinate direction), Figure 4.14 shows a general increase in speed in the $\hat{i}$ and $\hat{k}$ directions and a decrease in speed in the $\hat{j}$ direction. As the spacecraft moves closer to the asteroid towards the end of the orbit, the spacecraft has a net increase in speed that propels it away from the asteroid instead of impact. The speed increase is directly related to the mass of the asteroid; the higher the mass, the greater the change in velocity when compared to the baseline case.

The relative position vector shows the continuing trend. Figures 4.15– 4.19 show how the spacecraft formation flying with the asteroid of 25–tons still does not have too much of a change in trajectory. However as the mass increases, the effects are starting to become pronounced. The increase in speed in a non-collision course with the asteroid is causing the spacecraft to propel further away the closer the spacecraft initially starts relative to the asteroid. Though the relative range from the baseline as shown in Figure 4.13 is roughly the same for the 130–ton–mass case, Figure 4.18 clearly shows that the actual position is quite different. Though the range is similar, the spacecraft is clearly in a different position from the baseline.

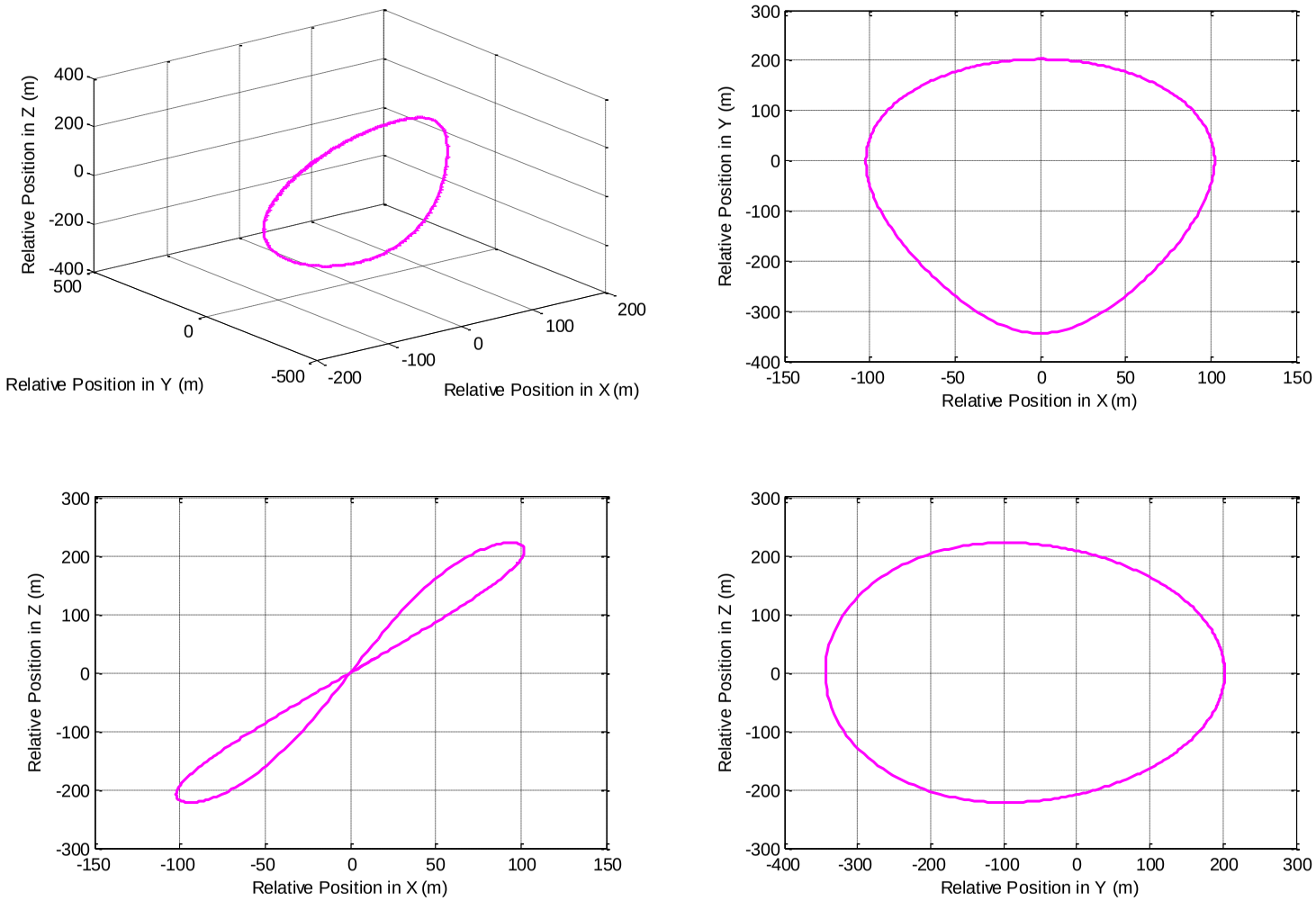

Figure 4.15. The spacecraft's relative position vector around the 0–ton asteroid at an initial distance of 202–m

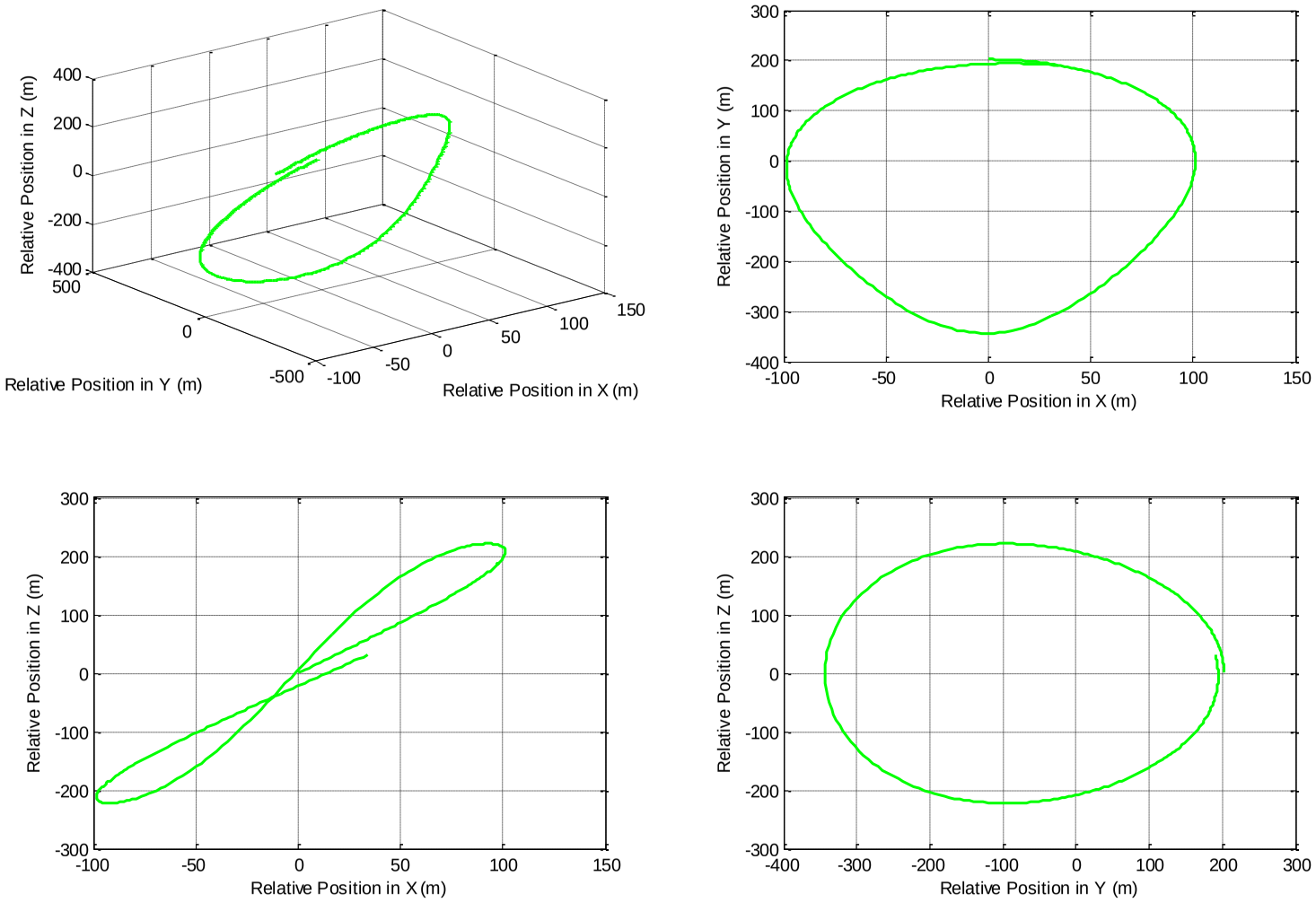

Figure 4.16. The spacecraft's relative position vector around the 25–ton asteroid at an initial distance of 202–m

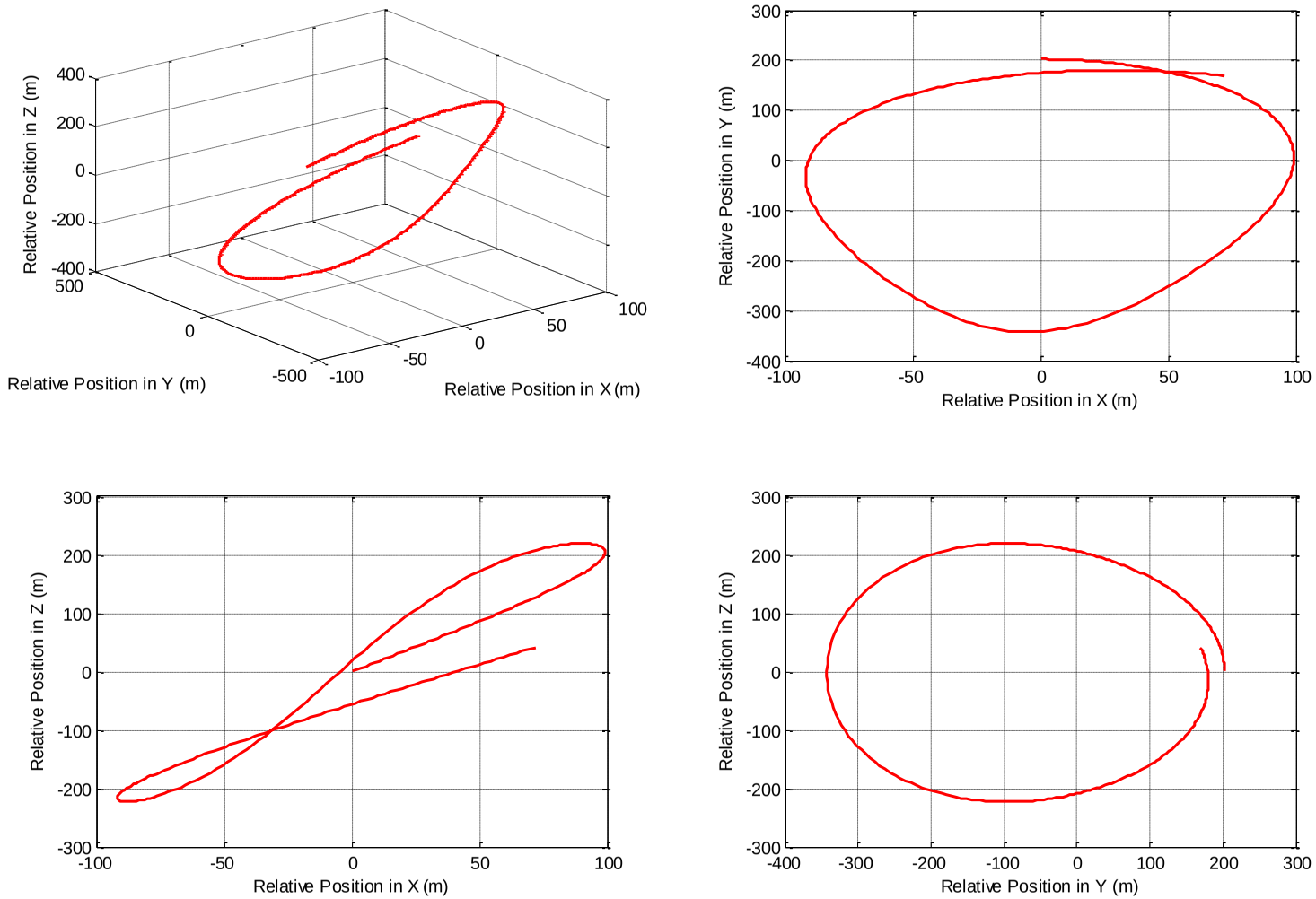

Figure 4.17. The spacecraft's relative position vector around the 75–ton asteroid at an initial distance of 202–m

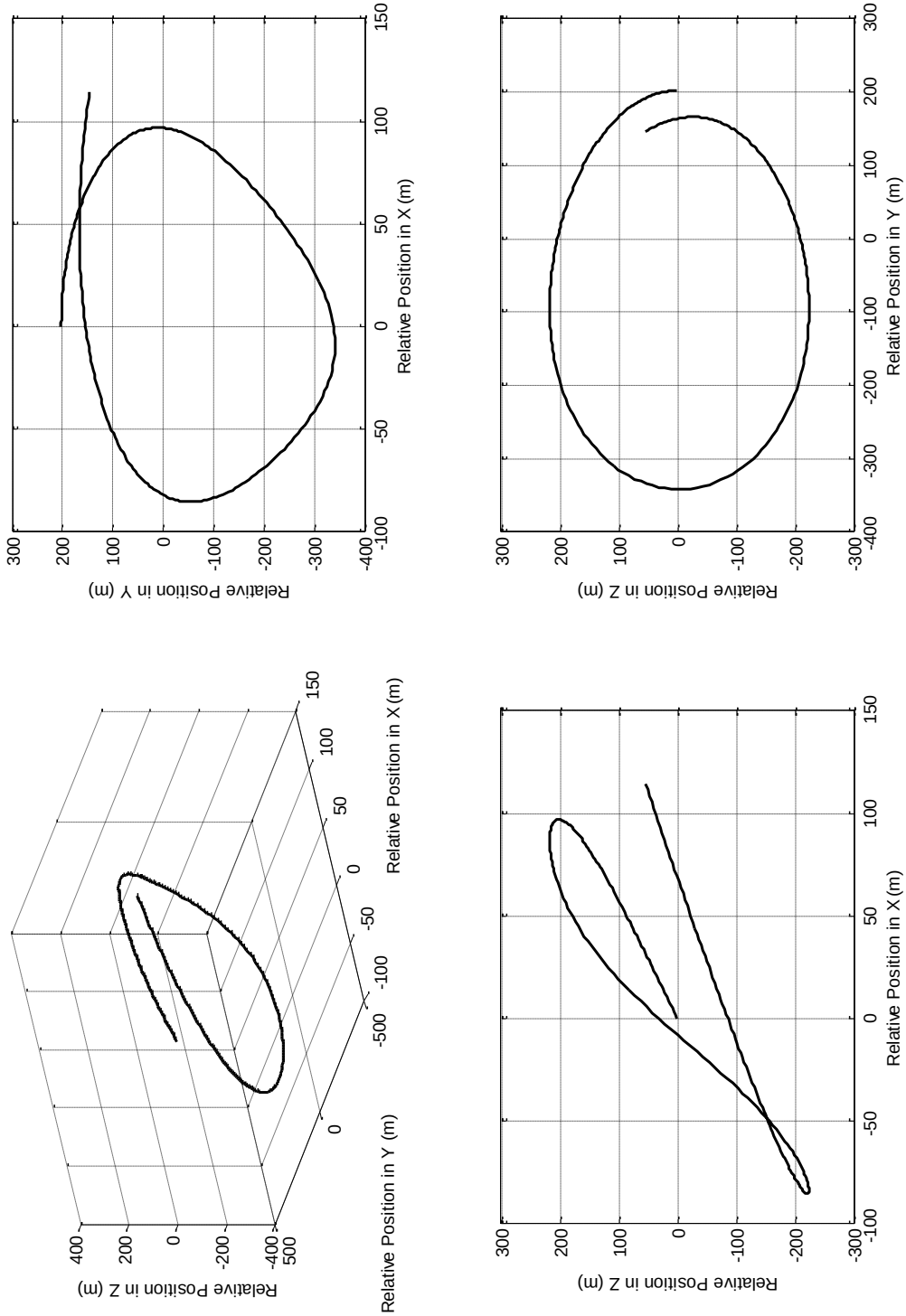

Figure 4.18. The spacecraft's relative position vector around the 130–ton asteroid at an initial distance of 202–m

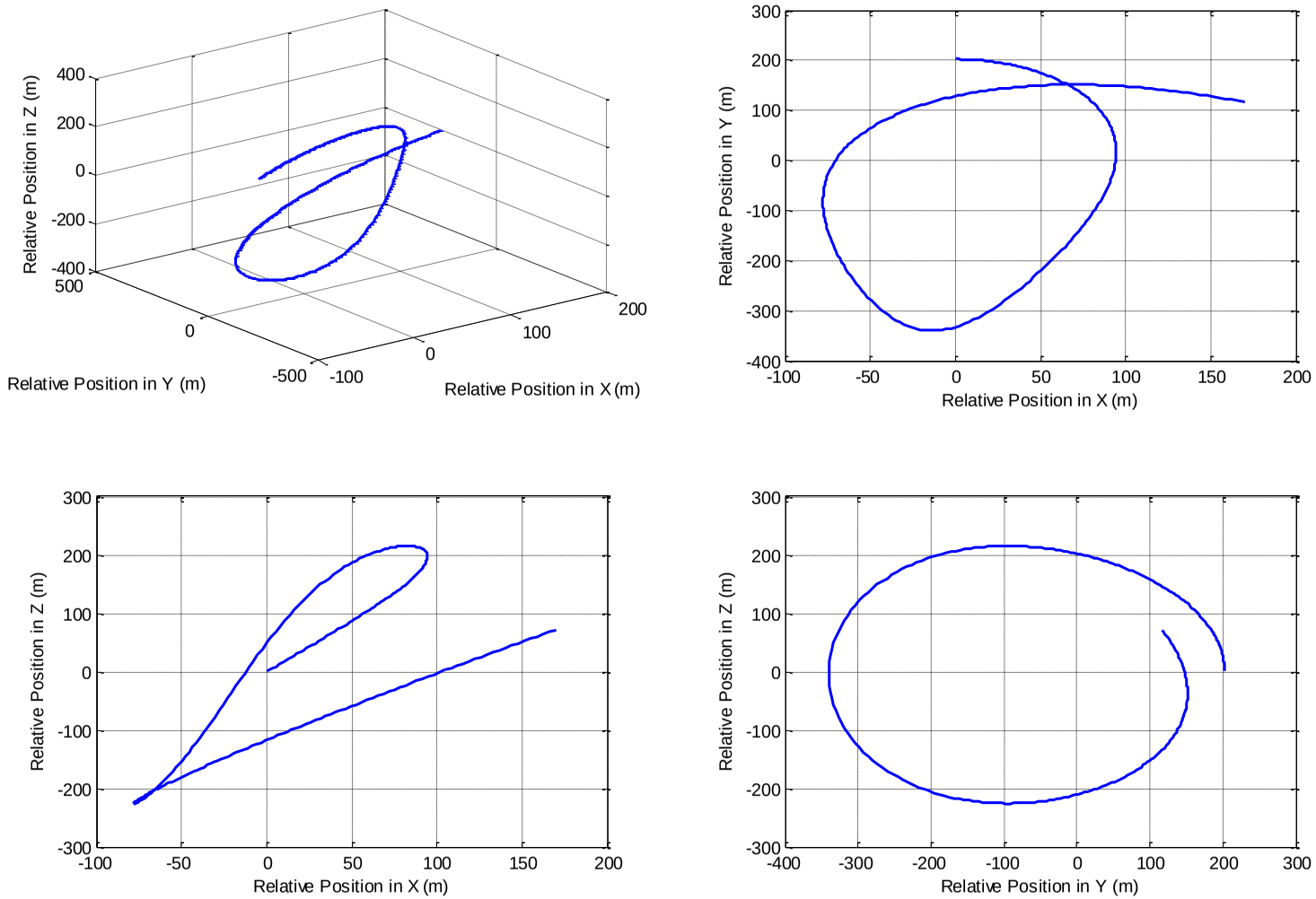

Figure 4.19. The spacecraft's relative position vector around the 200–ton asteroid at an initial distance of 202–m

At 172 and 151 meters respectively, the trend of the asteroid moving away from the asteroid towards the end of the orbit continues. Both Figures 4.20 and 4.21 show how the range between the asteroid and the spacecraft decreases a bit before the 8–day mark and then rapidly continues as the orbit completes. However, the case with the 25–ton–mass is still somewhat stable.

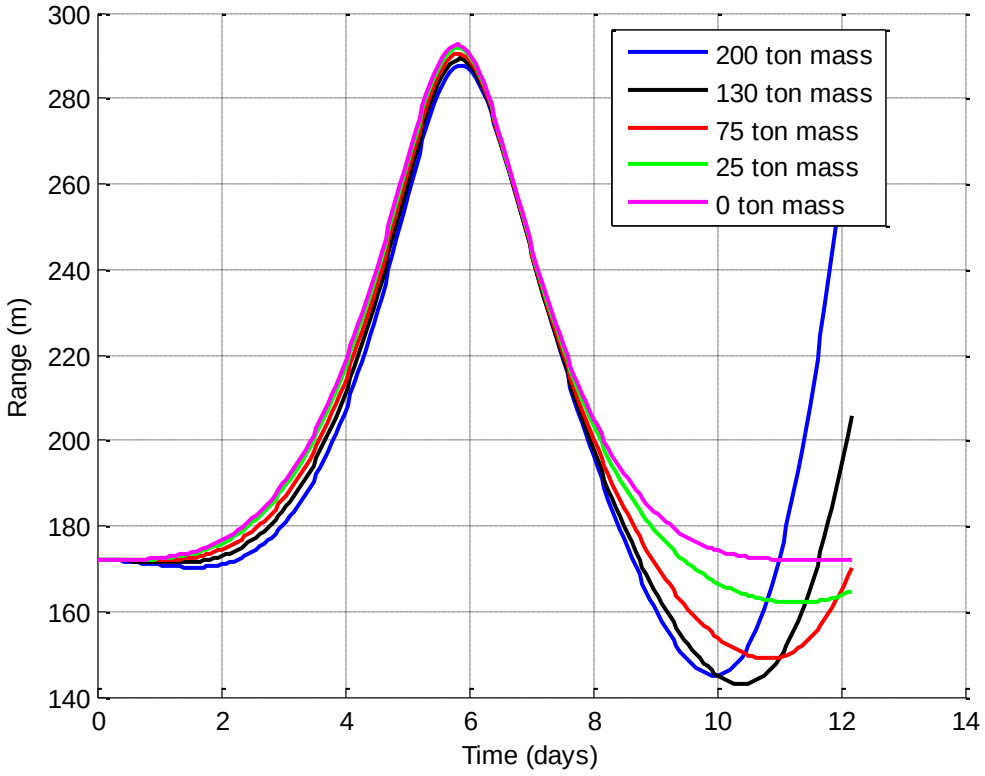

Figure 4.20. Range between spacecraft and asteroid with 172–m initial separation

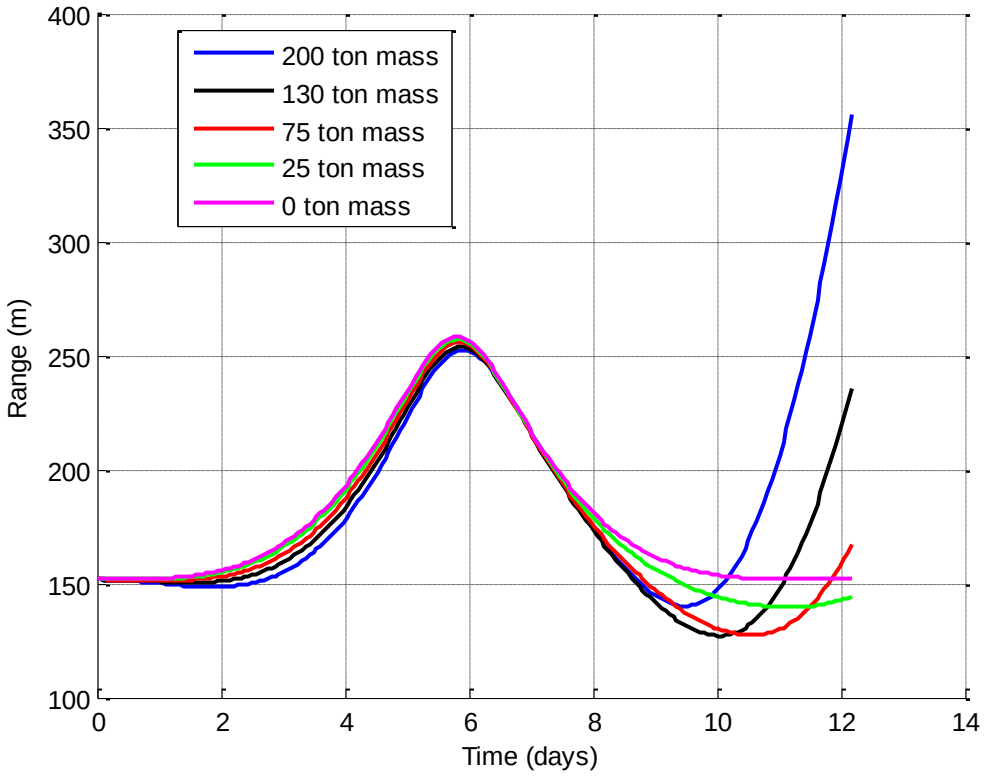

Figure 4.21. Range between spacecraft and asteroid with 151–m initial separation

Now, at an initial separation distance of 101 meters, the effects of the gravity are becoming more pronounced. The ranges depicted in Figure 4.22 show that the range starts dramatically increasing for the heavier masses a couple days earlier in the orbit than at previous initial ranges of separation. From examination of Figure 4.23, the relative ranges compared to the baseline range show that, after the initial movement towards the asteroid, the spacecraft heads away from the asteroid and does not return again like at previous initial separation distances.

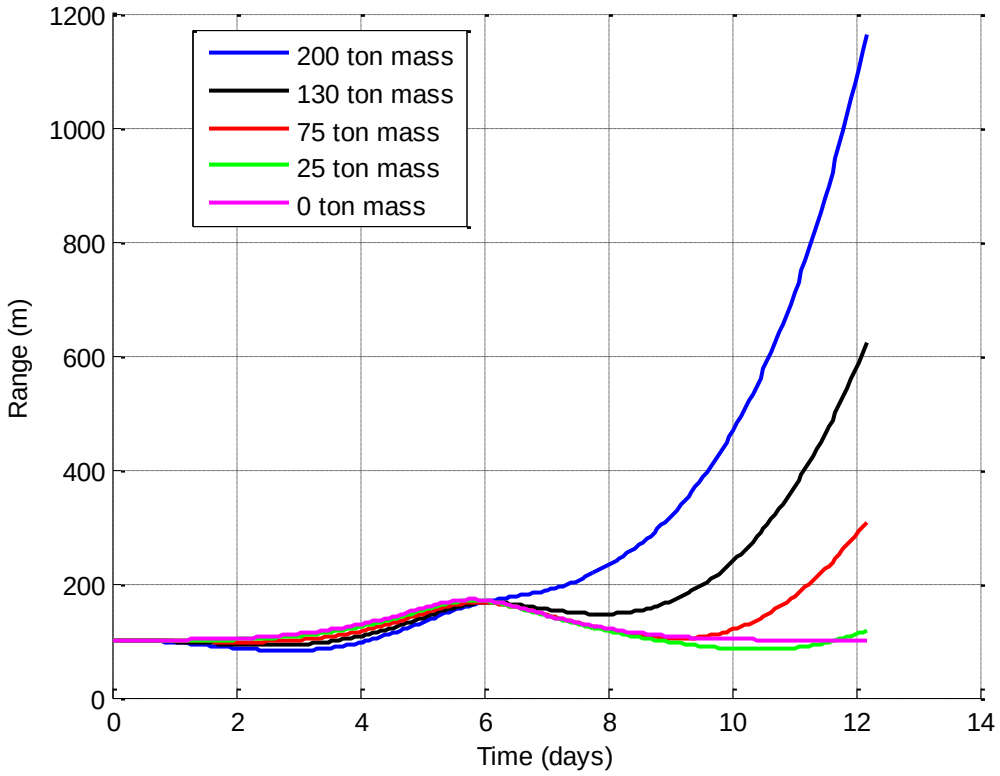

Figure 4.22. Range between spacecraft and asteroid with 101–m initial separation

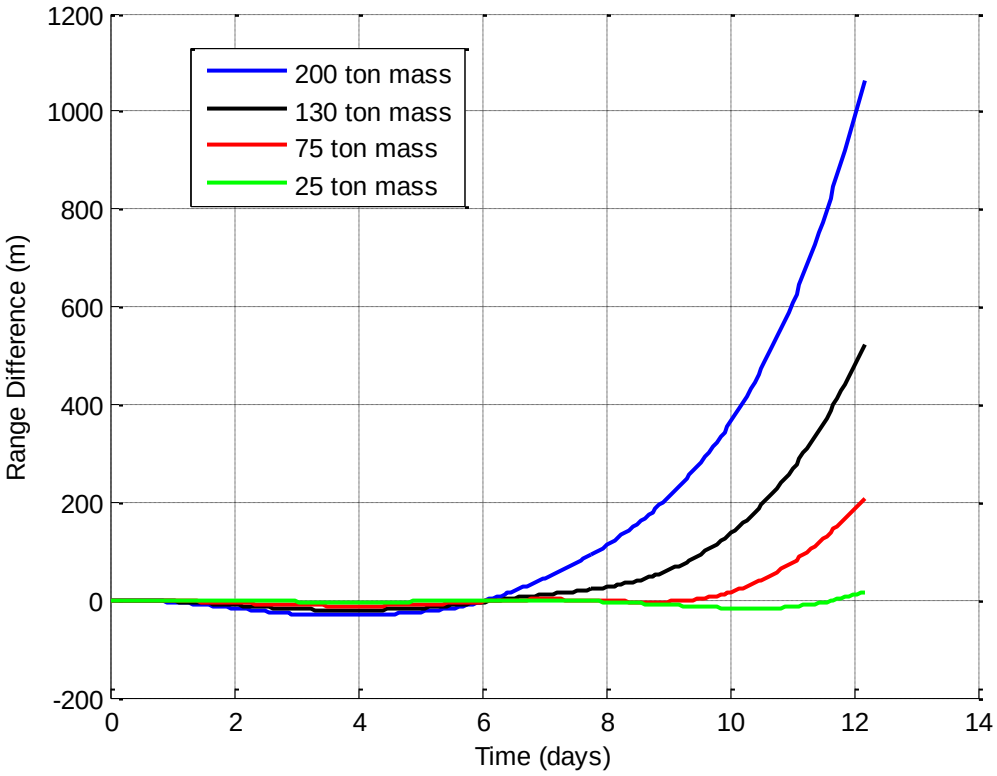

Figure 4.23. Range difference between spacecraft and massless asteroid from asteroids of varying mass with initial 101–m separation

The difference in range vectors shows the dramatic changes in the orbits, especially those with the heavier masses. Figures 4.24–4.28 demonstrate the instability of the orbits with the larger masses. As soon as the spacecraft is drawn closer to the asteroid, the net velocity dramatically increases as seen in Figure 4.29, causing the spacecraft to be sent on an outward bound trajectory. The integrity of the orbit is now lost as the spacecraft is sent on a trajectory away from the asteroid. Even the case for the 25–ton–mass asteroid is becoming unstable at this initial separation distance. Though the range from the asteroid is not too different from the baseline case as seen in Figure 4.23, the position relative to the asteroid from Figure 4.25 shows how the spacecraft has drifted from its baseline trajectory.

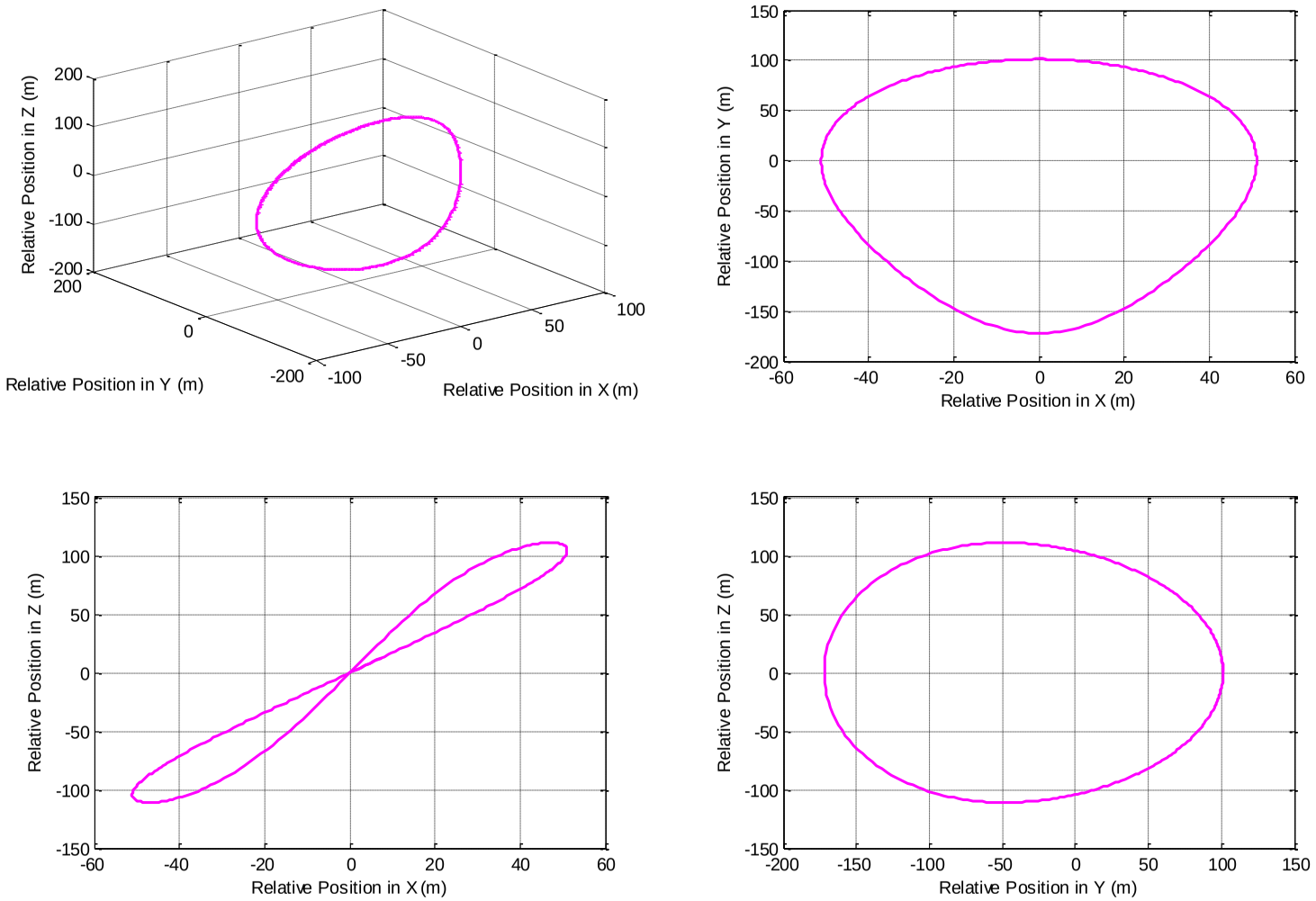

Figure 4.24. The spacecraft's relative position vector around the 0–ton asteroid at an initial distance of 101–m

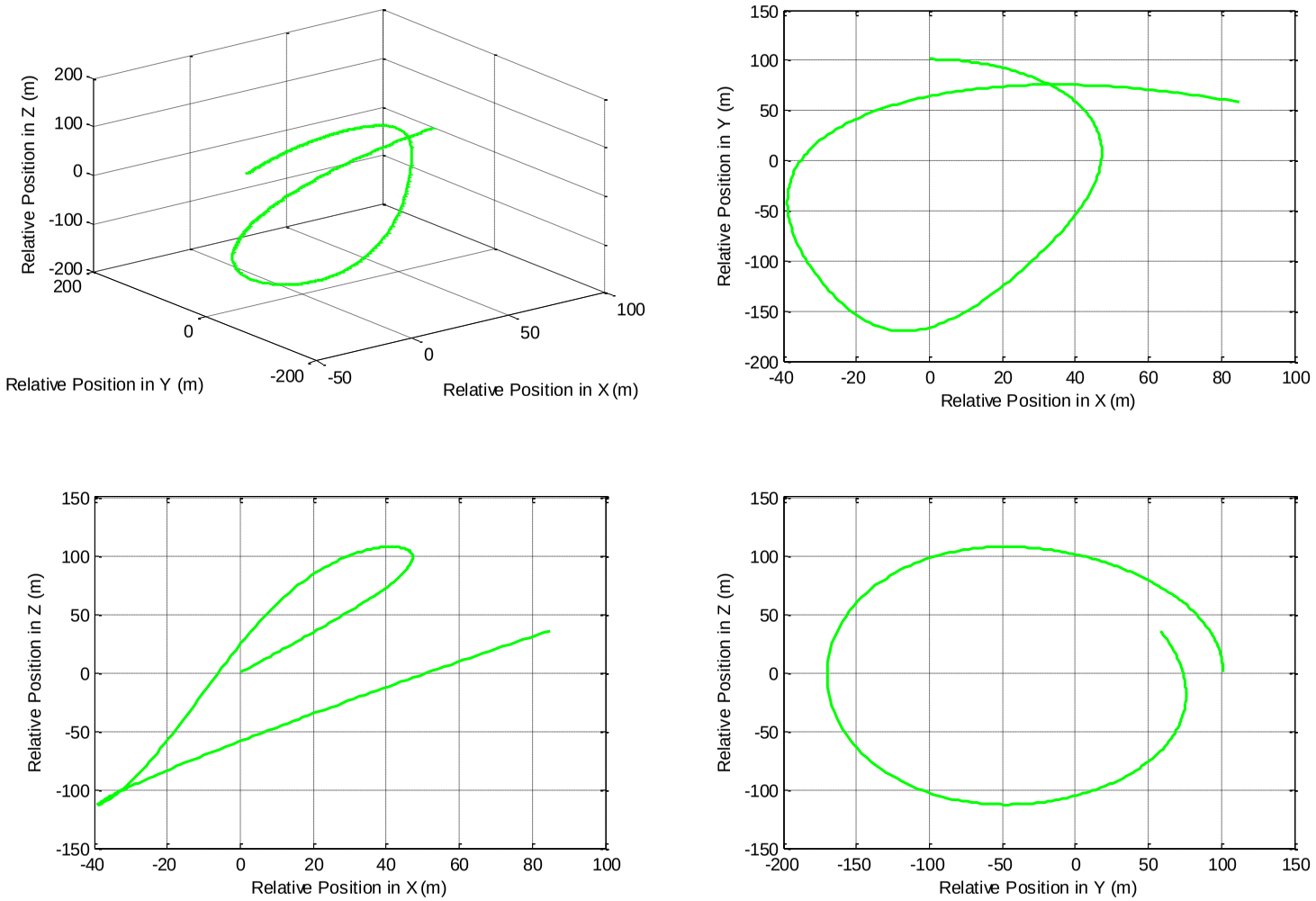

Figure 4.25. The spacecraft's relative position vector around the 25–ton asteroid at an initial distance of 101–m

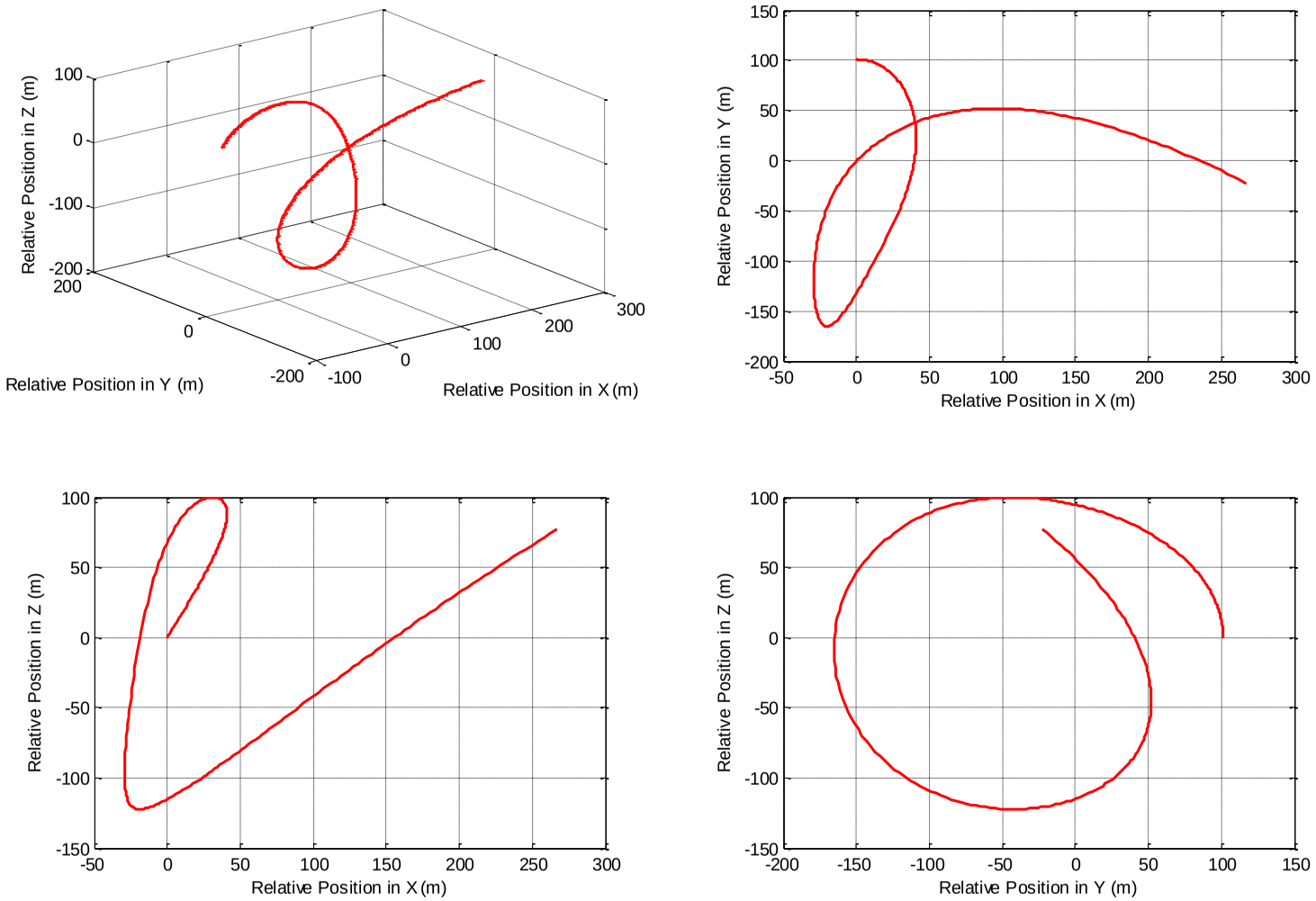

Figure 4.26. The spacecraft's relative position vector around the 75–ton asteroid at an initial distance of 101–m

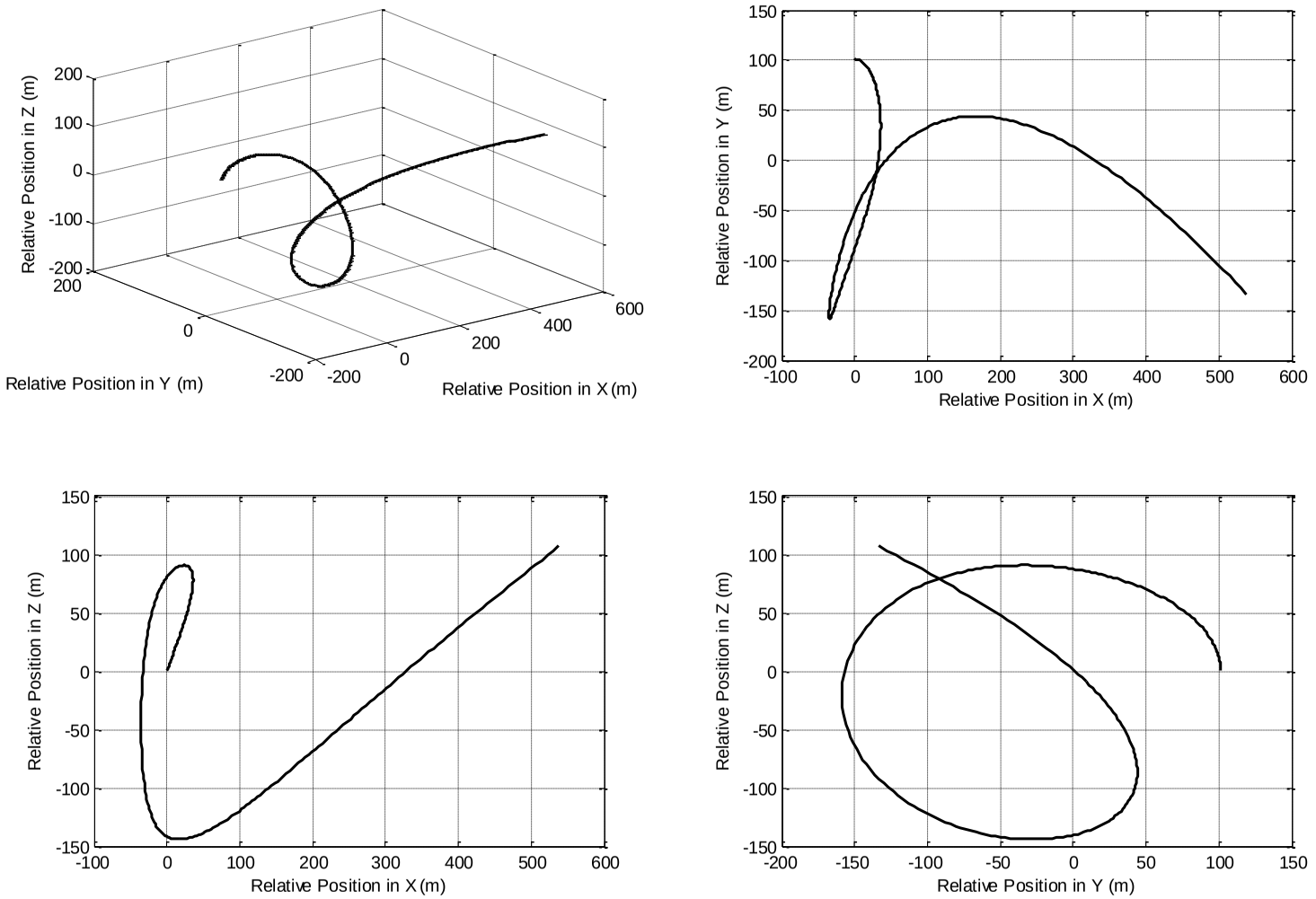

Figure 4.27. The spacecraft's relative position vector around the 130–ton asteroid at an initial distance of 101–m

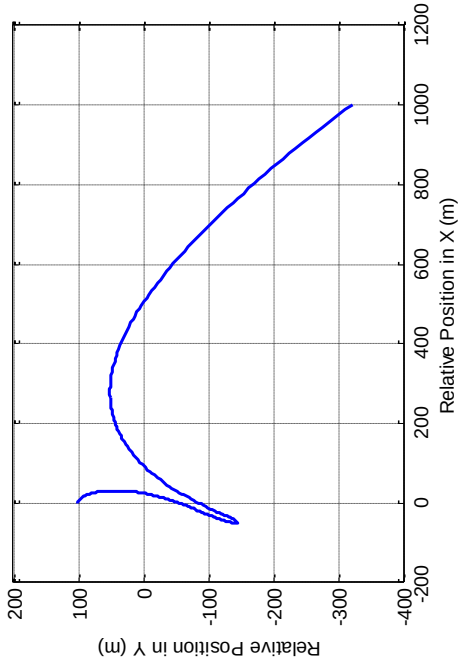

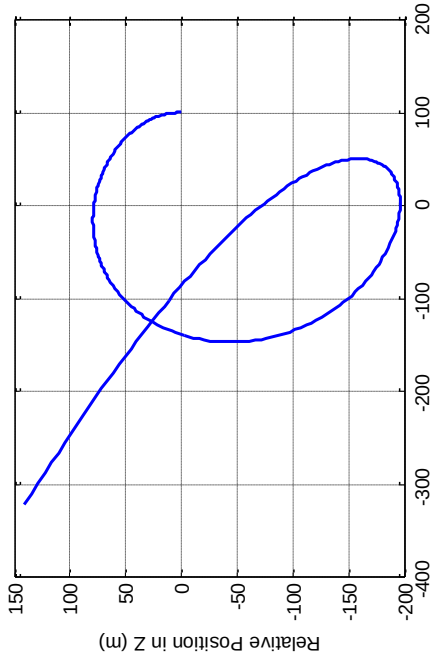

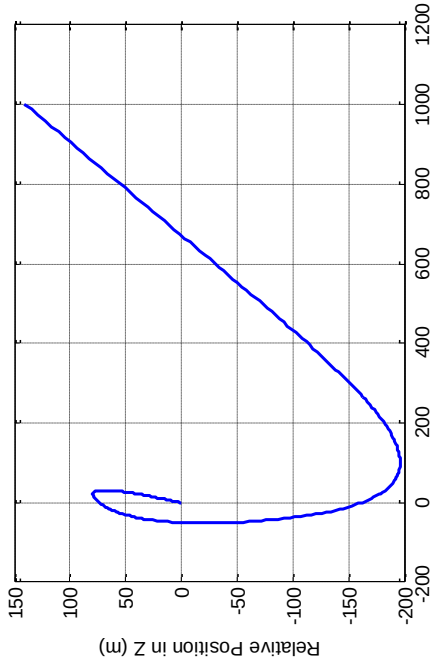

Figure 4.28. The spacecraft's relative position vector around the 200–ton asteroid at an initial distance of 101–m

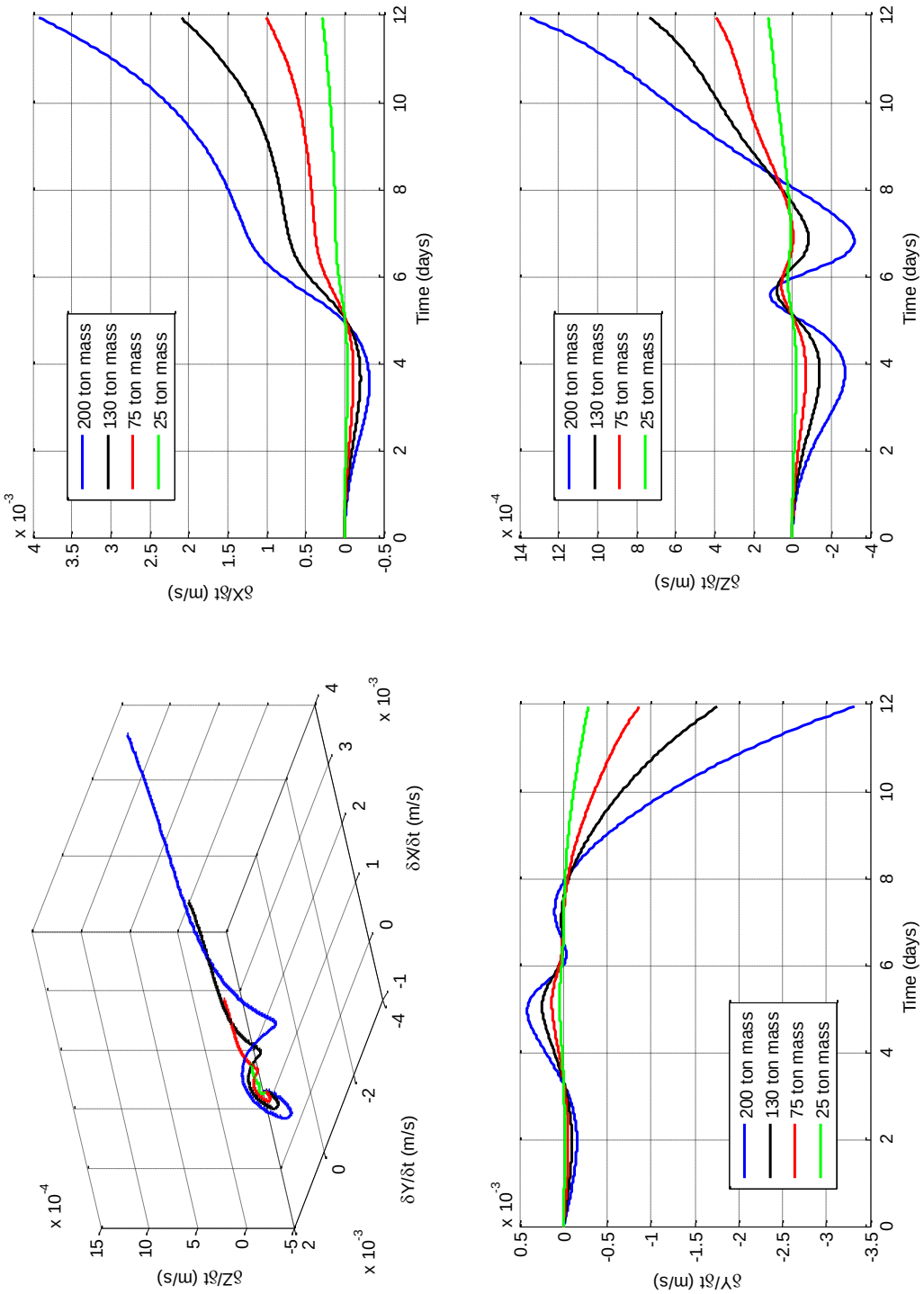

Figure 4.29. Relative velocity vector deviation from the baseline case at 101–m

When approaching an initial range of 71 meters, the previous trend continues as seen in the ranges of Figure 4.30. However, at this range, a near-miss of the asteroid takes place (as defined in Chapter 3) for the 200–ton–mass. A zoomed-in view of Figure 4.30 can be seen in Figure 4.31. In this figure, the radius of each asteroid is denoted by a dashed line. The exact values of the radii can be determined from Table 3.3, where half the upper limit of the diameter corresponds to the position of r_{200} through r_{25} in Figure 4.30. While it is not a direct hit with the asteroid, the spacecraft does pass very close to the asteroid such that it might be considered to be too close, based on the numerical accuracy for a mission. It should also be noted that at this initial range, the 25–ton–mass is finally having a dramatic effect on the spacecraft. This is not surprising given the trends for the heavier masses. The range for the 25–ton–mass can be viewed in Figure 4.32 without the other masses distorting the plot.

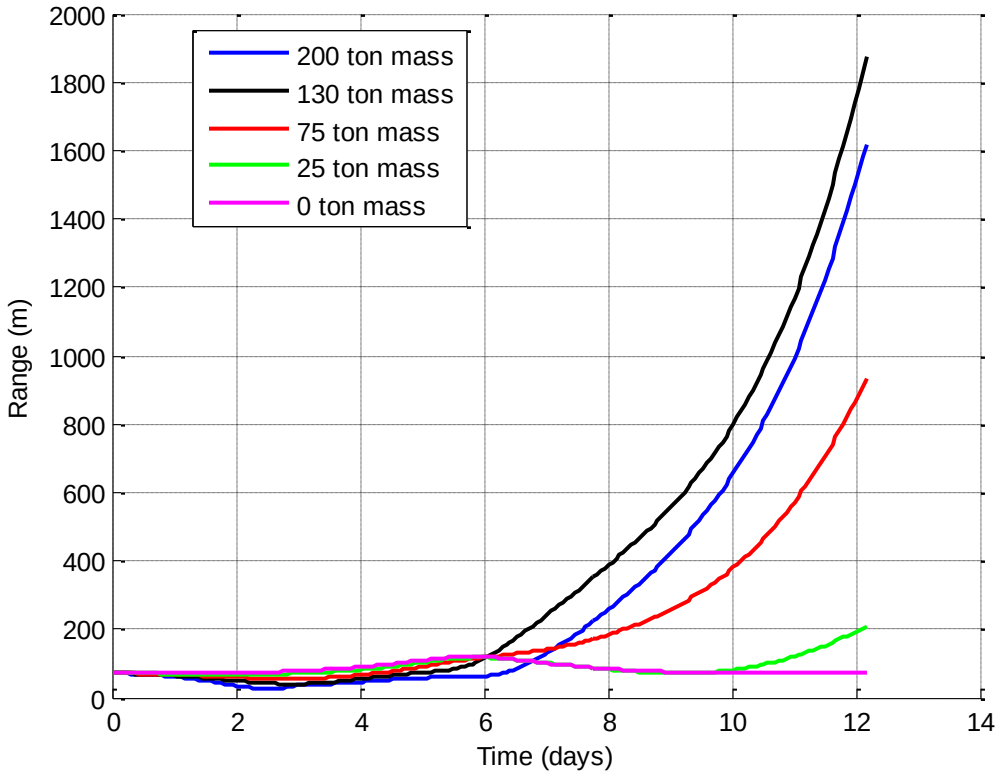

Figure 4.30. Range between spacecraft and asteroid with 71–m initial separation

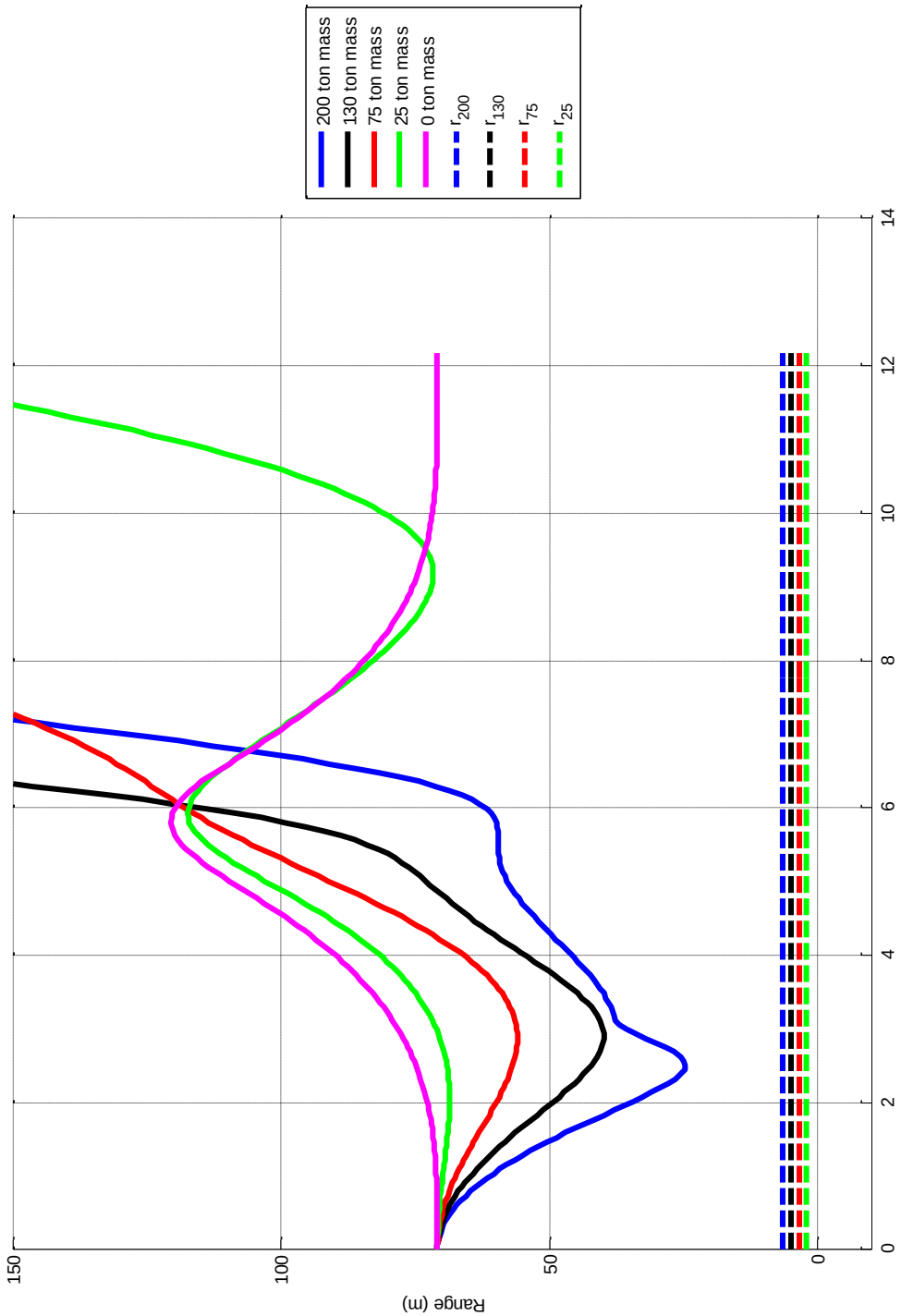

Figure 4.31. Near-miss of 200–ton asteroid by spacecraft at initial 71–m initial separation

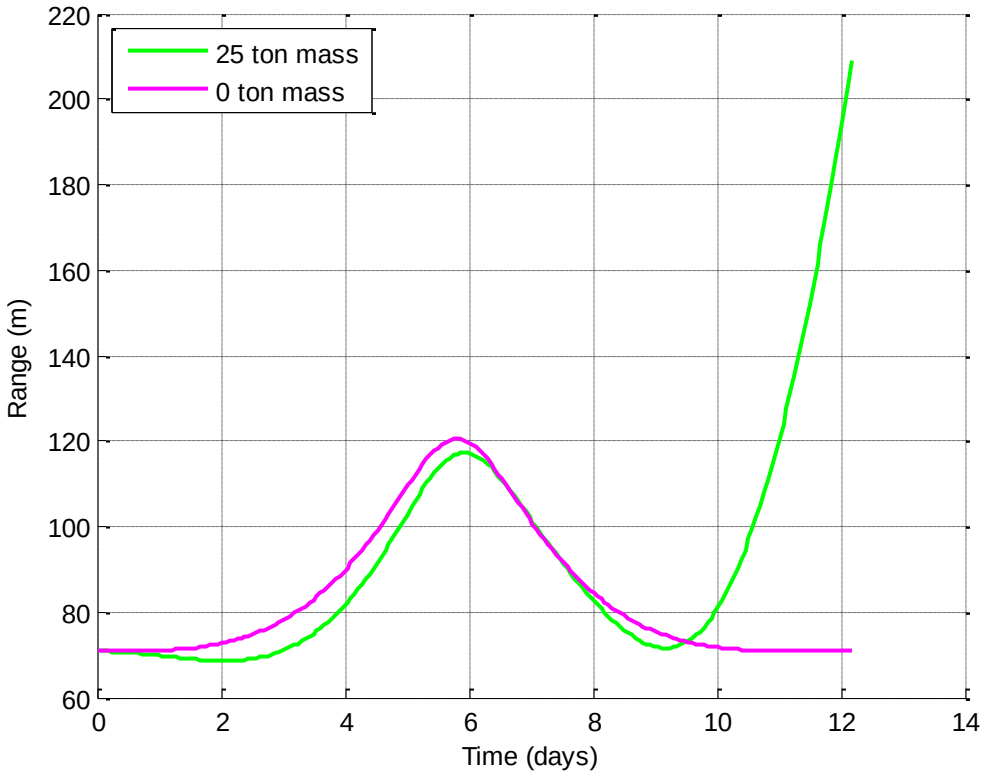

Figure 4.32. Range between spacecraft and asteroid with 71–m initial separation for the 25–and–0–ton–masses

Beginning at an initial separation distance of 50 meters, an impact occurs for the 200–ton–mass (Figure 4.33). The parameters of an impact were defined in Chapter 3. Both the 75- and 130–ton–masses have near-misses, whereas the 25–ton–mass continues to have a safe, albeit unstable, trajectory. At this range, most of the trajectories are unsafe and only continue to get worse the closer to the asteroid the spacecraft is initially. At an initial range of just 38–meters, the 130–and 75–ton–masses have a collision as seen in Figure 4.34. As the spacecraft passes within the radius of the asteroid denoted by r_{200}, r_{130}, r_{75}, and r_{25} for their respective masses, an impact occurs.

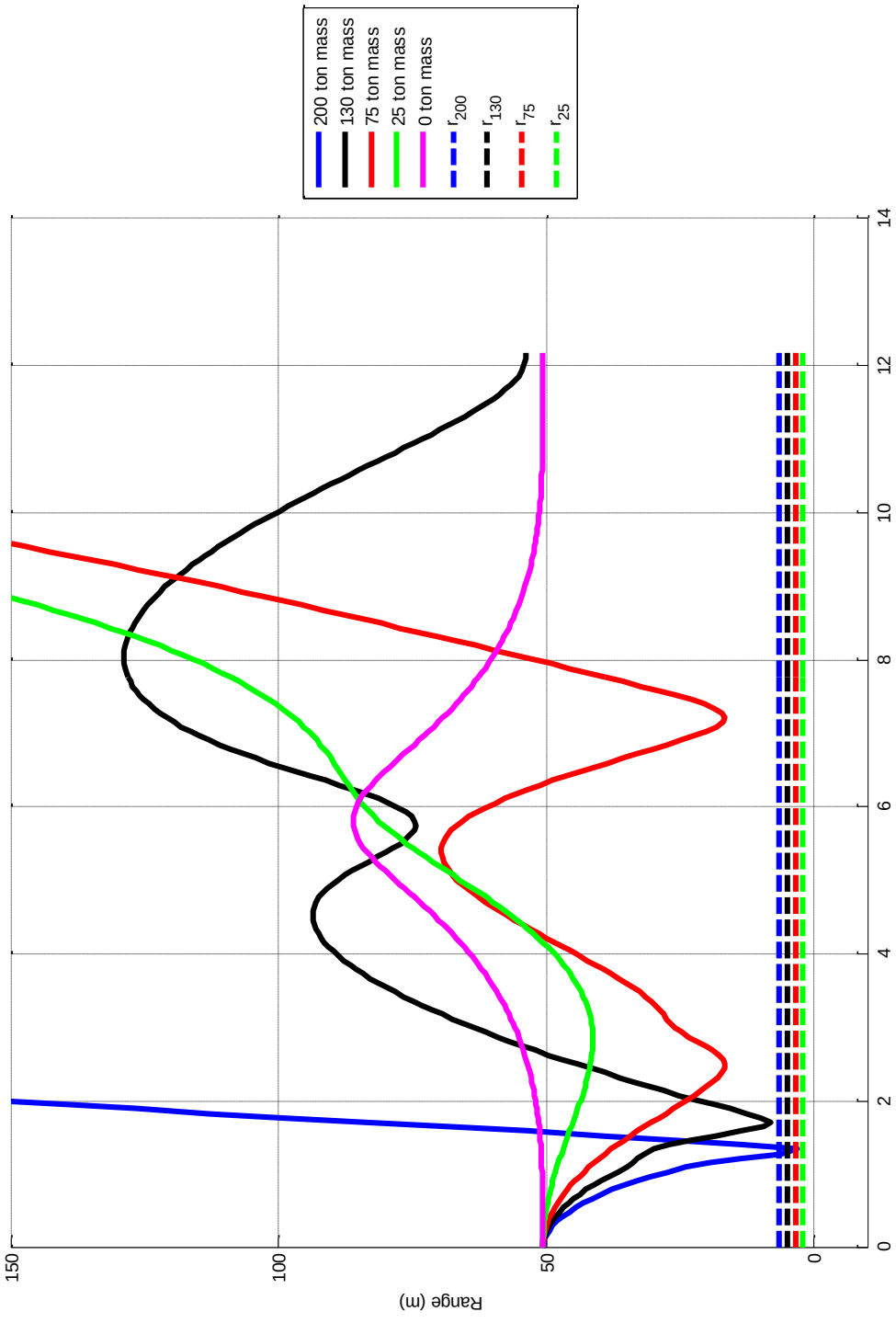

Figure 4.33. Impact with the 200–ton–mass and near-misses for the 7– and 130–ton–masses at initial separation of 50–m

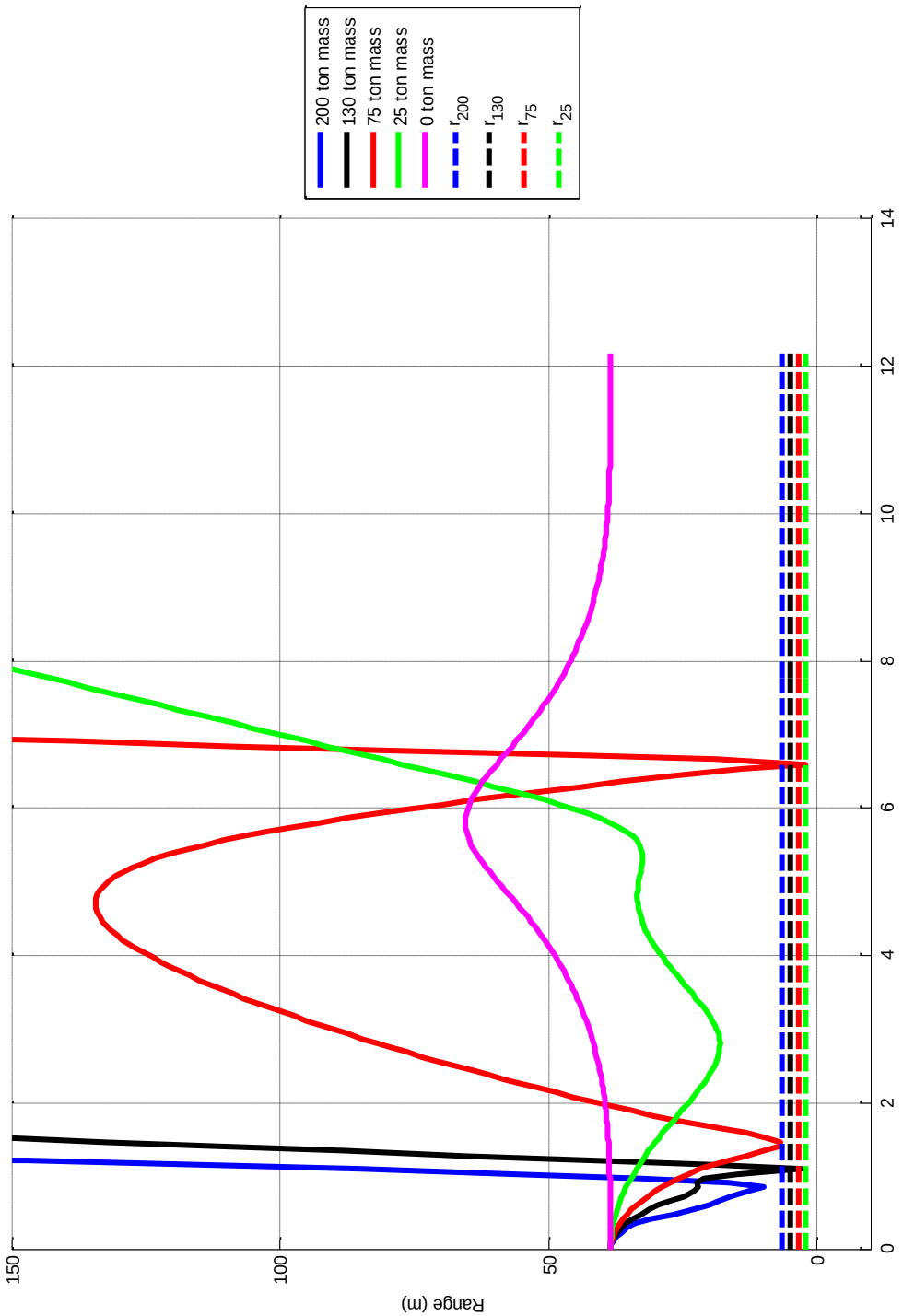

Figure 4.34. Impact with the 130– and 75–ton–masses at initial separation of 38–m

Getting any closer to the asteroid is superfluous as impacts will continue to occur and even the orbit for the 25–ton–mass at this range is unstable (Figure 4.35). At this juncture, the next section explores orbits over two.

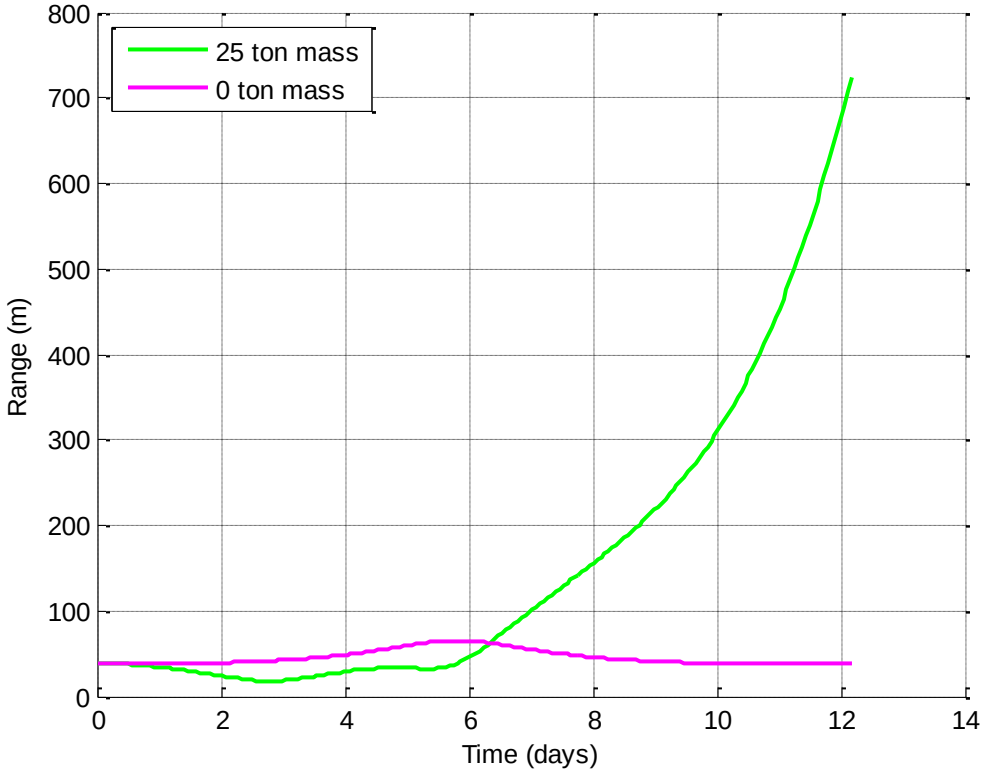

Figure 4.35. Range between spacecraft and asteroid with 38–m initial separation for 25-and 0–ton–masses

4.1.2 Spacecraft Trailing Asteroid Over Two Revolutions of Large Halo Orbit

Integrating over twice the orbital period, it is now time to determine the stability over a longer time period. Stability over twice the orbital period is much more difficult as even at an initial range of 506 meters, the spacecraft starts to drift far from the asteroid especially at heavier

masses. Figure 4.36 shows that the range between the spacecraft and the asteroid, while stable for the first period, begins to deviate at the start of the next period. Ultimately, part way through the second period, the spacecraft in the 200–, 130–, and 75–ton–mass cases is sent on an outward bound trajectory. The trend that developed in the previous section is already developing much earlier over two orbital periods.

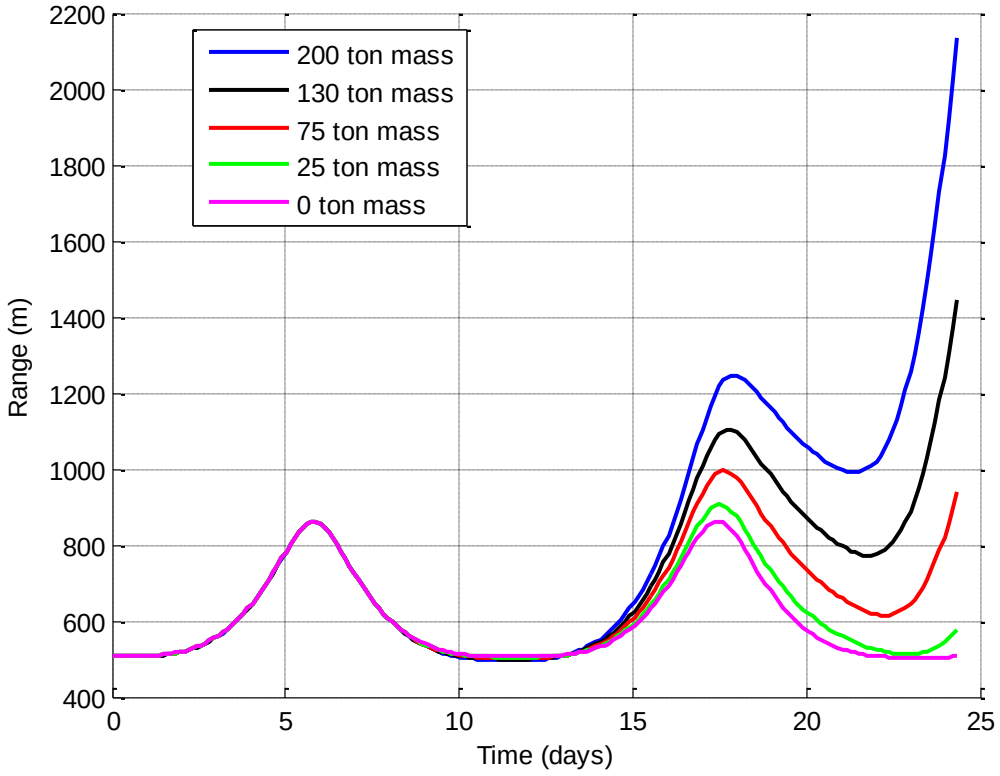

Figure 4.36. Range between spacecraft and asteroid with 506–m initial separation over two orbital periods

Examining the range difference between the cases with asteroids of mass and the baseline in Figure 4.37 show that the spacecraft after initially drifting away starts to come back towards the asteroid before moving further outward. Figures 4.38–4.42, showing the relative position vector, highlight the instability of the orbits with the heavier masses. Recall, that over this initial separation distance for one revolution, the orbit was stable. However, a second orbit with the

asteroid is enough to send the spacecraft on an outward bound trajectory relative to the asteroid. There is also a general instability in the halo orbit itself with no asteroid as seen in Figure 4.38. Over two revolutions, the stability of the orbit is naturally decaying due to the natural instability of libration point orbits. As in the case with only one orbital period, the net velocity of the spacecraft (Figure 4.44) increases within the second orbit driving the spacecraft away from the asteroid.

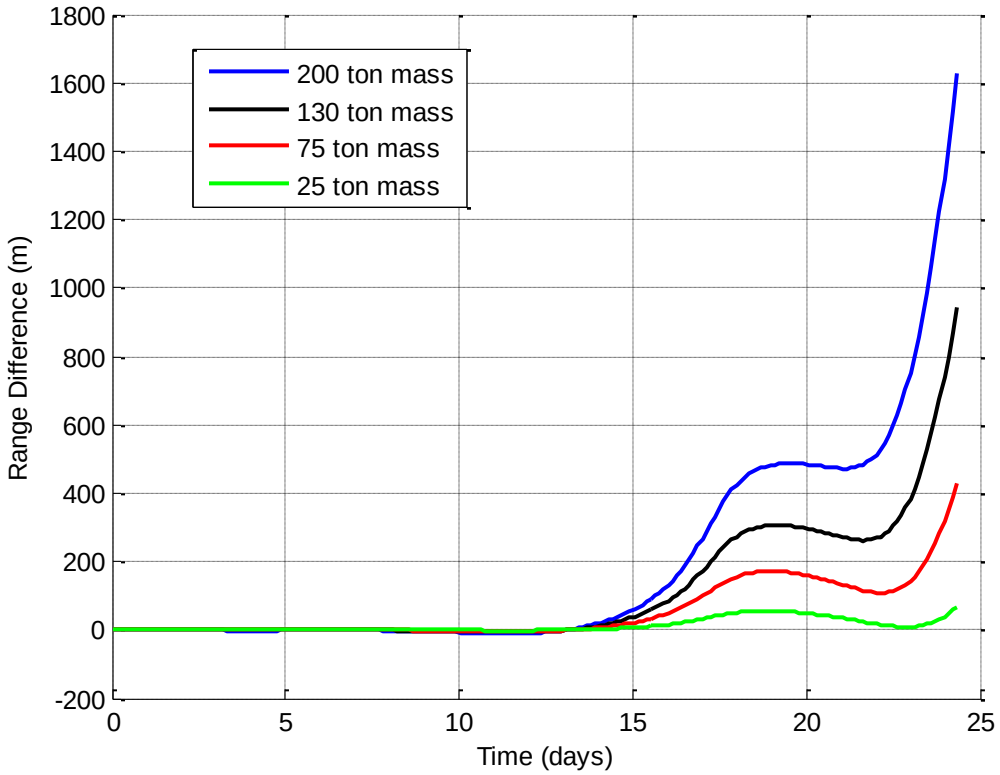

Figure 4.37. Range difference between spacecraft and massless asteroid from asteroids of varying mass with initial 506–m separation over two orbital periods

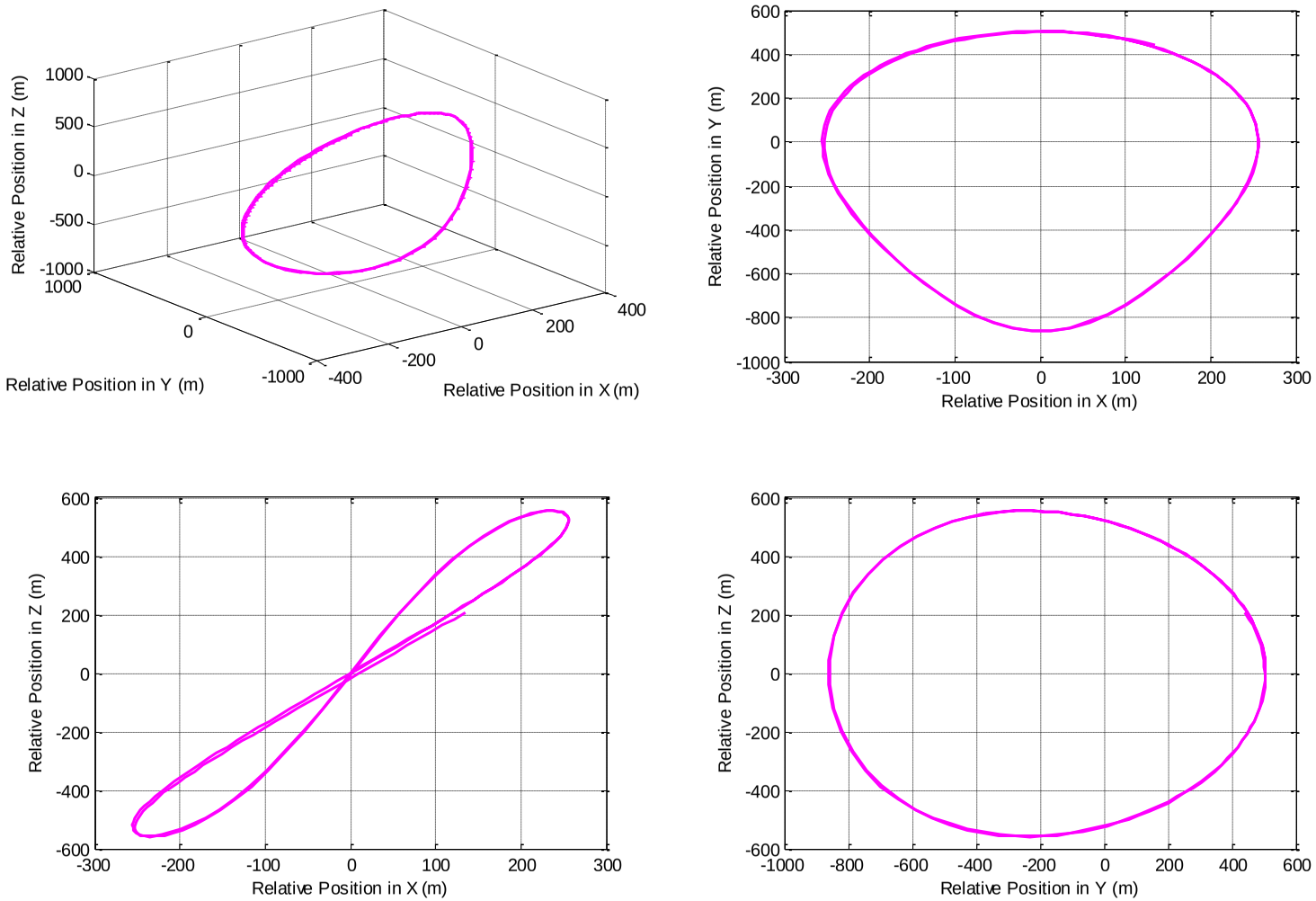

Figure 4.38. The spacecraft's relative position vector around the 0–ton asteroid at an initial distance of 506–m over two periods

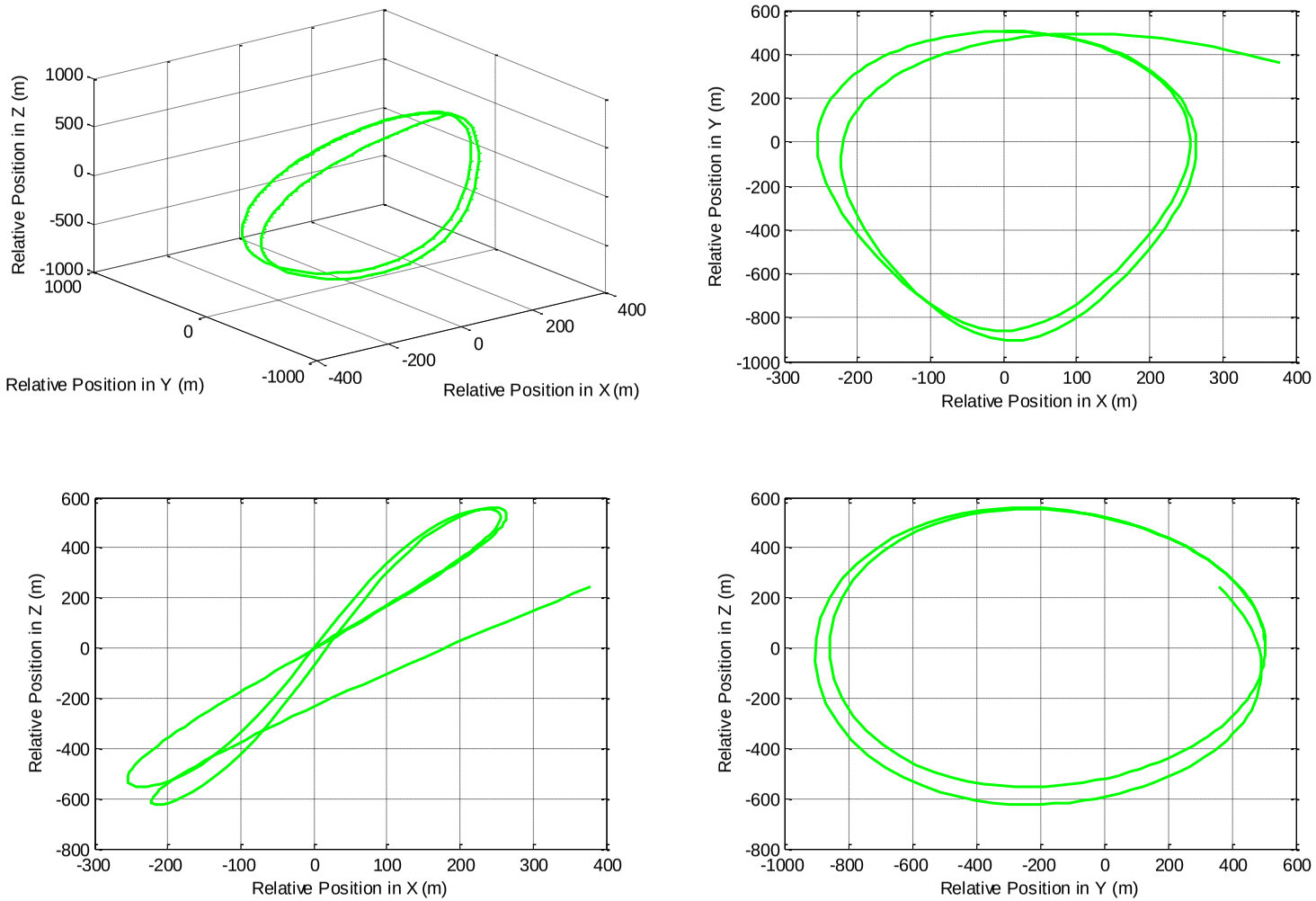

Figure 4.39. The spacecraft's relative position vector around the 25–ton asteroid at an initial distance of 506–m over two periods

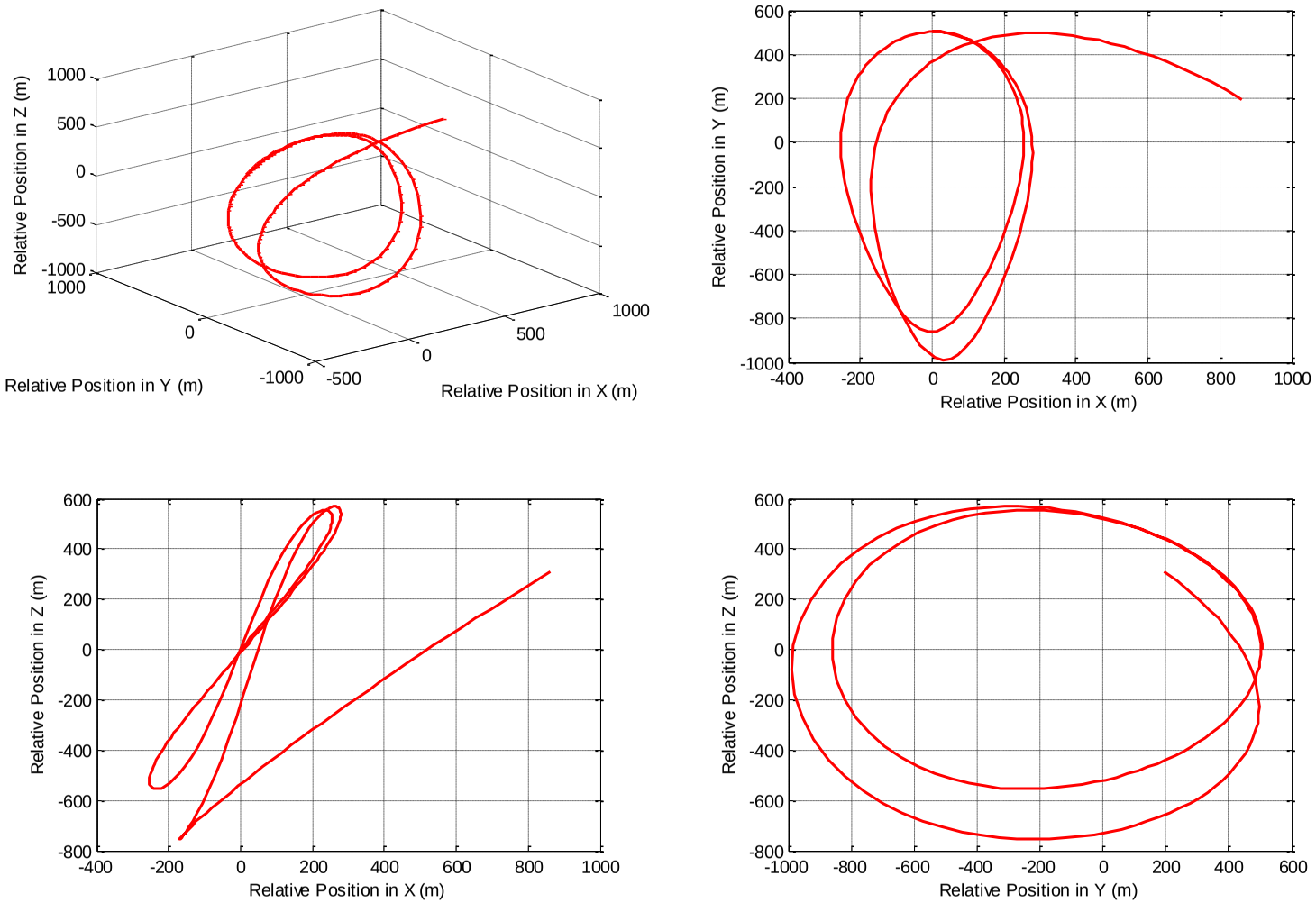

Figure 4.40. The spacecraft's relative position vector around the 75–ton asteroid at an initial distance of 506–m over two periods

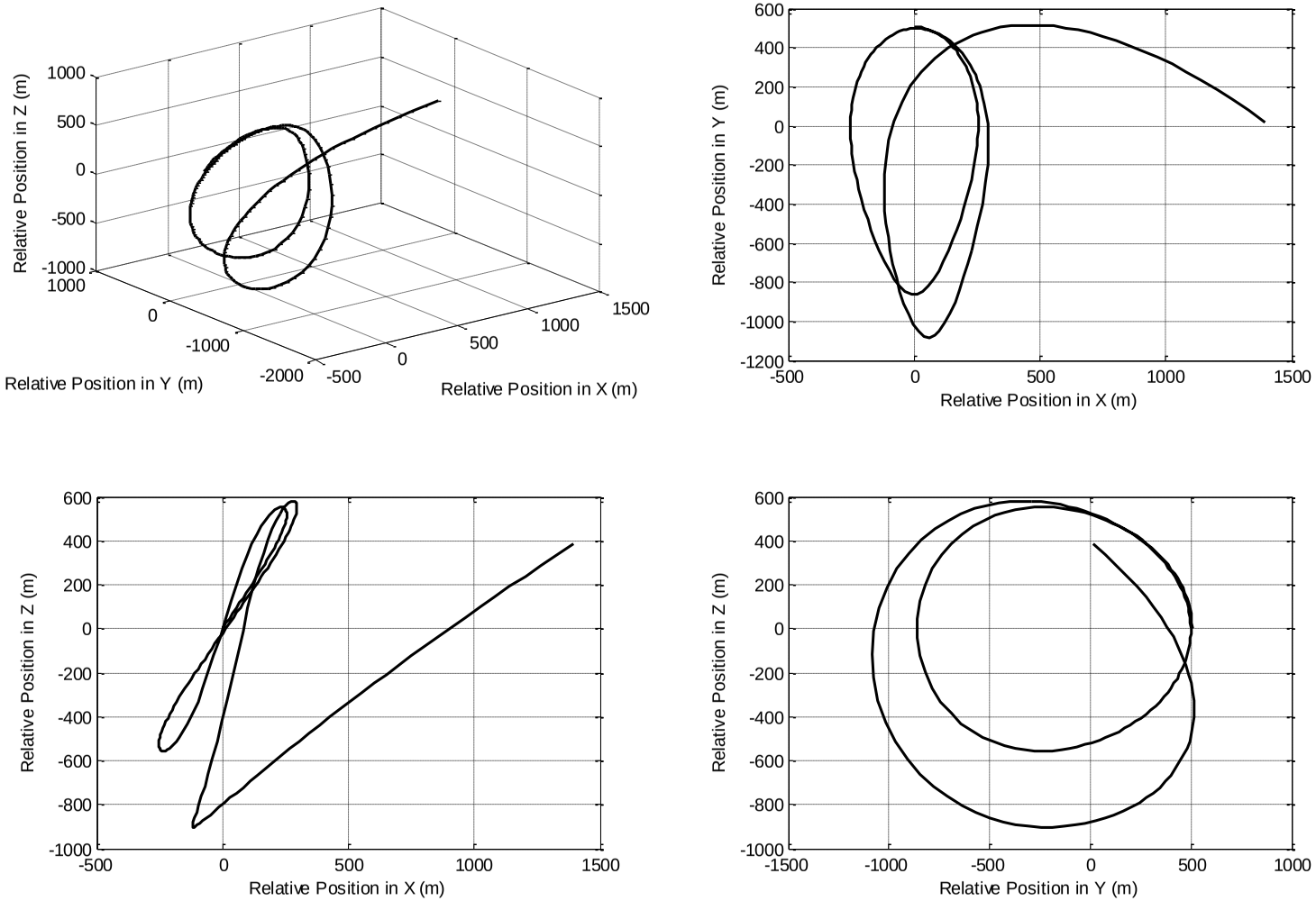

Figure 4.41. The spacecraft's relative position vector around the 130–ton asteroid at an initial distance of 506–m over two periods

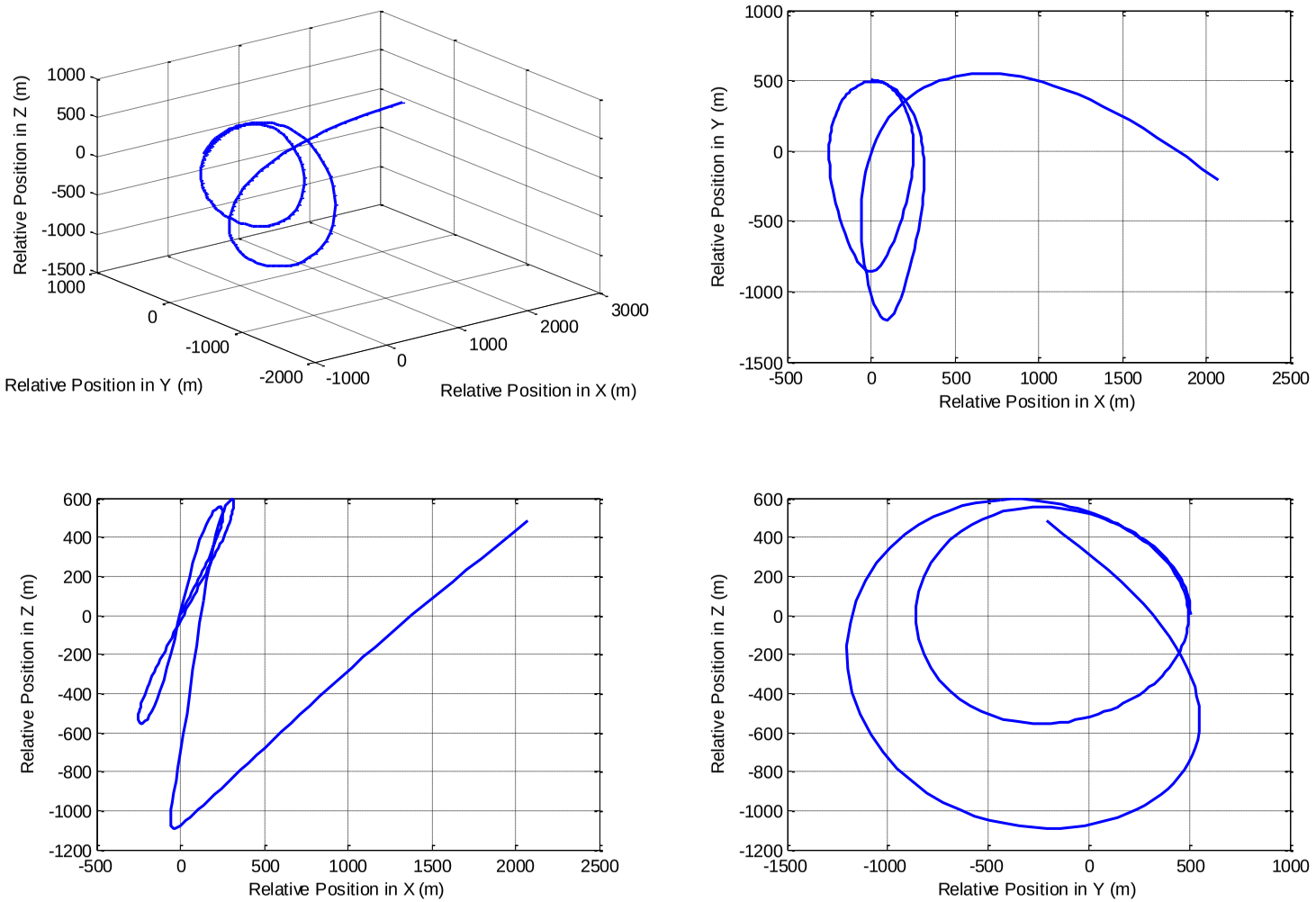

Figure 4.42. The spacecraft's relative position vector around the 200–ton asteroid at an initial distance of 506–m over two periods

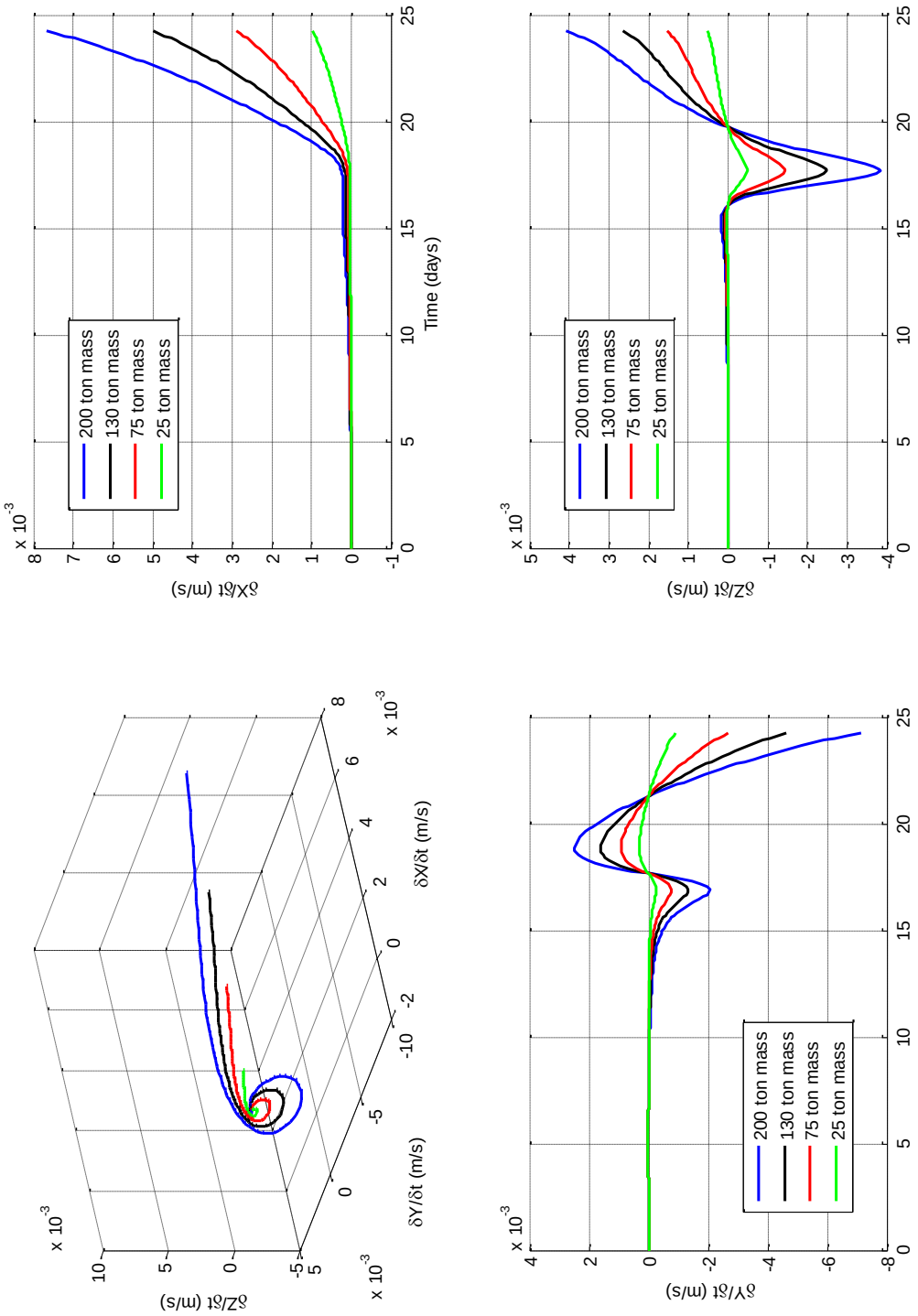

Figure 4.43. Relative velocity vector deviation from the baseline case at 506–m over two periods

To obtain stability over two periods, the spacecraft and asteroid need to be initially farther apart. At 910 meters, the orbits for all masses are stable as seen in the ranges of Figure 4.44. Looking at the relative ranges from the baseline range, Figure 4.45 shows that the deviations are not incredibly large at this range.

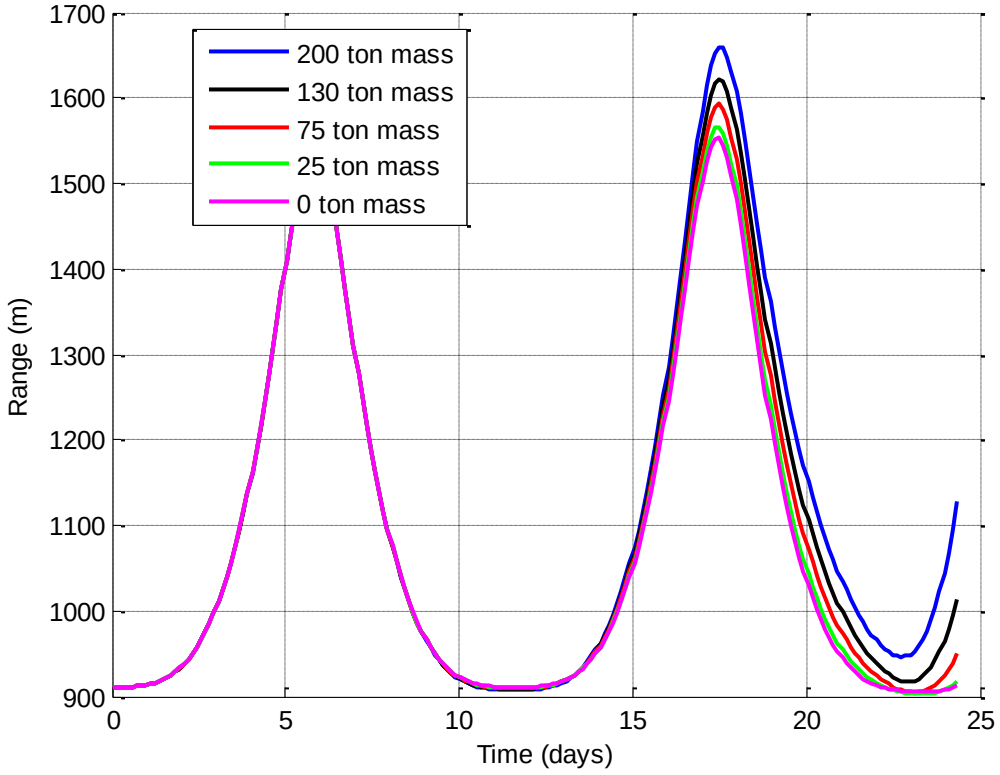

Figure 4.44. Range between spacecraft and asteroid with 910–m initial separation over two orbital periods

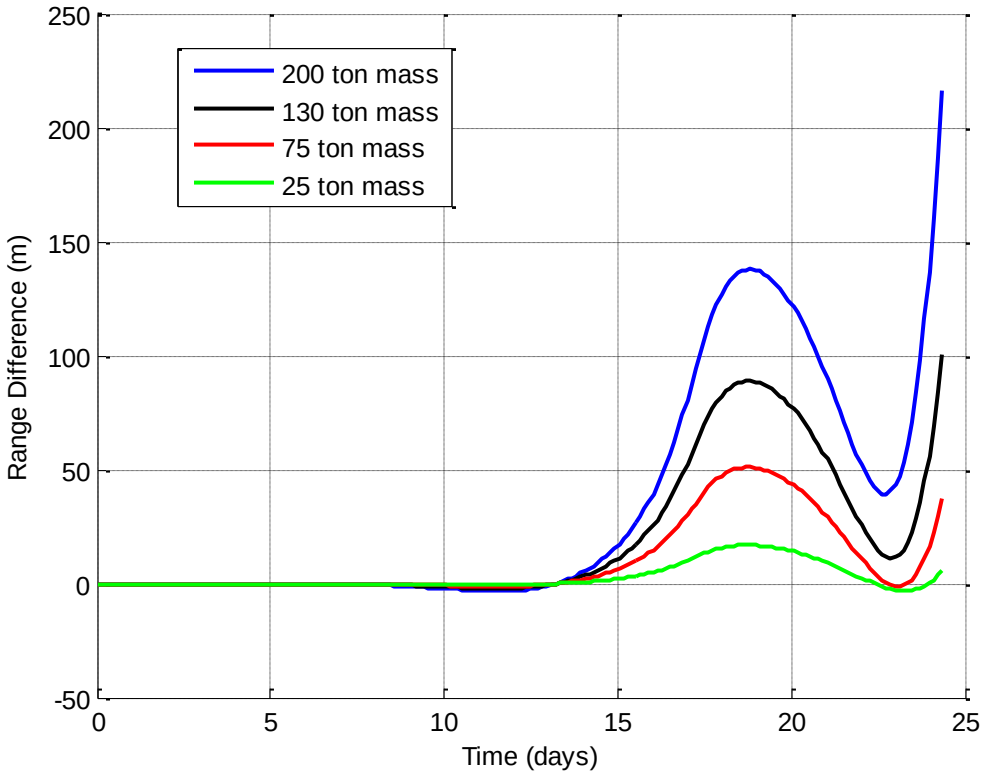

Figure 4.45. Range difference between spacecraft and massless asteroid from asteroids of varying mass with initial 910–m separation over two orbital periods

Moving any closer than the 506 meters is moot as the orbit becomes way too unstable. Figure 4.46 shows the range difference from the baseline at an initial separation distance of 202 meters. At this point, the difference in range from the baseline is on the order of several kilometers, which is undesirable for a mission. Furthermore, if impacts don't occur within the first orbital period, they won't occur within the second as the spacecraft is either stable or it just simply drifts too far away. The only concern over two orbital periods is the stability; impacts are not a factor.

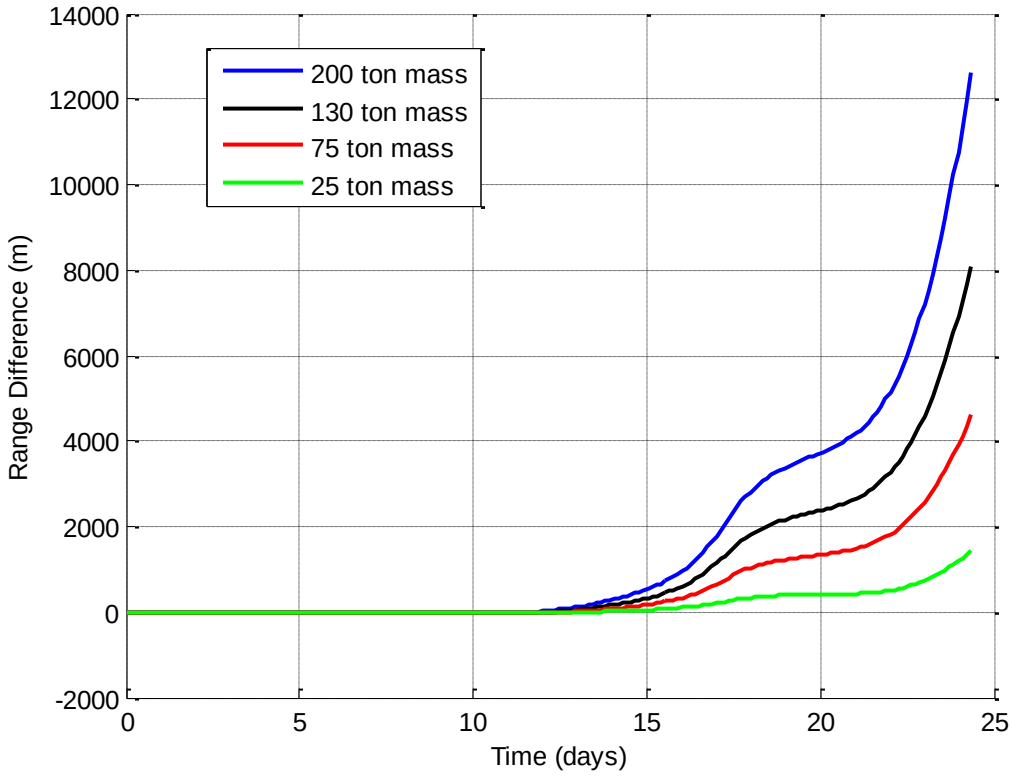

Figure 4.46. Range difference between spacecraft and massless asteroid from asteroids of varying mass with initial 202–m separation over two orbital periods

4.1.3 Trailing versus Leading Spacecraft in Large Halo Orbits

As it turns out, the effect of the orbit depending on whether or not the spacecraft leads or trails the asteroid does not matter. Looking at both the initial separation distances of 506 and 101 meters, both the range in Figures 4.47 and 4.48 and the relative range to the baseline range in Figures 4.49 and 4.50 are exactly the same as its counterparts from the Section 4.1.1. The deviations from the asteroid are the same and occur at the same point in the orbit. The only difference is in the relative position (Figures 4.51 and 4.52) and relative velocity (Figures 4.53

and 4.54) vectors, but that is only a sign change depending on which object is leading the other. Comparing these figures to their counterparts in Section 4.1.1 shows that the relative positions and velocities are the same except that they head in the opposite direction. As it doesn't matter which object trails or leads, it is up to the mission planner's preference as to the position of each object.

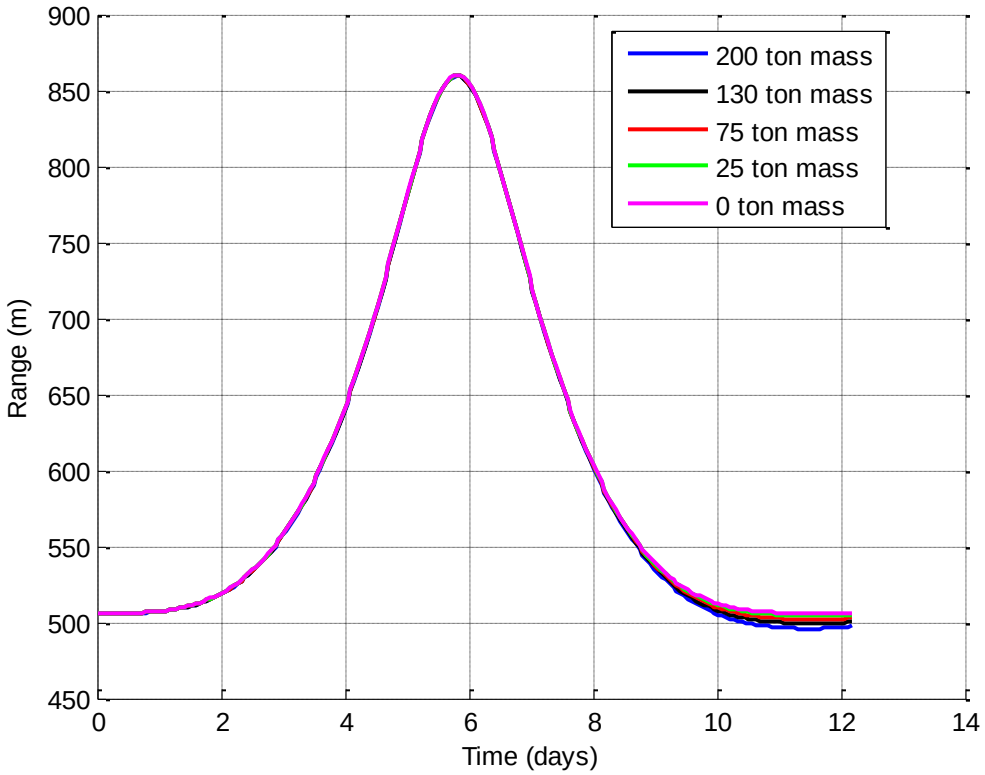

Figure 4.47. Range between leading spacecraft and asteroid with 506–m initial separation

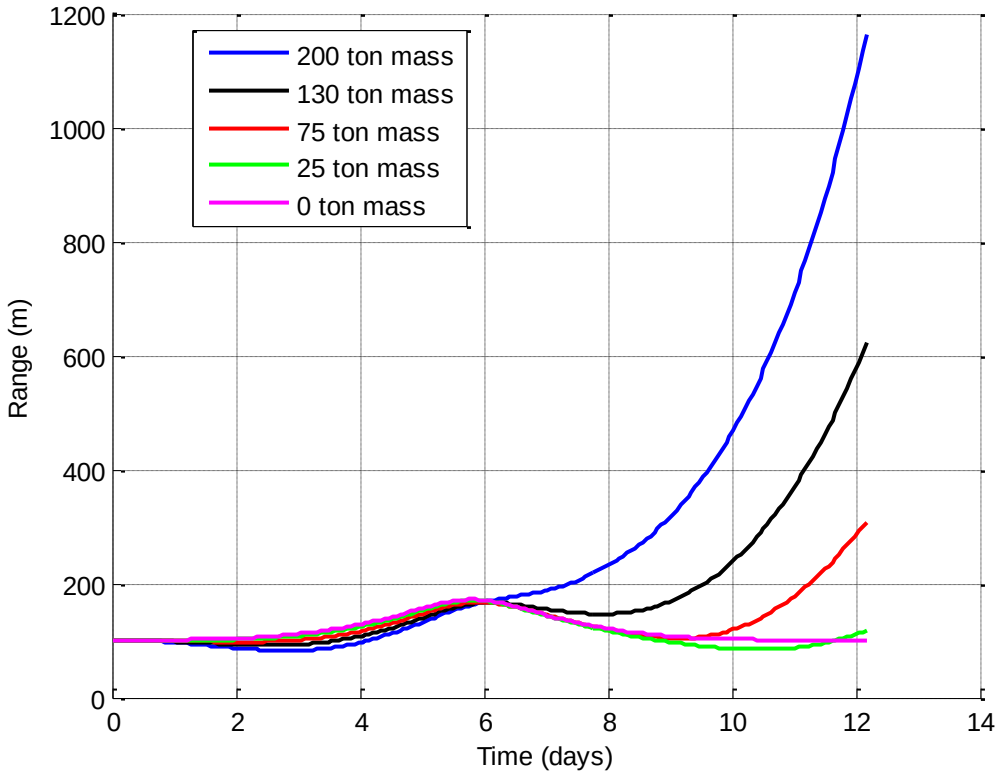

Figure 4.48. Range between leading spacecraft and asteroid with 101–m initial separation

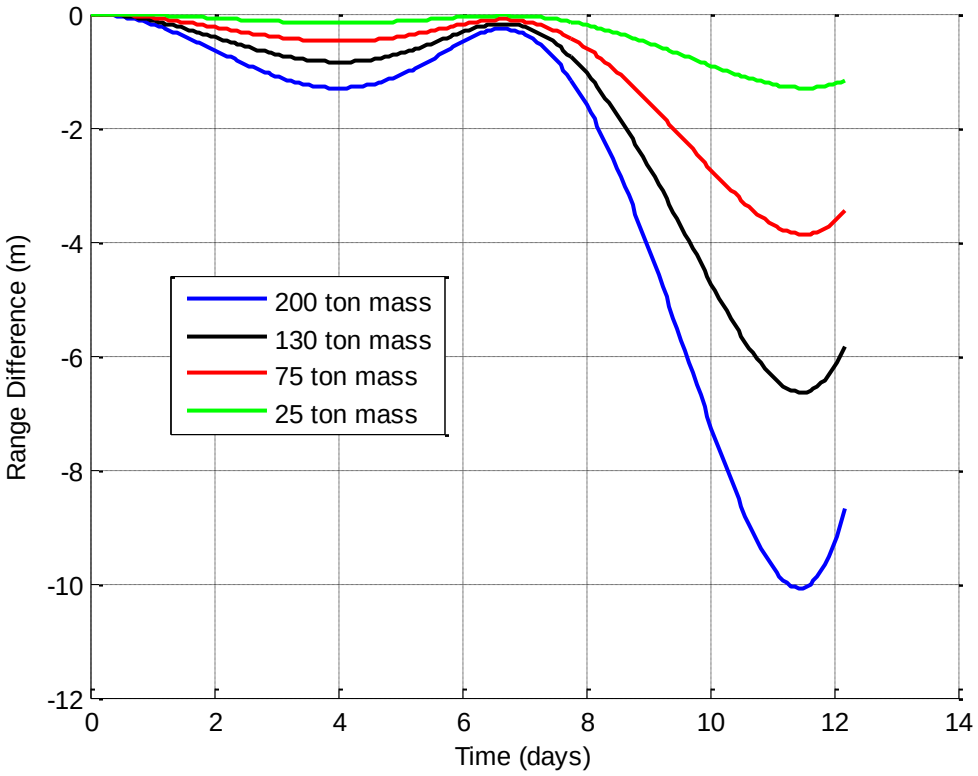

Figure 4.49. Range difference between leading spacecraft and massless asteroid from asteroids of varying mass with initial 506–m

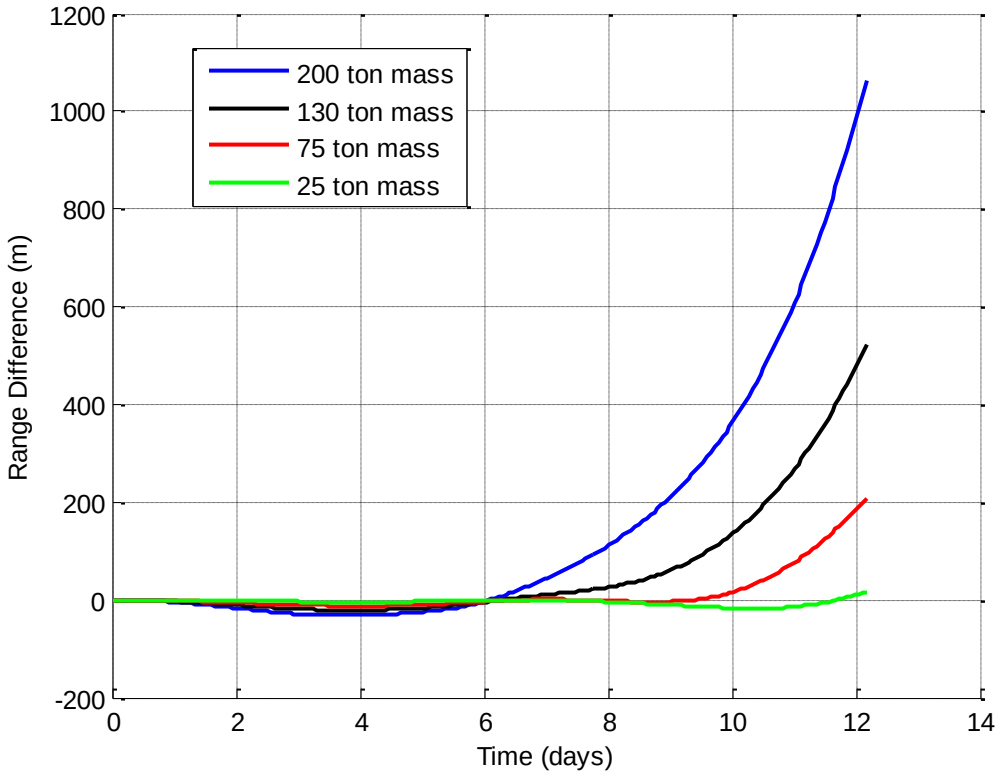

Figure 4.50. Range difference between leading spacecraft and massless asteroid from asteroids of varying mass with initial 101–m

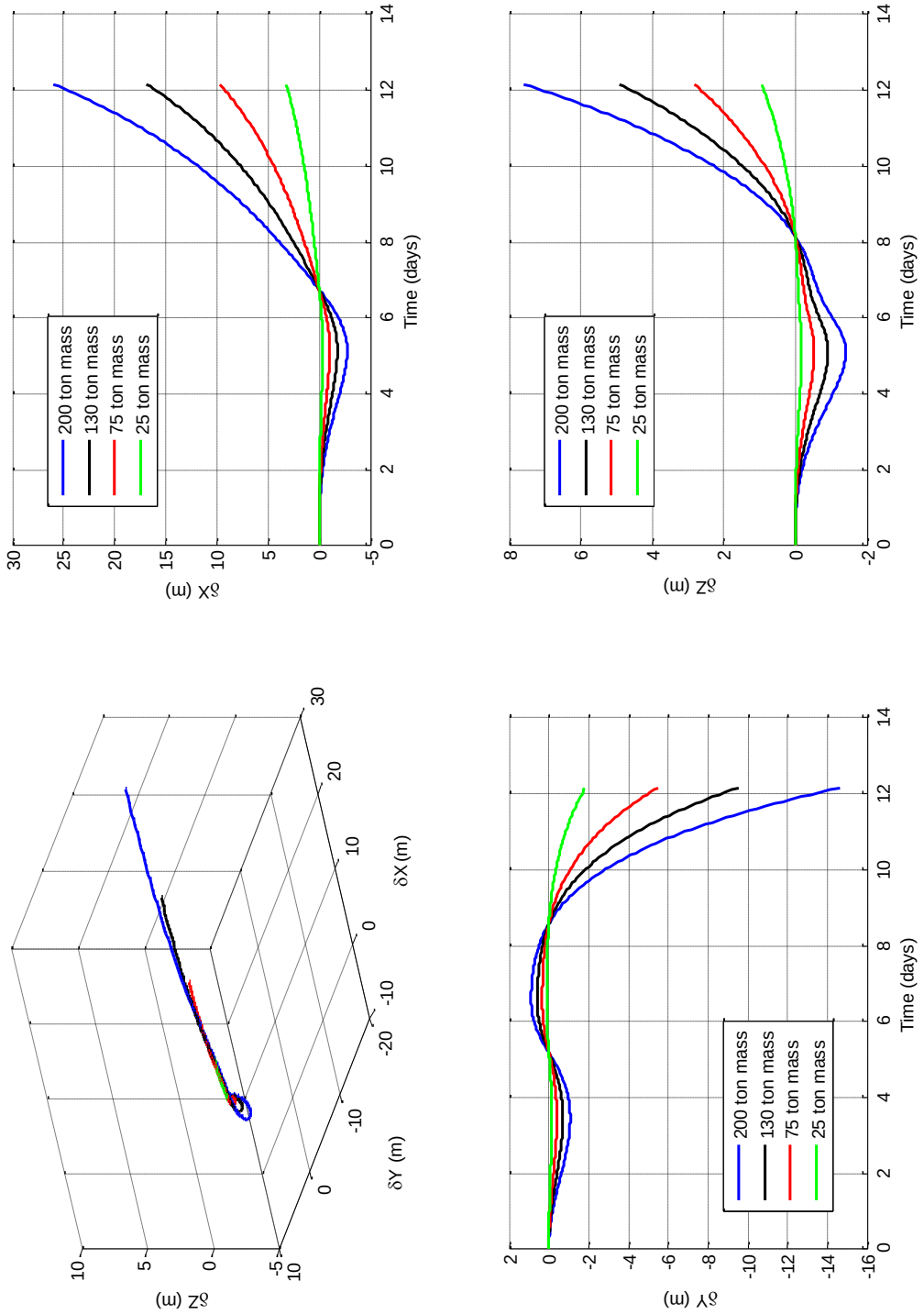

Figure 4.51. Relative position vector deviation from the baseline case at 506–m when spacecraft leads asteroid

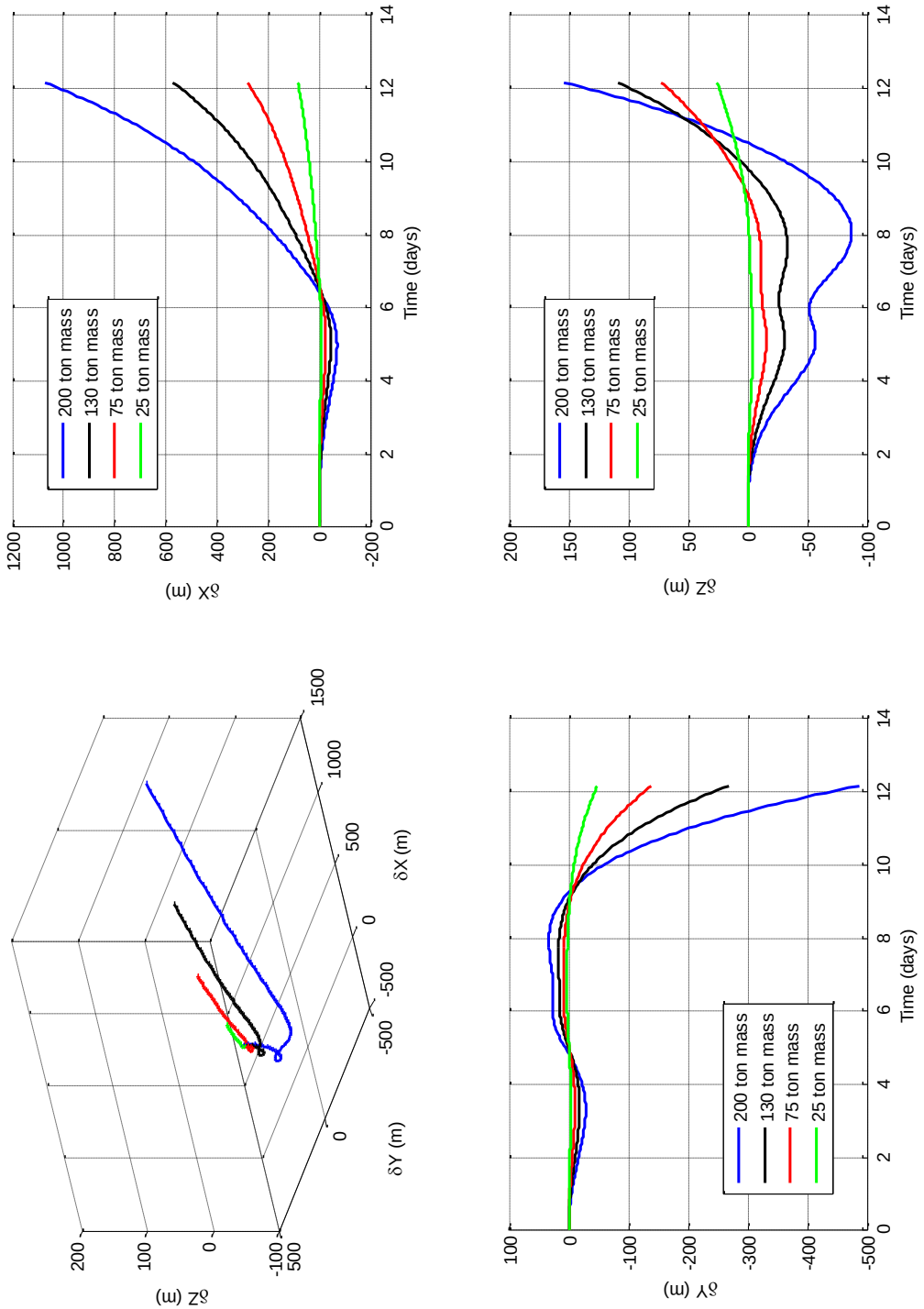

Figure 4.52. Relative position vector deviation from the baseline case at 101–m when spacecraft leads asteroid

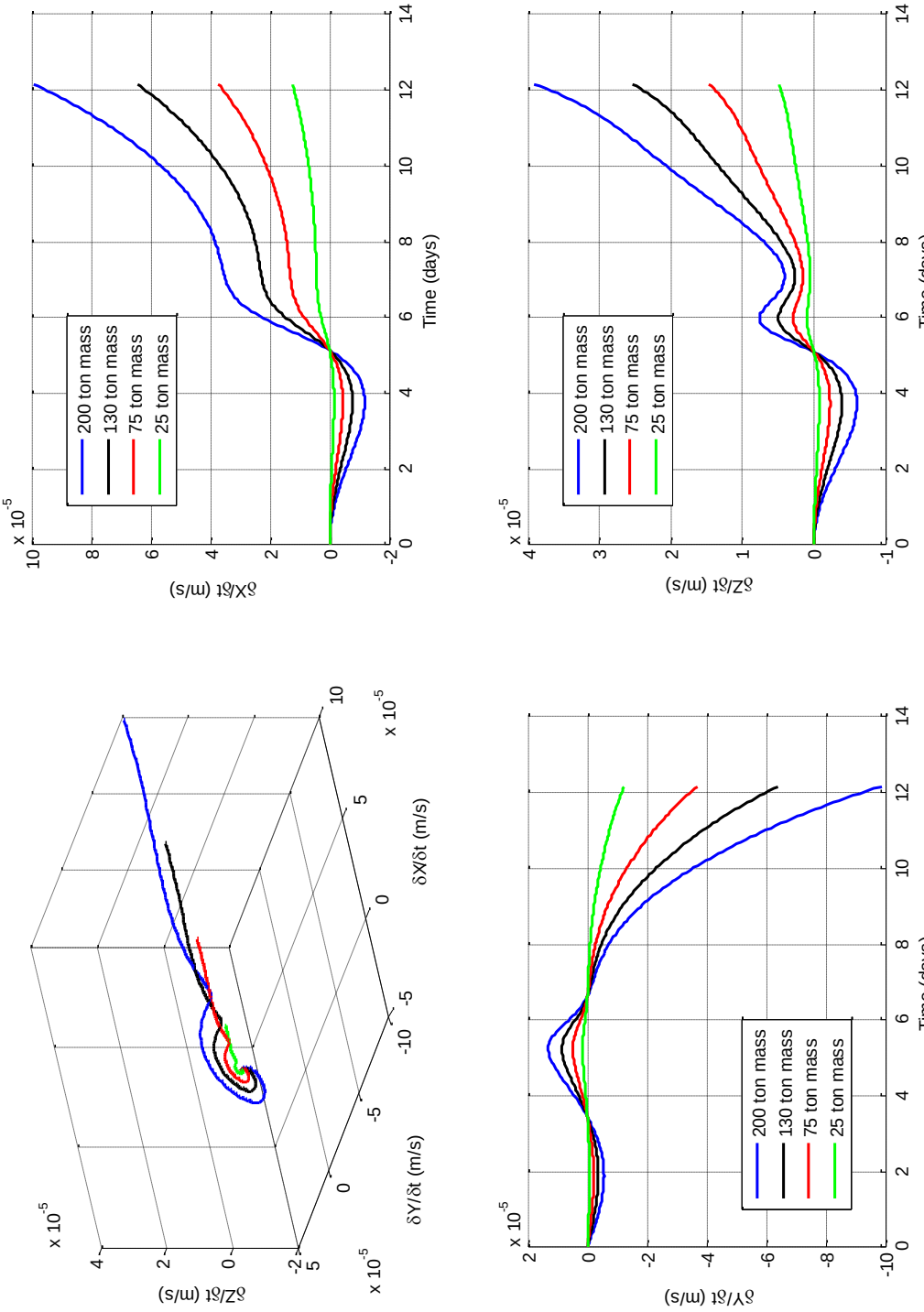

Figure 4.53. Relative velocity vector deviation from the baseline case at 506–m when spacecraft leads asteroid

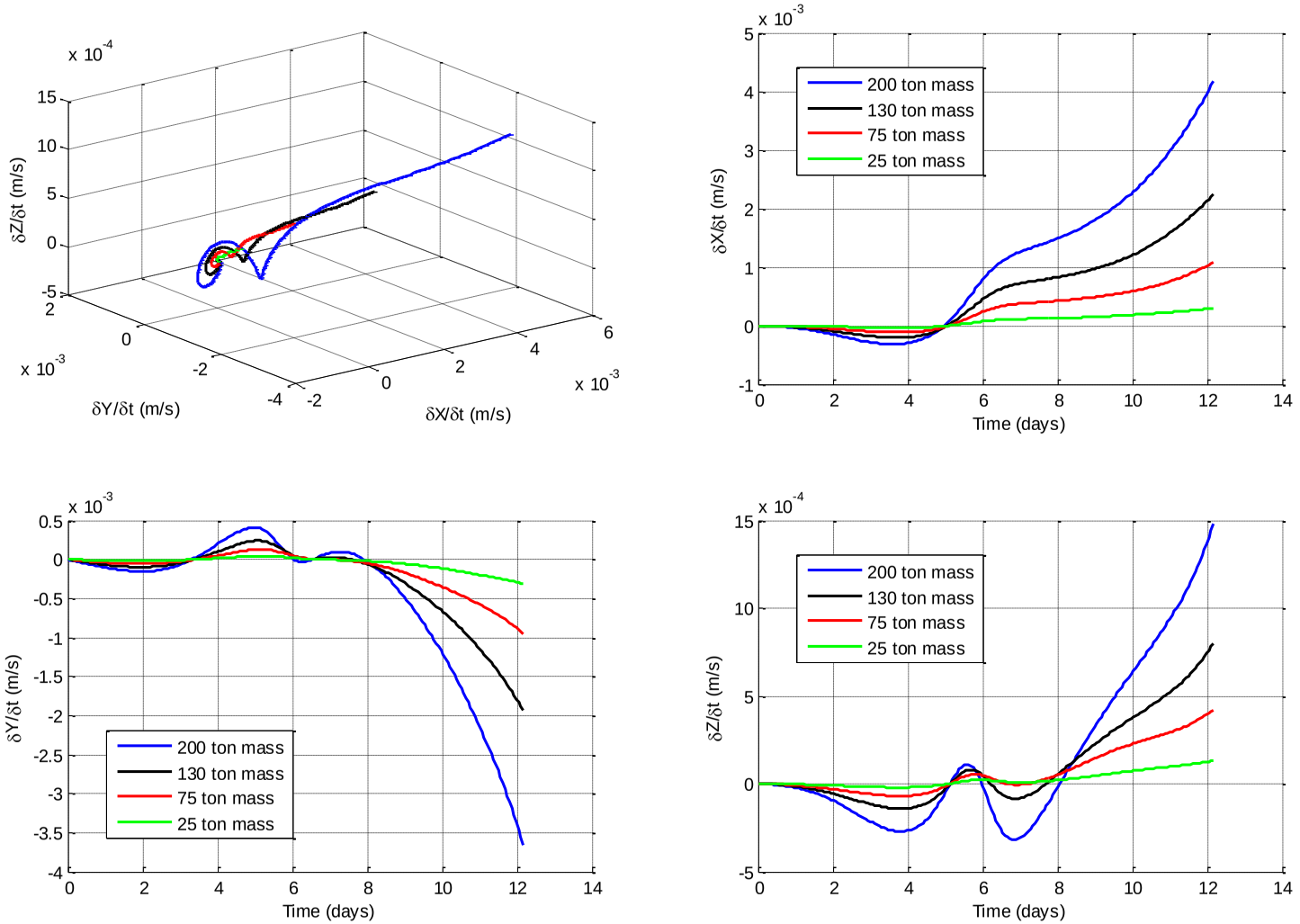

Figure 4.54. Relative velocity vector deviation from the baseline case at 101–m when spacecraft leads asteroid

4.2 Small Halo Orbit

In this section, as with the Section 4.1, the initial distances will be examined from largest to smallest. The dynamics covered in the aforementioned previous section will be the same except they will occur in a smaller orbit as seen in Figures 3.3 and 3.4. Again, the spacecraft trailing the asteroid over one period (11.948 days) will be examined first followed by the same case but over two periods. Lastly, the question of whether the spacecraft trailing or leading having any effect on the orbit is examined.

4.2.1 Spacecraft Trailing Asteroid over One Revolution of Small Halo Orbit

Looking at an initial separation distance of 811 meters, it can already be seen that small orbits are not optimal. The ranges between the spacecraft and asteroid as seen in Figure 4.55 are already deviating from the baseline case at a range of slightly over 300 meters over the maximum initial range from the large halo orbit. Furthermore, from examining the relative ranges compared to the baseline, Figure 4.56 demonstrates that the difference in range of the asteroids with mass from the baseline case is already greater than that of the initial 506–meter case for the large halo orbit (Figure 4.2).

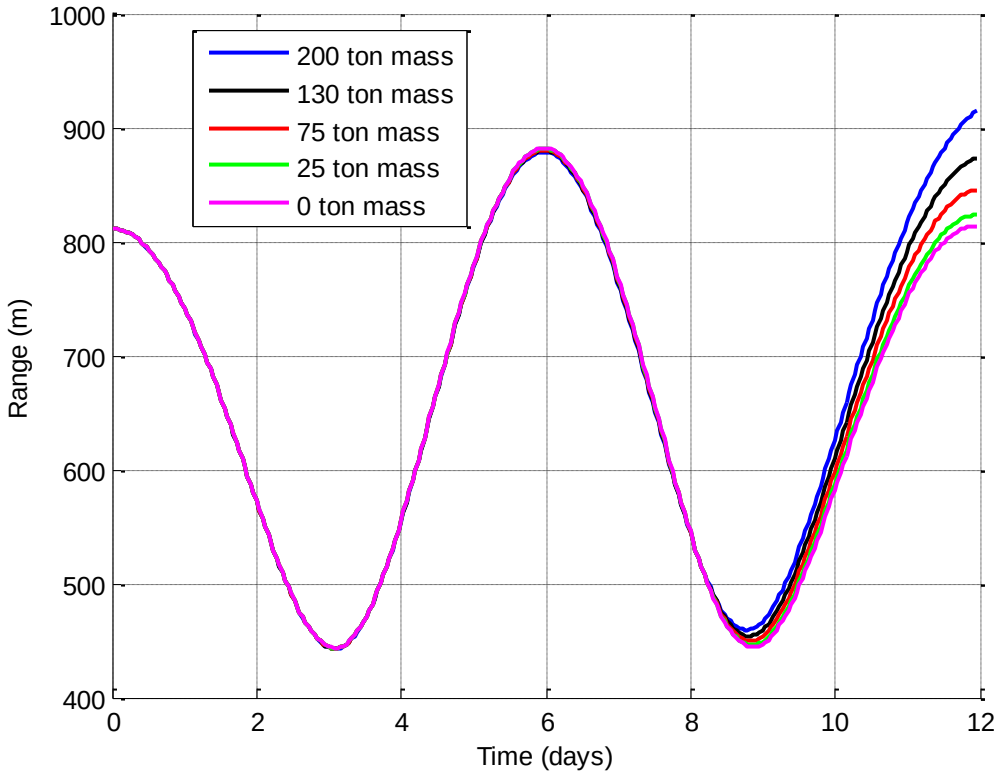

Figure 4.55. Range between spacecraft and asteroid with 811–m initial separation

The range difference to the baseline case shows a slightly different scenario than the one that occurred in the large halo orbit case with large initial separation distances between the asteroid and the spacecraft. Figure 4.56 shows that, at the first time the spacecraft is drawn closer to the asteroid, the spacecraft after moving away continues to do so even in the 25–ton–mass case. In contrast, the large halo orbit at large initial separation distances had a phenomenon where the spacecraft would move closer to the asteroid initially but then return to the position of the baseline case. This would be followed by a second movement away from the asteroid, which at closer initial separation distances would result in the spacecraft moving beyond the range of the

baseline case. Because of the fact that the small halo orbit at a large initial distance already has the early signs of instability shows that this orbit is not optimal.

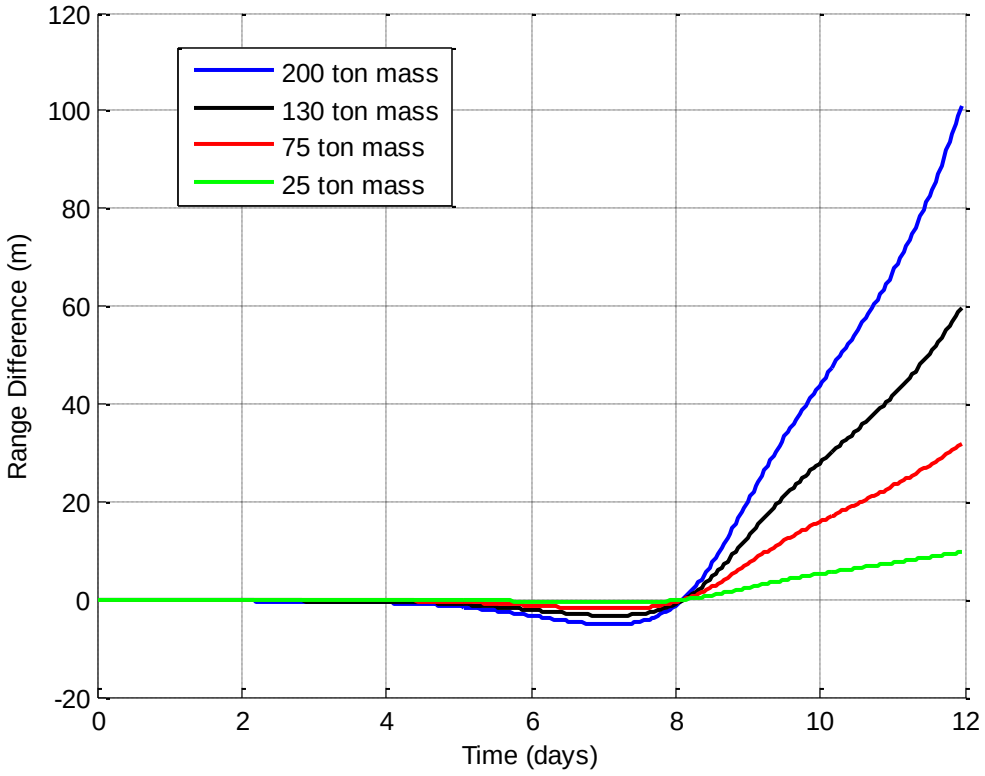

Figure 4.56. Range difference between spacecraft and massless asteroid from asteroids of varying mass with initial 811–m

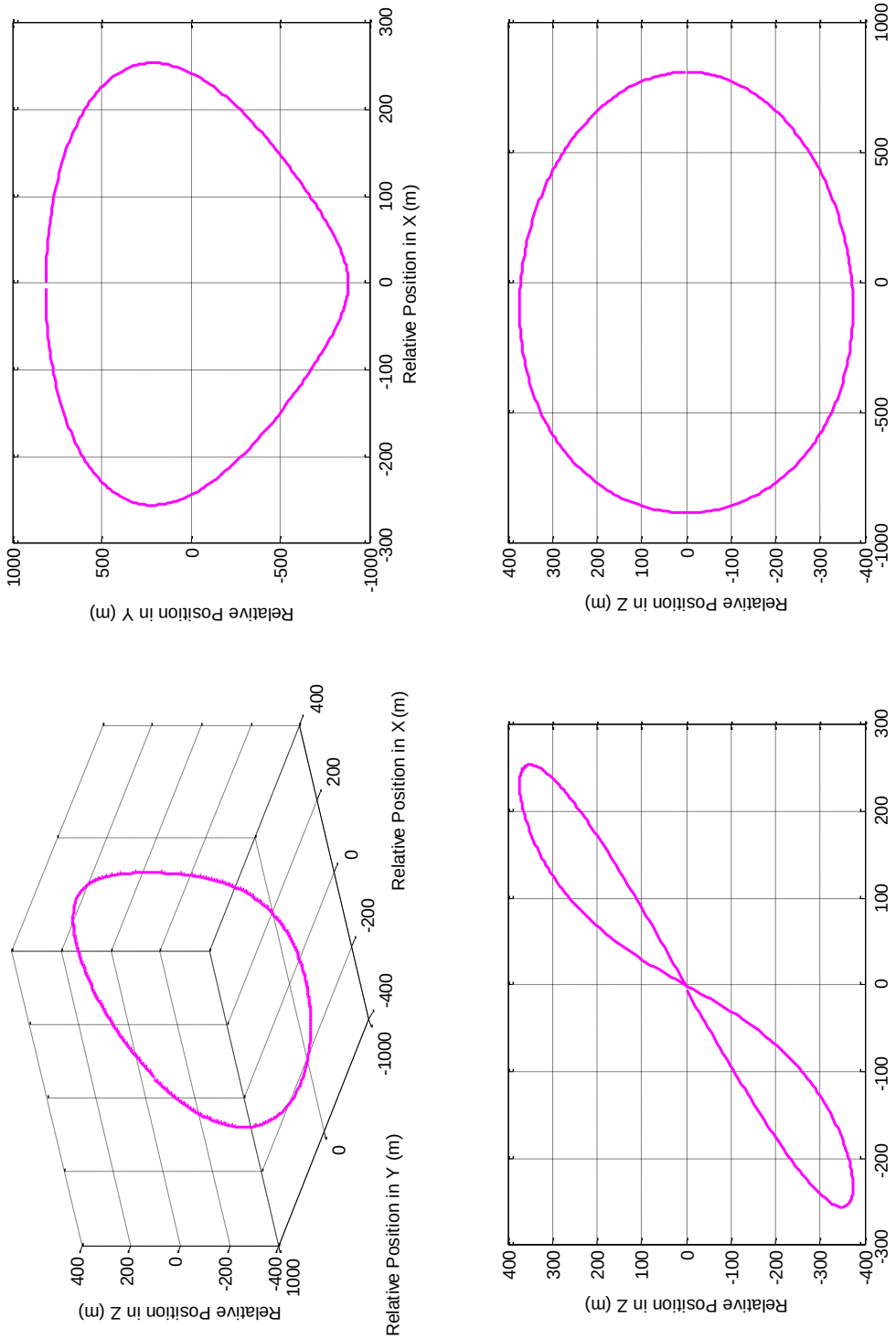

Figure 4.57. The spacecraft's relative position vector around the 0–ton asteroid at an initial distance of 811–m

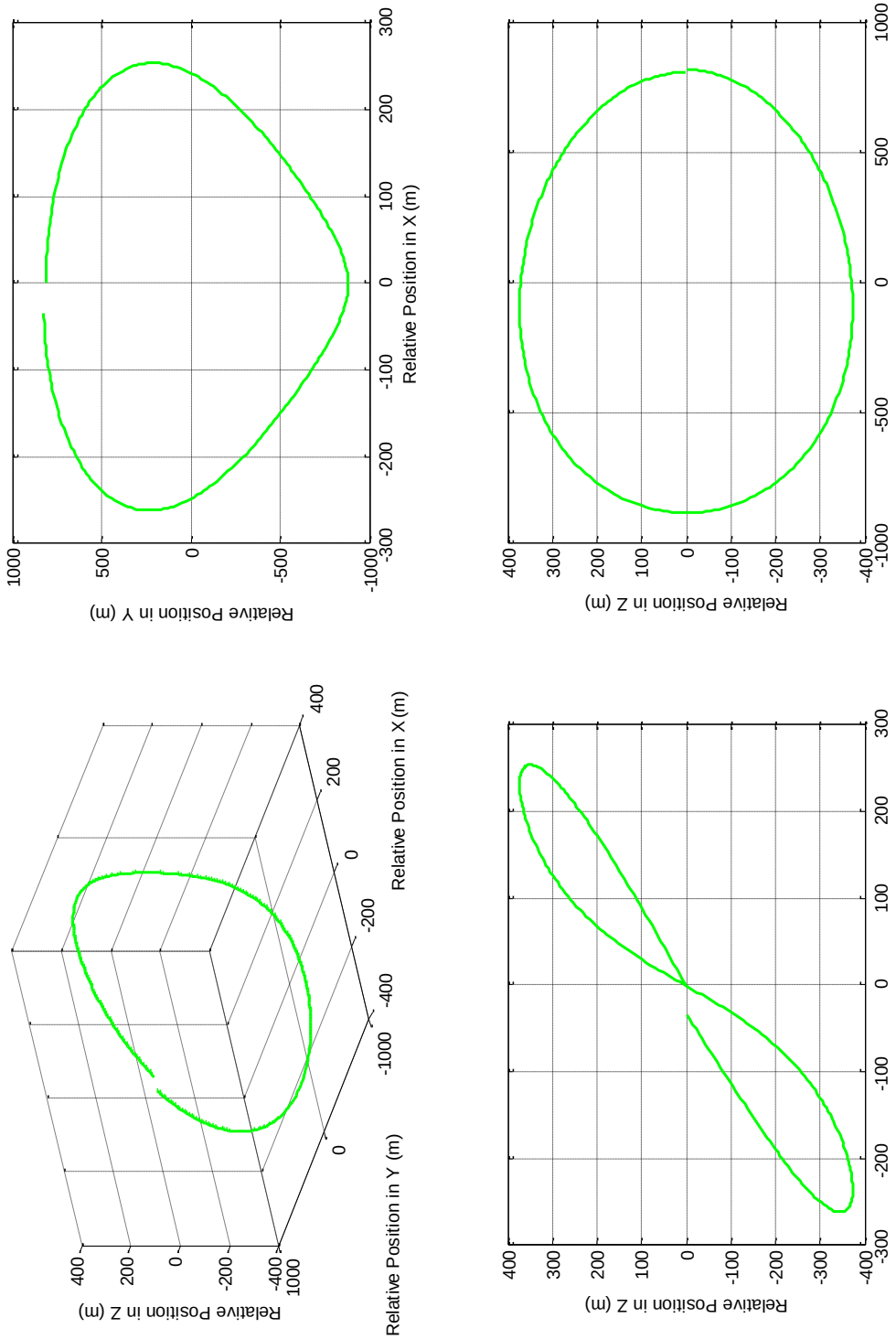

Figure 4.58. The spacecraft's relative position vector around the 25–ton asteroid at an initial distance of 811–m

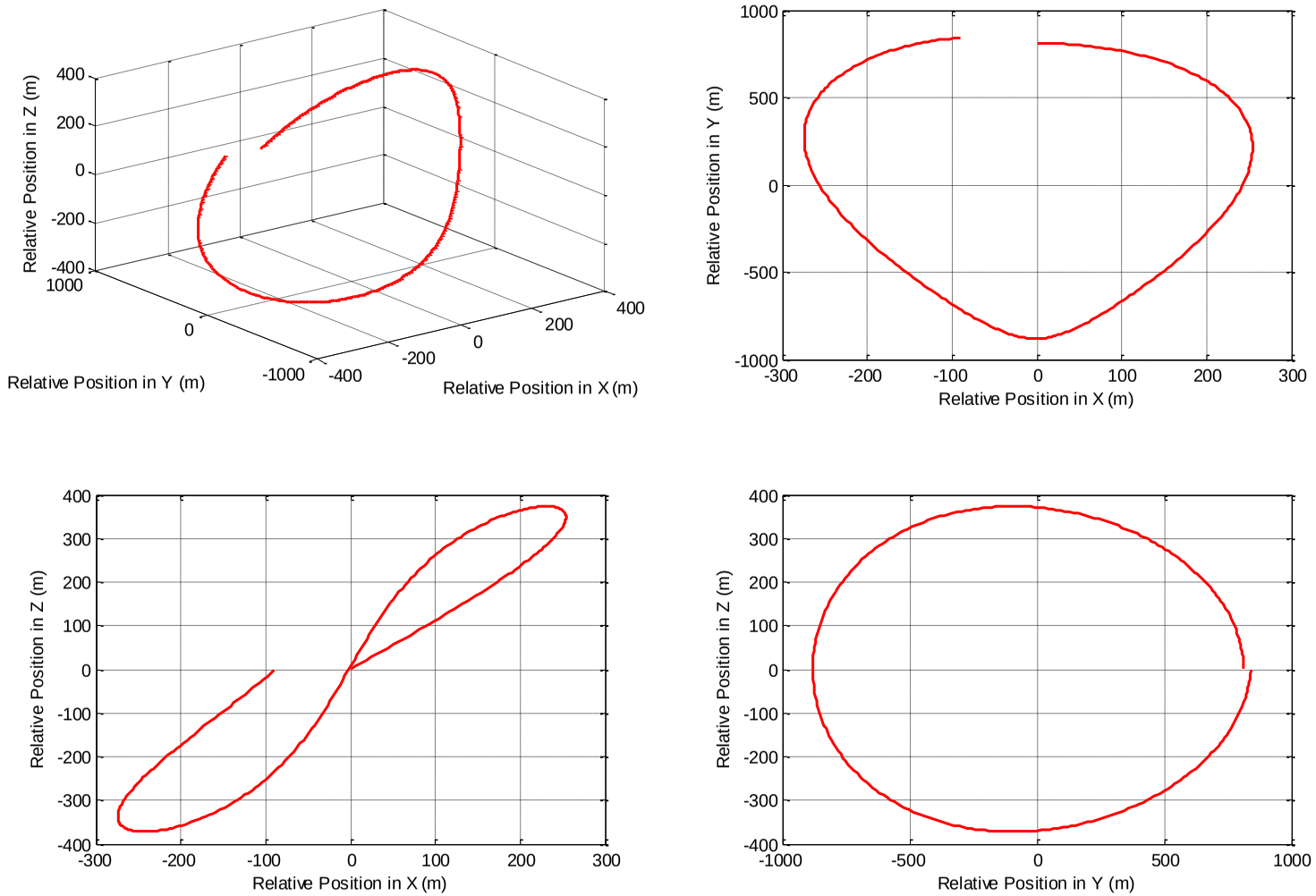

Figure 4.59. The spacecraft's relative position vector around the 75–ton asteroid at an initial distance of 811–m

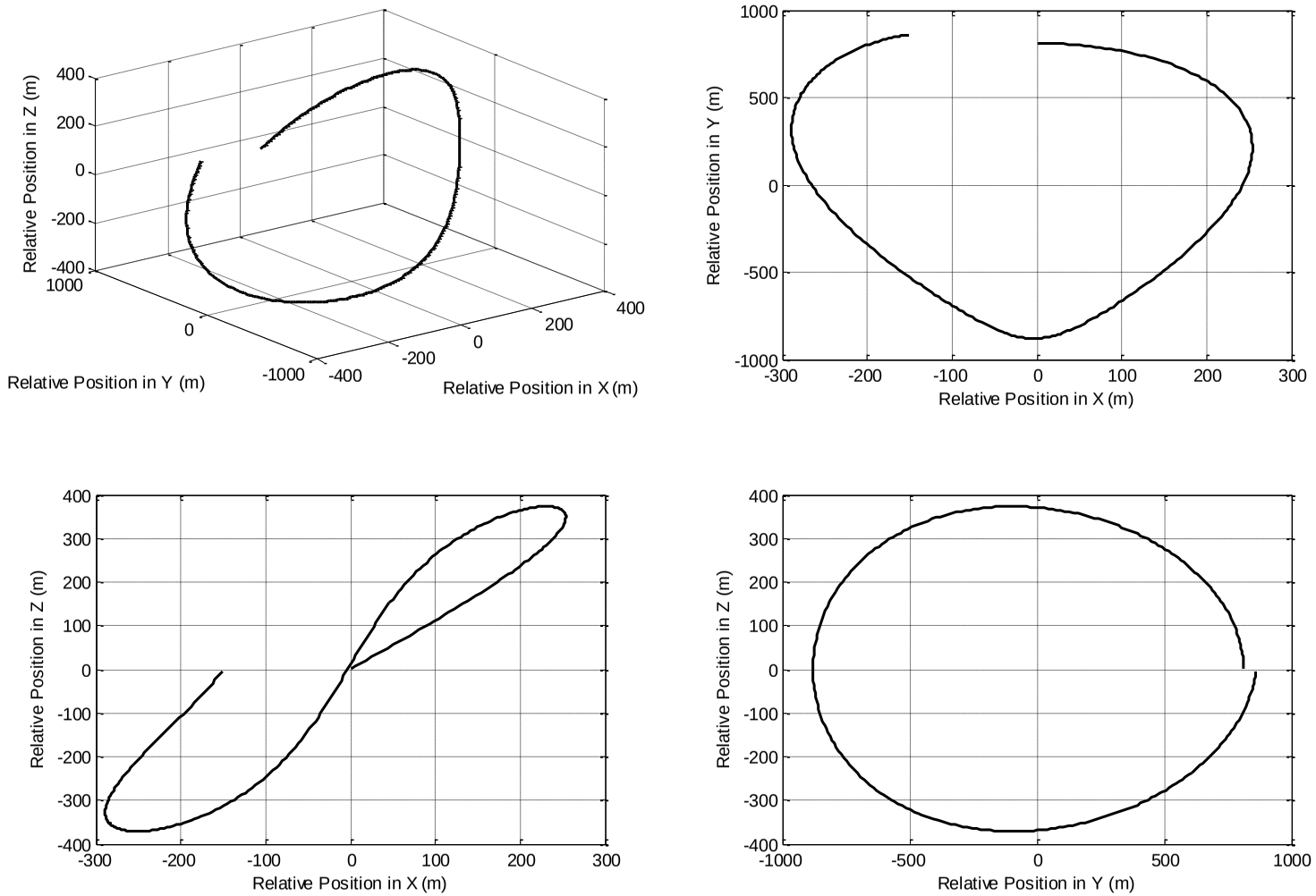

Figure 4.60. The spacecraft's relative position vector around the 130–ton asteroid at an initial distance of 811–m

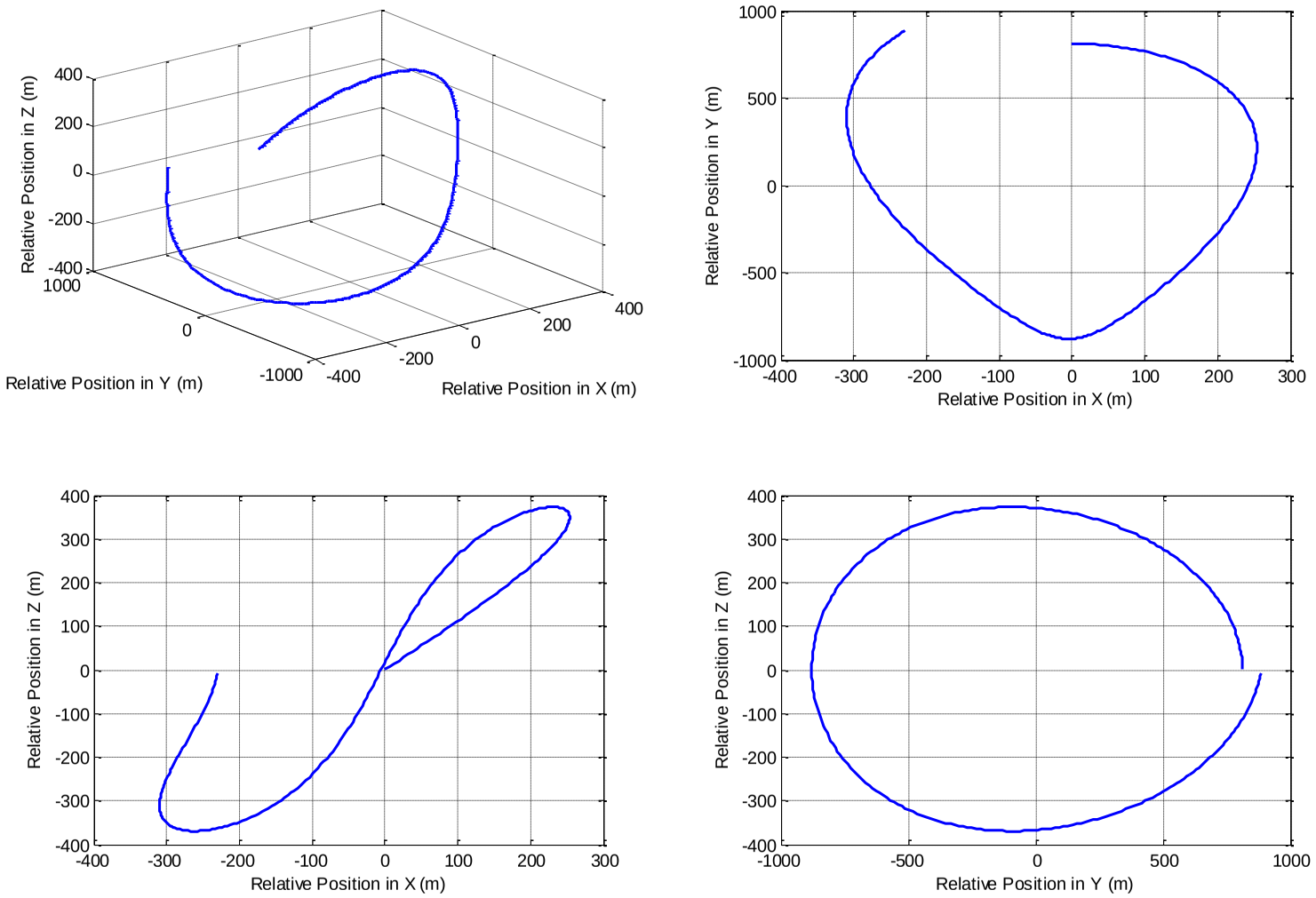

Figure 4.61. The spacecraft's relative position vector around the 200–ton asteroid at an initial distance of 811–m

From examining the relative position vectors in Figures 4.57–4.61, it can be seen that even in the 0–ton–mass case, the orbit is discontinuous as there is a small gap. Having used the smallest tolerances that MATLAB will allow, the conclusion that was reached is that the orbit is unstable which, is seen in the following section where the orbit over two periods will be examined. From the baseline case, the problem only worsens; a more sizable gap appears in the 25–ton–mass case and in the 75–ton case, the position in the $\hat{j}$ direction increases. The later cases with the heavier masses have even more pronounced effects. These changes in position are more easily seen in Figure 4.62, which shows the relative position vector. Instead of completing the orbit properly, the component in the $\hat{i}$ direction does not move toward the beginning of the orbital position relative to the baseline; this is shown by the negative values in the $\hat{i}$ direction. In the $\hat{j}$ direction, it can be seen that the position increases relative to the baseline, which is easily viewable in Figures 4.57–4.61 in the various planes as the spacecraft starts to change orbit. The component in the $\hat{k}$ direction increases but is followed by a sharp decline relative to the baseline.

This behavior contrasts from the large halo orbit in which the spacecraft would have an increase in the $\hat{i}$ and $\hat{k}$ components and a decrease in the $\hat{j}$ component. In other words, the spacecraft would complete the orbit but overshoot the initial start position in the $\hat{i}$ direction by a large margin especially at closer separation distances. The small halo orbit in contrast has an opposite effect where the spacecraft is undershooting its initial starting orbital position relative to the baseline.

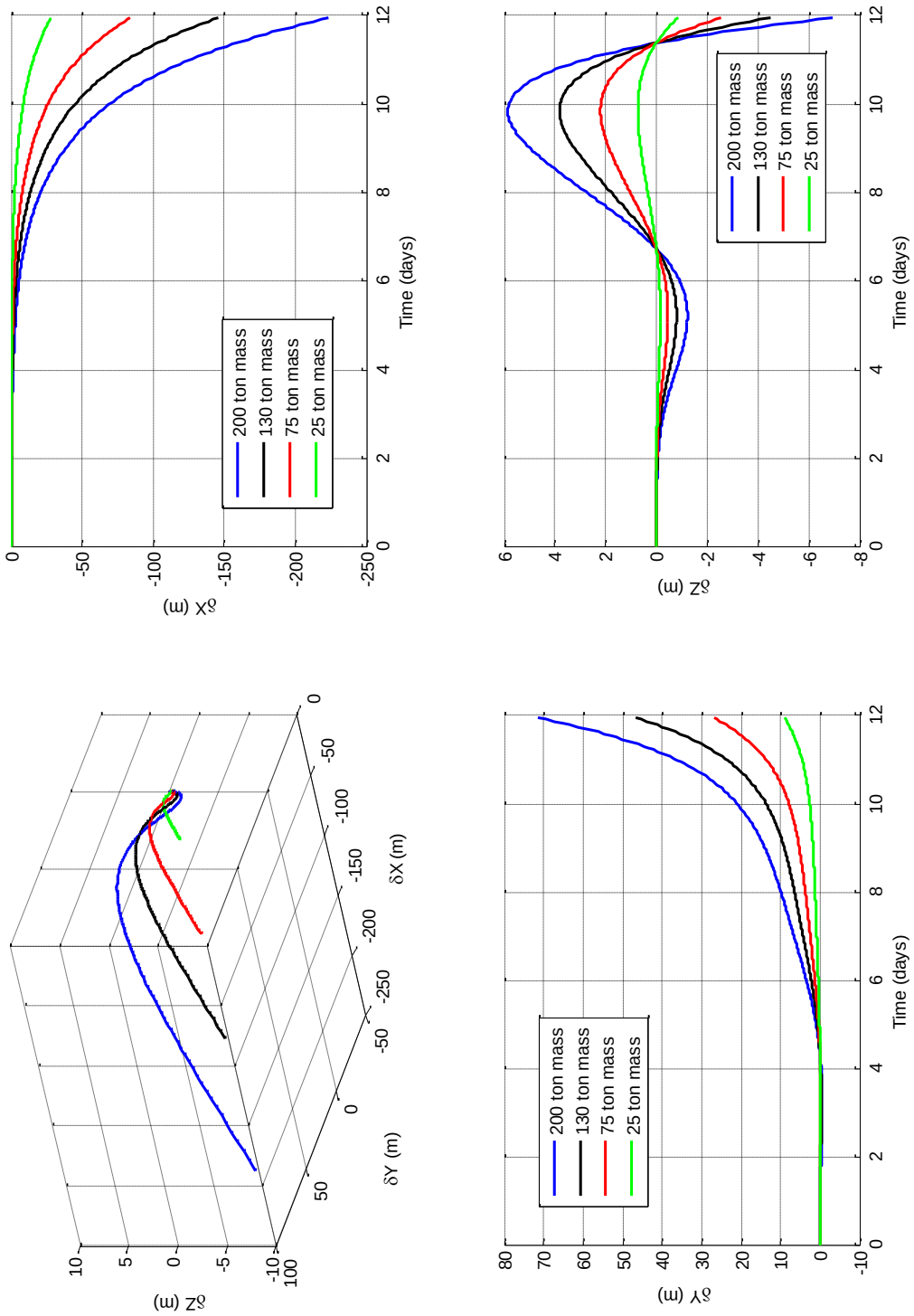

Figure 4.62. Relative position vector deviation from the baseline case at 811–m

The trends developing at the initial separation distance of 811 meters continue at an initial separation distance of 270 meters. Figure 4.63 depicting the range between the spacecraft and the asteroid show the ranges growing over the orbit.

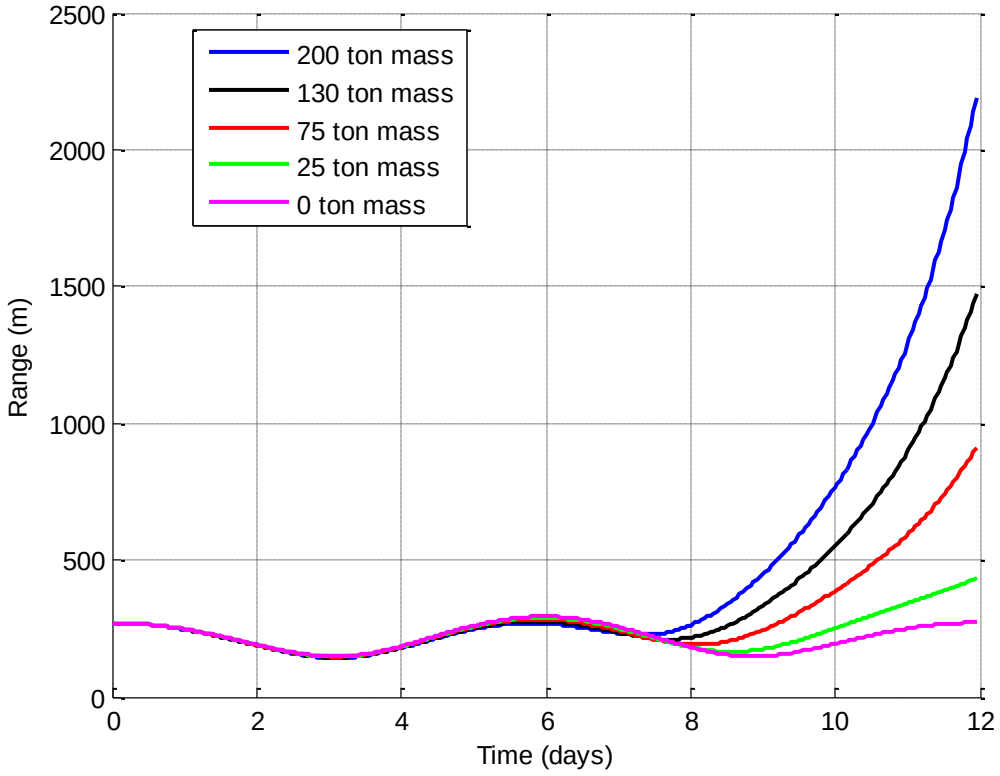

Figure 4.63. Range between spacecraft and asteroid with 270–m initial separation

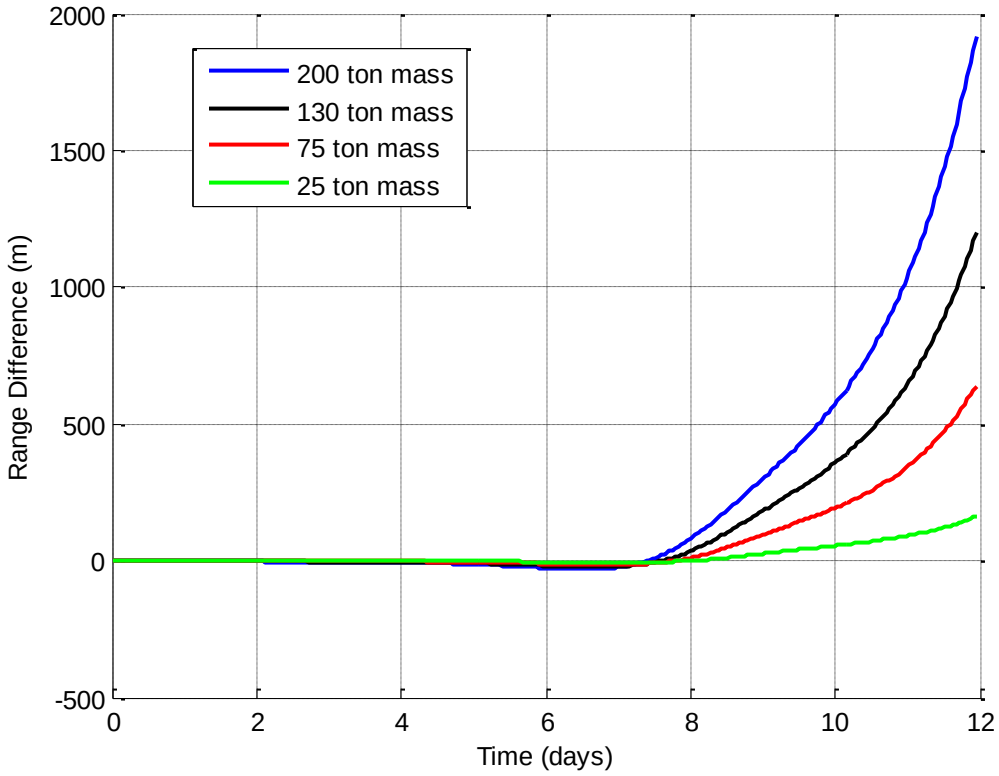

Figure 4.64. Range difference between spacecraft and massless asteroid from asteroids of varying mass with initial 270–m

When comparing the ranges to the baseline case as seen in Figure 4.64, the decrease in range is immediately followed by a large increase in the range between both objects. While it might seem that the range between the spacecraft and the asteroid for the 25–ton–mass case is not too large, this plot does not show the whole story. Figure 4.65 shows the relative position vector for the 25–ton–mass case where it can be seen that it has continued the established trend from the previous initial separation distance. As the spacecraft moves along its orbit, it radically changes its orbital plane and trajectory heading off in a completely different direction. The orbit is completely unstable and is naturally even worse for the larger masses.

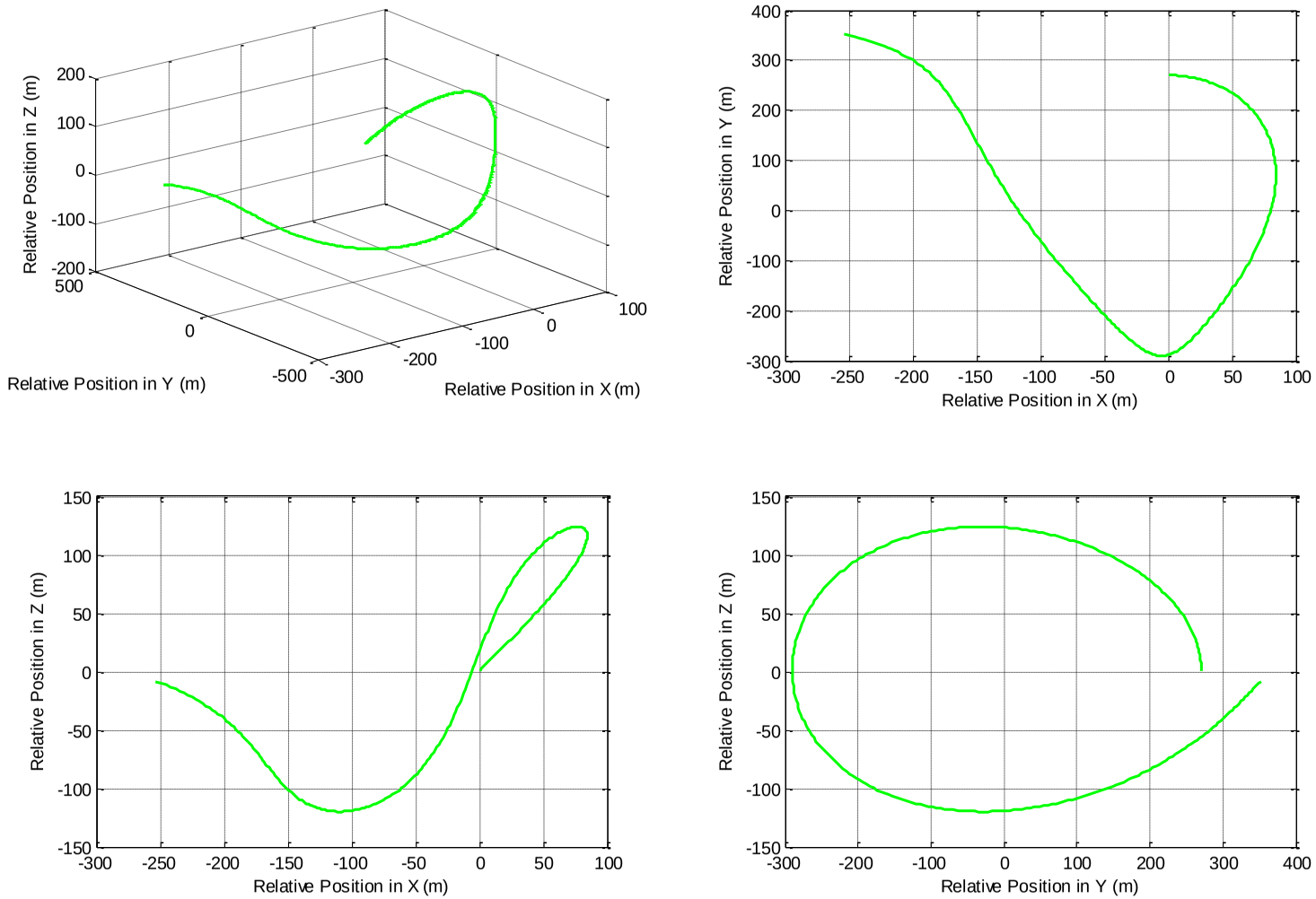

Figure 4.65. The spacecraft's relative position vector around the 25–ton asteroid at an initial distance of 270–m

At this juncture, it becomes clear that examining any cases with closer initial separation distances is superfluous. The orbital stability has already degraded to the point of uselessness. Finding the point at which the spacecraft might have a near-miss or collision with the asteroid is no longer pertinent as the stability is completely lost and the larger halo orbit is clearly the superior option.

4.2.2 Spacecraft Trailing Asteroid over Two Revolutions of Small Halo Orbit

As was mentioned in Section 4.2.1, the stability of the small orbit was in question even in the baseline case. Recalling back to the previous section, it was noted that a discontinuity existed in the relative position vector of the baseline case. Even further back in Chapter 3, it was noted that the orbit itself possessed a minor but noticeable gap hinting at the potential issues. Integrating over twice the orbital period greatly exacerbates the problem. From Figure 4.66, it can be seen that the orbit of the spacecraft is completely unstable over two periods. The spacecraft is flying alone with no asteroid and is simply moving under the principles of the circular three-body problem. The instability is not due to the asteroid but rather due to the instability of the libration point orbit.

Conducting a trade study over two periods for the small halo orbit is thus unnecessary as the orbit is inherently unstable and thus would not be a good candidate for a mission.

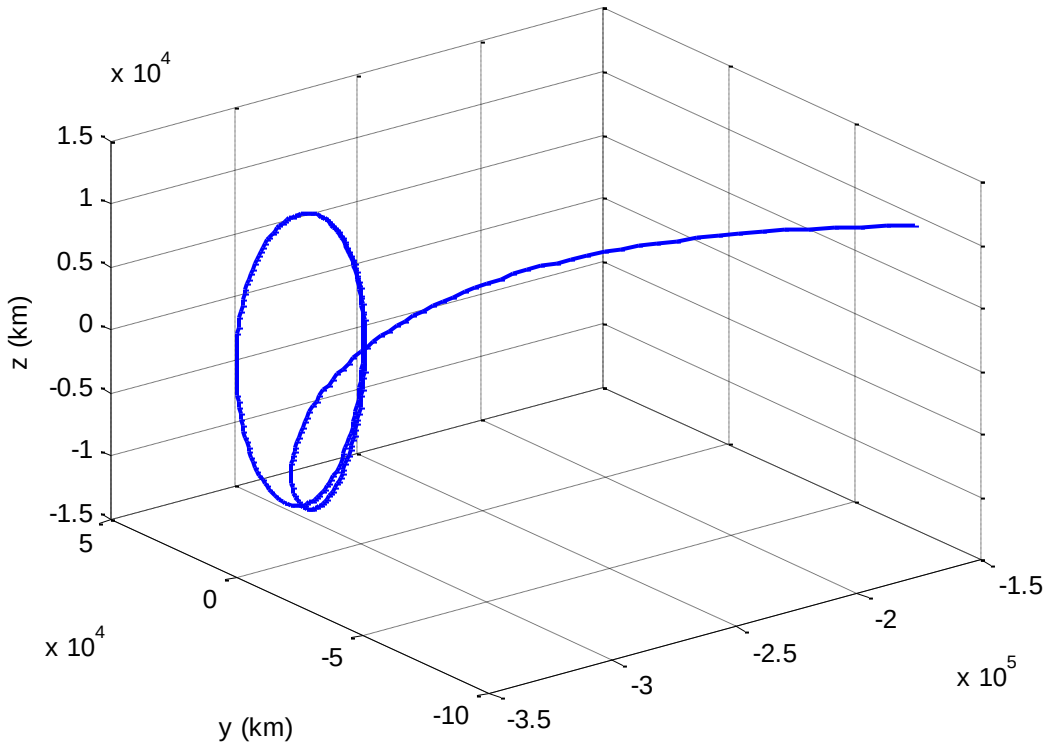

Figure 4.66. Orbit of spacecraft over two periods

4.2.3 Trailing versus Leading Spacecraft in Small Halo Orbits

Just like with the large halo orbit, the effect of the trailing versus leading spacecraft has no effect on the orbit. Examining the range of Figure 4.67 and the range difference from the baseline of Figure 4.68 shows the same exact plots as Figures 4.55 and 4.56 from Section 4.2.1. Again, the only differences are in the relative position and velocity vectors but that is only due to a difference in the sign; the magnitudes are exactly the same.

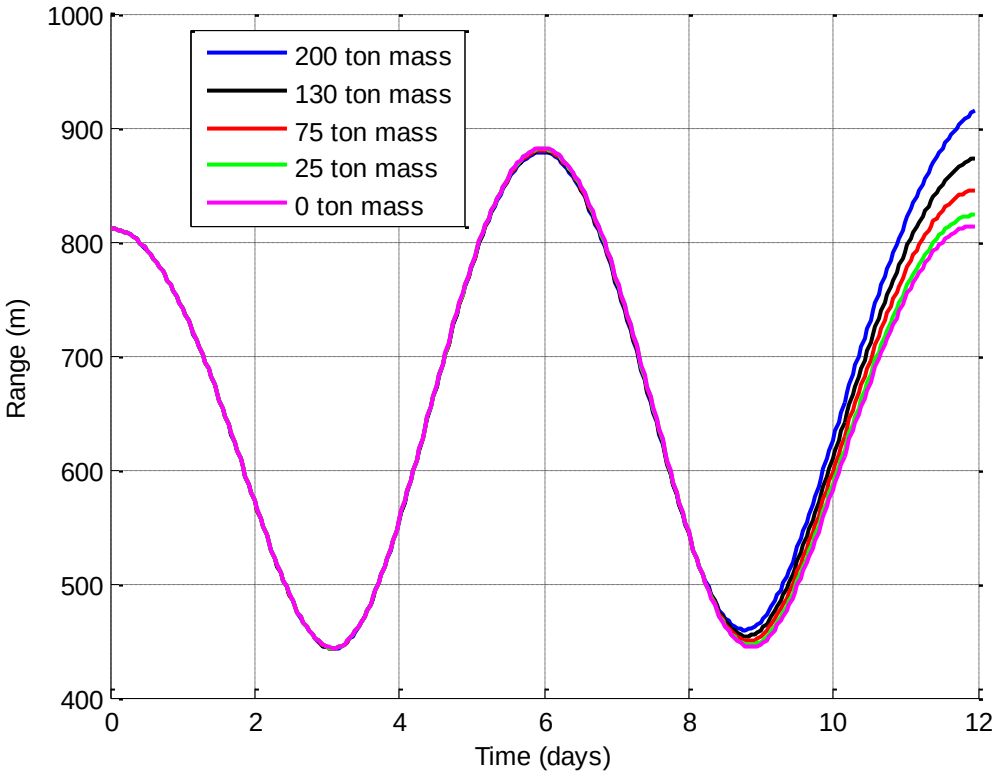

Figure 4.67. Range between leading spacecraft and asteroid with 811–m initial separation

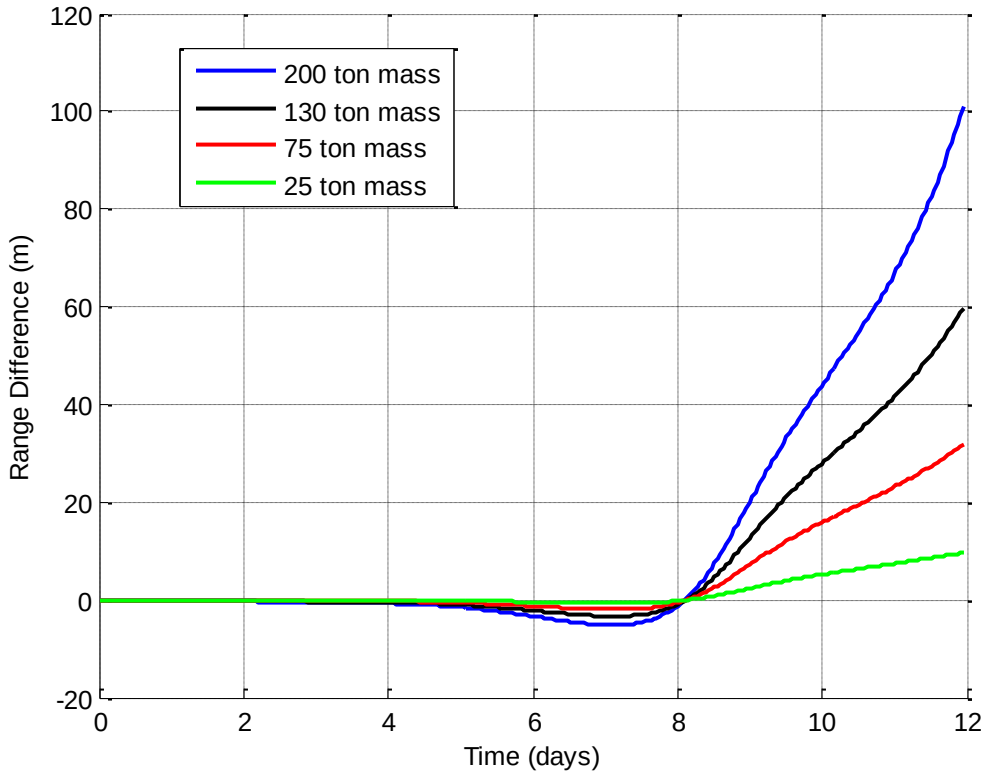

Figure 4.68. Range difference between leading spacecraft and massless asteroid from asteroids of varying mass with initial 811–m

Chapter 5

Conclusions and Future Work

5.1 Conclusions

Clearly the size of the orbit has a profound effect on the stability. Larger orbits produce better results and thus should be the only ones considered for this libration point orbit. In addition, it does not matter whether the spacecraft leads or trails the asteroid, so this aspect is purely up to mission planners' preference.

The possibility of impacts as seen in the large halo orbits only occur when the orbit is already unstable. The orbits generated between the 101 and 50 meters were already becoming unstable before impacts started occurring at the later initial separation distance. As a result, any stable orbit that is chosen will not be in any danger of impacts or near-misses which is good for mission planning. Given these range of masses, the spacecraft in the stable orbits would have their trajectories altered more for the higher masses within the range studied. The orbits were quite stable within the 300–500 meter range and thus would be viable depending on how conservative the mission planning would be. In the 200–meter range, the largest deviation from the baseline range was the 200–ton–mass asteroid at around 35 meters closer to the asteroid relative to the baseline. However, at this range, the larger masses began to have noticeable stability issues. At 300 meters, this shrinks to less than 25 meters and at the 500–meter range, the effects are practically negligible. An initial separation of 303 meters had minimal stability issues for the largest asteroid and thus would be an acceptable range for the spacecraft relative to the

asteroid for all masses. The bottom line is that it is up to the mission planner to decide as to how much deviation from the baseline orbit is acceptable.

Within the aforementioned ranges at which the orbits are stable, the resulting trajectory of the spacecraft is fairly independent of the mass of the asteroid (within the range of masses used) except for the borderline 200–meter case for the largest asteroid only. This is counterintuitive and an interesting result of the trade study. This gives mission planners the flexibility in designing orbits independent of the mass of the asteroid.

The length of the orbit also has a dramatic effect on the stability. As seen from integrating over twice the orbit, stability was only viable over a 900–meter range between the spacecraft and the asteroid. It was also found that the orbit itself with no asteroid mass was completely unstable for a small halo orbit. As a result, the size of the orbit is especially imperative for a mission over this duration. Furthermore, if a mission were designed so that it took place over less than one orbital period, then closer initial distances could be considered. Orbits such as the one generated with an initial distance of around 150 meters were stable for roughly a week before stability started to become an issue. Basically, the longer the mission, the further the initial distance between the spacecraft and the asteroid needs to be.

The minimum stand-off distance is dependent on the stability of the orbit. While the spacecraft had safe trajectories within an initial separation distance of 100 meters from the asteroid, the orbits were unstable. As a result, only the minimum ranges from the surface of the asteroid for the stable orbits are considered for the minimum stand-off distance. At an initial separation distance of 506 meters, the spacecraft formation flying with the 200–ton asteroid approaches 485 meters from the asteroid's surface. For the initial separation distance of 303 meters, the spacecraft comes to within 270 meters of the asteroid.

Due to the fact that the mass of the asteroid has predictable effects on the motion of the spacecraft, the accumulated data can be used to determine the mass of an asteroid if the mass is

unknown. Given the range data from an asteroid, the mass can be determined based on the trajectory of the spacecraft using similar methods described by Tapley et al. [17].

5.2 Future Work

This research only considered the circular restricted four-body problem (CR4BP); further work could be done using the elliptical restricted four-body problem (ER4BP). In this paradigm, the orbits of the Earth–Moon system are not considered to be circular but rather their realistically elliptical motion. This would also create more instability in the libration point as it would oscillate in this model as the Moon changes its range relative to the Earth.

Future work could also look at even larger halo orbits; it was clearly shown that the large halo orbit was clearly the more viable option over a smaller orbit. Perhaps many different orbits of various sizes and orbital periods can be examined to determine the most optimal orbit. In addition, different types of orbits could be analyzed; the viability of orbits like lissajous orbits could be analyzed.

Perhaps another avenue of future work could be a study of how much ΔV would be required to maintain more stable orbits at closer initial separation distances. An entire trade study could be conducted on this aspect alone to determine the most optimal use of ΔV over a given range

References

[1]Bando, Mai and Ichikawa, Akira, "Formation Flying Along Halo Orbit of Circular-Restricted Three-Body Problem," *Journal of Guidance, Control, and Dynamics*, Vol. 38, Issue 1, DOI: 10.2514/1.G000463, 123-129, 2015.

[2]Gurfil, Pini and Meltzer, Dani, "Stationkeeping on Unstable Orbits: Generalization to the Elliptic Restricted Three-Body Problem," *The Journal of the Astronautical Sciences*, Vol. 55, Issue 1, 29-51, 2006.

[3]Wang, Yue, Xu, Shijie, and Zhu, Mengping, "Stability of Relative Equilibria of the Full Spacecraft Dynamics Around an Asteroid with Orbit-Attitude Coupling," *Advances in Space Research*, Vol. 53, Issue 7, 1092-1107, 2014.

[4]Scheeres, D. J., Williams, B. G., and Miller, J. K., "Evaluation of the Dynamic Environment of an Asteroid: Applications to 433 Eros," *Journal of Guidance, Control, and Dynamics*, Vol. 23, Issue 3, DOI: 10.2514/2.4552, 466– 475, 2000.

[5]Brucker, Eytan and Gurfil, Pini, "Analysis of Gravity-Gradient-Perturbed Rotational Dynamics at the Collinear Lagrange Points," *The Journal of the Astronautical Sciences*, Vol. 55, Issue 3, 271-291, 2007.

[6]Scheeres, Daniel J., "Orbit Mechanics About Asteroids and Comets," *Journal of Guidance, Control, and Dynamics*, Vol. 35, Issue 3, DOI: 10.2514/1.57247, 987-997, 2012.

[7]Scheeres, Daniel J., "Spacecraft at Small NEO," http://arxiv.org/abs/physics/0608158

[8]Szebehely, Victor, Theory of Orbits The Restricted Problem of Three Bodies, Academic Press Inc., 1967.

[9]Curtis, H.D., "Orbital Mechanics for Engineering Students," Elsevier Butterworth-Heinemann, Second Edition, New York, NY, 2009.

[10]Guelman, Mauricio, "Closed-Loop Control of Close Orbits Around Asteroids," *Journal of Guidance, Control, and Dynamics*, Vol. 38, Issue 5, DOI: 10.2514/1.G000158, 854-860, 2013.

[11]Mok, Sung-Hoon, Choi, Yoonhyuk, Bang, Hyochoong, and Leeghim, Henzeh, "A Delayed Impulse Control Strategy for Spacecraft Formations," *Journal of the Astronautical Sciences*, Vol. 60, Issue 3, 338-365, 2015.

[12]Broschart, Stephen B. and Scheeres, Daniel J., "Control of Hovering Spacecraft Near Small Bodies: Application to Asteroid 25143 Itokawa," *Journal of Guidance, Control, and Dynamics*, Vol. 28, Issue 2, 343-354, 2004.

[13]Morrow, Esther, Scheeres, Daniel J., and Lubin, Dan, "Solar Sail Orbit Operations at Asteroids," *Journal of Spacecraft and Rockets*, 279-286, 2001.

[14]Tardivel, Simon, Scheeres, Daniel J., Michel, Patrick, Van wal, Stefaan, and Sànchez, Paul "Contact Motion on Surface of Asteroid," *Journal of Spacecraft and Rockets*, Vol. 51, Issue 6, DOI: 10.2514/1.A32939, 1857-1871, 2014.

[15]Prussing J., and Conway, B., Orbital Mechanics, Oxford University Press, UK, 1993

[16]Huang, Su-Shu, Very Restricted Four-Body Problem, NASA-TN-D-501, September, 1960.

[17]Tapley, Byron D., Schutz, Bob E., and Born, George H., Statistical Orbit Determination, Elsevier Academic Press, 2004